University of Pisa

PhD School in Morphology and Function of Normal and Pathological Cells and Tissues

(XXIV cycle)

2009-2011

Doctor of Philosophy Thesis in

Functional and morphological study of cells in connected culture in response to interactions associated with nanoparticles

(SSD BIO/13)

Candidate

Nadia Ucciferri

_____

Supervisor

Prof. Francesco Fornai

_____

Prof. Arti Ahluwalia

_____

Advisor

Dr. Claudio Domenici

_____

Prof. Claus-Michael Lehr

_____

Table of Contents

Abstract

The improvement of *in vitro* and *in vivo* models for tissue engineering, pharmacology, or metabolic studies, is largely requested. In fact, while *in vitro* models are usually preferred due to their convenience and compatibility with the 3Rs, unfortunately they lack biochemical interactions, for instance cell-cell cross-talk or important bio-barriers leading to non-physiologically relevant results.

The aim of this thesis is to develop a new *in vitro* system able to recreate the main barrier through ingestion, the intestinal epithelium as well as a connected target organs, the vascular endothelium and the liver. The thesis is focused on the study of nanoparticle (NP) fate after ingestion, the ability of NPs to cross the intestinal barrier and the effects on relevant target tissues. In order to achieve this aim simplified models were firstly used so that the complexity of the system could be increased stepwise to include additional cell types, more complex 3D models of tissues, and more sophisticated and specific tests of cellular responses to the presence of nanoparticles.

The system developed is a new body-on-a-plate device able to study the physiologically relevant doses that actually reach the systemic circulation after intestinal absorption. It has a microfluidic flow which transports messaging molecules from cell to cell and stimulates them with a constant low shear stress.

Hence, the results obtained with this new model were compared with data generated in conventional static cell cultures in order to validate the system and gain a better insight on the systemic effects of NP toxicity.

Besides the study of the toxicity of nanoparticles of industrial and environmental interest, this thesis demonstrates the importance of advanced *in vitro* testing, pointing out the differences in results from standard simple cultures with respect to those obtained from more relevant physiological model.

Section I

Introduction

Chapter 1

In vitro models for Toxicology Testing

1. TOXICOLOGY

Toxicology is the study of the adverse effects of chemical, physical or biological agents on people, animals, and the environment. Many studies are required to ensure the safety of medicines, household and gardening chemicals, and industrial and natural chemicals to which everybody is continuously exposed.

Toxicologists know that no substance is risk-free. Paracelsus, in the 16th century, summarized this concept in the sentence “All things are poison, and nothing is without poison; only the dose permits something not to be poisonous", or more commonly, "the dose makes the poison". That is to say, substances considered toxic are harmless in small doses, and conversely an ordinarily harmless substance can be deadly if over-consumed.

For this reason, toxicology research is important for ensuring the health of humans, animals, and their environments. This research is intended to identify harmful effects of potential new products and to provide understanding of the mechanisms by which chemical substances cause injury, in order to use this information in the treatment of poisonings.

Toxicology represents an area of science of growing importance, largely as a consequence of the rapid increase in environmental and safety legislation. A further driver of toxicology is the continuing growth of the industrial sector which develops a greater number of new materials and compounds.

All organisms are composed of chemicals, and chemical reactions power all life processes. When a substance is introduced into a body, it can interact in many places and effects upon one process can cause unexpected consequences in others.

The use of animals in this kind of experiments is fundamental because such complexity cannot be duplicated in normal cell culture or in non-living systems. For example, toxicity can be influenced by the speed with which the substance enters the system, how the metabolic organs change it and how it is taken up by and interacts with various body tissues.

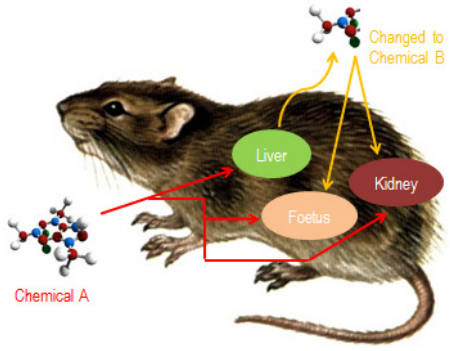

Fig. 1: Schematic diagram explaining how a chemical can change into another thanks to internal metabolism. Adapted from [1].

Moreover, because "the dose makes the poison" at the level of the individual organ, we need to be able to analyze not only how a chemical acts, but the relationship between the dose given to the animal and the dose delivered to the different organs and tissues in the body. Studies in whole animals are required to ensure the proper use of beneficial chemicals such as medicines, because the tissue or organ receiving the beneficial effect might be harmed if exposures are greater than needed. In many cases, laboratory tools simply cannot duplicate these complicated phenomena [2]. Ultimately, animal testing is the best method to detect effects such as cancer and birth defects, even if it sometimes is difficult to identify the right model to test as demonstrated by the Thalidomide case whose

teratogenicity was found only occasionally in the huge set of different animals and species tested [3].

2. THE ANIMAL TESTING DEBATE

The ethical questions raised by performing experiments on animals are subject to much debate, and viewpoints have shifted significantly over the 20th century [4].The case for animal experiments is that they will produce such great benefits for humanity that it is morally acceptable to harm a few animals. The equivalent case against is that the level of suffering and the number of animals involved are both so high that the benefits to humanity don't provide moral justification.

Animal welfare, and animal rights organizations (such as PETA -People for the Ethical Treatment of Animals- and BUAV -British Union for the Abolition of Vivisection-) question the legitimacy of animal testing, arguing that it is cruel, poor scientific practice, poorly regulated, that medical progress is being held back by misleading animal models, that some of the tests are outdated, that it cannot reliably predict effects in humans, that the costs outweigh the benefits, or that animals have an intrinsic right not to be used for experimentation.[3]

Heavy pressure from these associations leads to a high interest of scientist and governments to address the animal testing issue. Moreover, as technology has advanced, new ways to stop animal testing have come into the picture. In 1959, Russel and Burch published *The Principles of Humane Experimental Technique* in which “the 3 R’s principles” were proposed to encourage scientist reducing the impact of research on animals.

“The 3 R’s” stand for reduce, refine and replace and means:

Reduction:

- Reducing the number of animals used in experiments by:
  - Improving experimental techniques

- Improving techniques of data analysis
- Sharing information with other researchers

Refinement:

- Refining the experiment or the way the animals are cared for so as to reduce their suffering by:
  - Using less invasive techniques
  - Better medical care
  - Better living conditions

Replacement:

- Replacing experiments on animals with alternative techniques such as:
  - Experimenting on cell cultures instead of whole animals
  - Using computer models
  - Studying human volunteers
  - Using epidemiological studies

In November 2008 the European Union put forward proposals to revise the directive of 1986 for the protection of animals used in scientific experiments in line with the three Rs principle of replacing, reducing and refining the use of animals in experiments. The proposals have three aims:

- to considerably improve the welfare of animals used in scientific procedures
- to ensure fair competition for industry
- to boost research activities in the European Union [5].

Now EU rules for animal experimentation are more restrictive, requiring that experiments where animals are used be subject to authorization and state that alternatives to testing on animals must be used when available and that the number of animals used in projects be reduced to a minimum [6].

The Commission and industry have set up the European Partnership for Alternative Approaches to Animal testing (EPAA) whose aim is to promote

the development of new '3R' methods as alternative approaches to the use of animals in safety assessment.

Another thing to take in account about the reducing of animal testing issue is that concerning the Cosmetics industry. The 7th amendment to the Cosmetics Directive (76/768/EEC) foresees a testing and marketing ban on cosmetics tested on animals. The directive on animal testing (86/609/EEC) does not amend the rules provided for in other pieces of EU legislation. The sales ban means not only that cosmetics' testing is mostly ended in the European Union but also that even products tested elsewhere cannot be sold there.

The testing ban on cosmetics has been in application since 2009 when testing was prohibited irrespective of alternatives to animal testing being available. The marketing ban applies unconditionally to all human health effects with the exception of three toxicological effects such as repeated-dose toxicity, reproductive toxicity and toxicokinetics. The year 2013 is foreseen as the deadline for a ban on these specific health effects.

The interest for non-animal methods is clearly really high.

3. *IN VITRO* MODELS

In vitro models are the obvious solution to the replacement of animal testing. ***In vitro*** refers to studies in experimental biology that are conducted using components of an organism that have been isolated from their usual biological context in order to permit a more detailed or more convenient analysis than can be done with whole organisms. Common examples of *in vitro* experiments include:

- cells derived from multicellular organisms (cell culture or tissue culture)
- subcellular components (e.g. mitochondria or ribosomes)
- cellular or subcellular extracts (e.g. wheat germ or reticulocyte extracts)

- purified molecules in the test tube (proteins, DNA, or RNA, either individually or in combination) [4].

In vitro studies allow scientists to isolate specific cells, bacteria, and viruses and study them without the complexity of a whole organism. This permits an enormous level of simplification of the system under study, so that the investigator can focus on a small number of components [7]. For example, the knowledge of the mechanism by which a protein target recognizes and binds to a receptor is the result of the extensive use of *in vitro* work that means isolate the proteins, identify the cells and genes that produce them, study the physical properties of their interaction with molecules, and identify how those interactions lead to cellular signals that activate other components of the response pathway.

In toxicology, *in vitro* testing methods are employed primarily to identify potentially hazardous chemicals and/or to confirm the lack of certain toxic properties in the early stages of the development of potentially useful new substances such as therapeutic drugs, agricultural chemicals and direct food additives

In vitro toxicity testing:

- provides rapid and effective means of screening and ranking chemicals in food or environment for a number of toxicology endpoint
- allows the understanding of the mechanism by which a toxic lead effects at both the cellular and molecular level, and of both causal and adaptive responses
- is essential for bridging between experimental animal and human, and addressing the correct species choice
- provides well defined and simplified system for studying structure-activity relationship
- provides a means for identification of key molecular events that are involved in toxicity, enabling the development of effective biomarkers of effect

- enables detailed analysis of the toxicological consequences of genetic variation within the population
- enables assessment of cell-specific (e.g. liver, cardiac, kidney, neural, immune system) and, where possible, tissue-specific (e.g. embryo) effects;
- allows establishing the nature of concentration-effect relationships and the existence of effect-specific thresholds in cells from different species and different tissues [8].

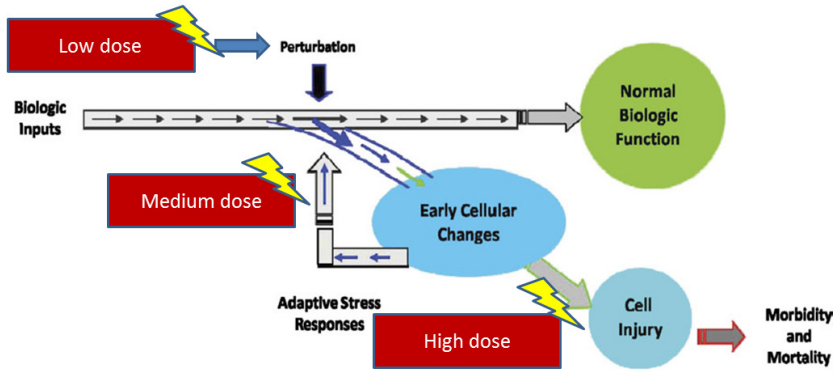

Fig. 2: Progressive activation of toxicity pathways from perturbation of initial target low dose, through activation of stress controlling pathways (medium dose), to overtly toxic responses (high dose). Biologic responses from exposure results in perturbation of biologic pathways, accumulation and high dose lead to toxicity and disease. Adapted from [9].

As already mentioned, *in vitro* assays for xenobiotic toxicity are recently carefully considered by key government agencies (e.g. EPA; NIEHS/NTP; FDA) due to the social movement to reduce the use of animals in research, and a desire to better assess human risks.

Most toxicologists believe that *in vitro* toxicity testing methods can be a useful, time and cost-effective supplement to toxicology studies in living animals. However, it is generally accepted that the available *in vitro* tests are not presently adequate to entirely replace animal toxicology tests.

For example, the hazardous properties of chemicals cannot be sufficiently determined using currently available *in vitro* testing methods, as noted in a report published by the European Centre for the Validation of Alternative methods (ECVAM). Until prediction of metabolism can be more reliably accomplished through computational toxicology and *in vitro* testing, some degree of highly targeted testing using whole animals may be needed to identify metabolites and to assist in developing pharmacokinetic models for the distribution of test compounds and their metabolites in humans [9].
Relying solely on vitro methods can underestimate the potentially hazardous properties of chemicals that could be harmful to humans and the environment.

***In vitro* models**	**Advantages**	**Disadvantages**
2-D cell culture model (conventional monolayer model)	Easy and convenient to maintain, increased viability	Loss of organ-specific cell-to cell interactions and differentiated functions
2-D co-culture model	Interactions between multiple cell types	Cell-cell competition, complicated and conflicting culture requirements
3-D cell culture model (hydrogels, multicellular spheroids, and multilayer cell culture)	Well-defined geometry, co-cultivation of multiple cell types, mimics the *in vivo* situation very closely, and 3-D scaffold for mechanical stability	Poor viability, diffusion and action of chemicals altered, multicellular resistance, and expensive
Tissue slice/Grafting model	3-D representation of cellular environment, preserve cell-to-cell & cell-to-matrix environment, realistic preclinical model, and	Viability is limited, morphological evaluation alters with the slice, difficult to reproduce, and limited availability for human models

	preserve the functional and morphological heterogeneity	
Micro-scale cell culture model (microfluidic cell culture system)	Mimics the *in vivo* situation very closely, controlled microenvironment, allow reproduction of biotransformation *in vitro*, short reaction times, portability, low cost, and small consumption of reagents and cells	Complex fluidic connection and flow control required, expensive detection and analysis system, and formation of air bubble

Tab.1: Commonly used *in vitro* models in toxicology: advantages and disadvantages. Adapted from [10].

The most commonly used *in vitro* model is represented by cells in culture. Normally, these cells are cells lines, then derived from tumors or immortalized and are therefore transformed. Another *in vitro* approach is to use primary cells that can be kept in culture only for a certain time. Both cell cultures can result in loss of differentiated properties, different metabolic components and modified functionality. The weakness of those *in vitro* tests result from the fact that the cells are isolated from their natural environment and are no longer integrated into an ordered tissue and organ topology.

Metabolic conversions of xenobiotics would be studied using subcellular fractions *in vitro* approach. These systems usually favor only the specific biotransformation step, depending on the type of isolation procedure, on the cofactors added, on the source of tissue, and on the expression level of the involved enzymes. However, the balance of metabolic activation and inactivation requires a highly ordered interplay of many enzymes and cofactors in most cases.

Also, it is difficult to study effects on integrated and at the same time diffusely organized systems like the neuro, immuno and endocrino systems.

Hence, to study effects on these organ systems *in vitro* is not an easy task [8].

4. ADVANCED *IN VITRO* MODELS AND BODY ON A CHIP MODEL

In this scenario, new tools and technology for *in vitro* toxicology testing are highly required by industries and governments as an alternative to animal testing but also as an improvement of available cell culture systems.

In 2004, the U.S. Environmental Protection Agency (EPA) and the U.S. National Institute of Environmental Health Sciences (NIEHS) asked the U.S. National Research Council (NRC) to conduct a review and a long-term strategic plan to update and advance toxicity testing. The NRC Committee on Toxicity Testing and Assessment of Environmental Agents produced two reports. The final report outlined four design criteria, which should guide the development of a new toxicity-testing paradigm:

1. achieving broad coverage of chemicals, chemical mixtures, outcomes, and life stages;
2. diminishing the cost and time required for toxicity testing;
3. developing a better scientific basis for assessing human health effects of environmental chemicals, including knowledge of modes of action;
4. minimizing the use of animals in toxicity testing [11] .

The new paradigm has to integrate with the widely used four-stage risk assessment framework originally proposed by the NRC in 1983 in the so-called Red Book: hazard identification, dose-response assessment, exposure assessment, and risk characterization.

The newest techniques, such as *in silico* models, -*omics* technologies and high-throughput screens, have been considered in this advanced *in vitro* toxicology.

Tool	Application
High-throughput screens	Efficiently identify critical toxicity pathway perturbations across a range of doses and molecular and cellular targets
Stem cell biology	Develop *in vitro* toxicity pathway assays using human cells produced from directed stem cell differentiation
Functional genomics	Identify the structure of cellular circuits involved in toxicity pathway responses to assist computational dose-response modeling
Bioinformatics	Interpret complex multivariable data from HTS and genomic assays in relation to target identification and effects of sustained perturbations on organs and tissues
Systems biology	Organize information from multiple cellular response pathways to understand integrated cellular and tissue responses
Computational systems biology	Describe dose-response relationships based on perturbations on cell circuitry underlying toxicity pathway responses giving rise to thresholds, dose-dependent transitions, and other dose-related biological behavior
Physiologically based pharmacokinetic models	Identify human exposure situations likely to provide tissue concentrations equivalent to *in vitro* activation of toxicity pathways
Structure-activity relationships	Predict toxicological responses and metabolic pathways based on the chemical properties of environmental agents and comparison to other active structures
Biomarkers	Establish biomarkers of biological change representing critical toxicity pathway perturbations
Molecular and genetic epidemiology	Incorporates molecular markers of exposure and biological change into population-based studies; integrates the knowledge of the human genome into epidemiological studies to understand genetic susceptibility and gene-environment interaction in disease causation

Tab. 2: New *in vitro* toxicity testing tools and their application in the risk assessment. Adapted from [11].

An approach to overcome *in vitro* test limits is to perform a more realistic model that mimics animal and human response accurately, increasing

control over cell–cell and soluble cues typical of *in vivo* cell environments. Cells sense most extracellular signals (including proteins, peptides and carbohydrates) via transmembrane receptors that activate complex biochemical cascades which regulate cell physiology. Moreover, cells are sensitive to the presence of neighboring cells of similar or different type and often make long-lasting mechanical and biochemical connections to them [12], [13].

The first step in this direction is to combine microfabrication of 3D extracellular matrix (ECM) structures and microfluidic networks that transport soluble factors such as nutrients and oxygen. In this way mechanical strain, through shear, in the physiological range is also created [14].

Recent advances in using microfabrication with cell culture technology resulted in the rise of a new research field often referred to as cells-on-chip technology, which has allowed researchers to have precise control over *in vitro* biological systems with microscale resolution [15].

Body on a chip models are physiologically more relevant than single or co-culture *in vitro* models, stimulating the multi-tissue interactions and crossing-talk given by fluid flow condition.

Those systems also achieve one of the aspects of new desired tools that is the high-throughput screening of several compounds in a cheaper and less time consuming manner.

Microfabrication techniques allow the creation of devices with structures of sizes relevant to biological systems such as cell sizes (on the order of 10 μm) and the sizes of human blood vessels with spacing between capillaries on the order of 100 to 200 μm. The result is a more physiological growth environment with relevant shear stress, liquid-to-cell ratios, and physiological fluid residence times in tissue compartments. Devices that are design with regard to the structure of the human body in scale are known as micro Cell Culture Analog device (μCCA).

Sung and Shuler, in 2009, demonstrated the importance of *in vitro* microfluidic mimics device in drug testing [16]; their system, contained liver cells (HepG2/C3A), colon cancer cells (HCT-116), and myeloblasts (Kasumi-1) was used to test Tegafur, an oral prodrug of the cancer drug 5-fluorouracil (5-FU), with better bioavailability than that of 5-FU.
The μCCA was able to reproduce the metabolism of Tegafur, in the liver cell compartment, in order to let 5-FU travelled through the microfluidic connections to the cancer cell compartment and caused its action as a decrease in cell viability.
Viravaidya and collaborators developed a μCCA with liver and lung cells to assess toxicity of chemical as naphthalene [17]. Naphthalene is known to cause oxidative stress with subsequent glutathione (GSH, anti-oxidative molecule) depletion assuming due to its metabolite naphthalene epoxide; in this study it was demonstrated that the observed toxicity on lung cells is caused by naphthoquinone rather than naphthalene epoxide being the half-life of naphthalene epoxide in aqueous medium 3.6 min, and the residence time in the other tissue/debubbler compartment is approximately 50 min, so the epoxide cannot reach the lung cells to cause the oxidative stress.

Other technologies can be useful in development of more physiological devices.
Mathematical models can be used to foresee complex processes, for example the absorption, distribution, metabolism, and elimination (ADME) of a new compound. ADME processes are important because determine the concentration-time profiles in the bloodstream and in the tissues of organs. Pharmacokinetic (PK) and pharmacodynamic (PD) models and more complex physiologically based pharmacokinetic (PBPK) models can predict the time-dependent pharmacological effects of a drug and increase the predictability of human response leading to higher success rates in clinical trials.

PBPK models and μCCAs can be used in combination to inform each other. In the development of multicompartment devices, representations of the human body such as PBPK models can be used to guide the device design with regard to the arrangement of chambers and fluidic channel connections. In this way, furthermore, the resulting systems are physical representations of PBPK models and the reactions are that described by the equations of the model. Because PBPK models rely on the input of already known mechanisms, conversely, data obtained with these systems may be used to test and refine mechanistic hypotheses and to amplify the model with new pathways and reactions to reach a more complete system. The μCCA and PBPK model can be used in an iterative manner to test modifications in the proposed mechanism and to validate each others.

Next step in advanced *in vitro* models is the implementation of body-on-a-chip devices with analytical and detection technology. The 'micro-total-analysis-system' (μTAS) framework seeks to create microsystems incorporating several steps of an assay into a single system [14]. Integrated microfluidic devices perform rapid and reproducible measurements on small sample volumes while high sensitivity of analytical methodologies is required due to the small physical dimensions of culture systems inherently contain small numbers of cells, leading to mass-limited quantities of analyte molecules. Optical and electrical techniques have found extensive application in these devices owing to their ready compatibility with microfluidic formats and relative ease of operation. Such systems can provide near-real-time analysis. Indicator testing compound such as autofluorescent substrate can be added to the device to evaluate change in the metabolite fluorescence or absorption in order to evaluate the ability of the cells to perform that metabolic reaction.

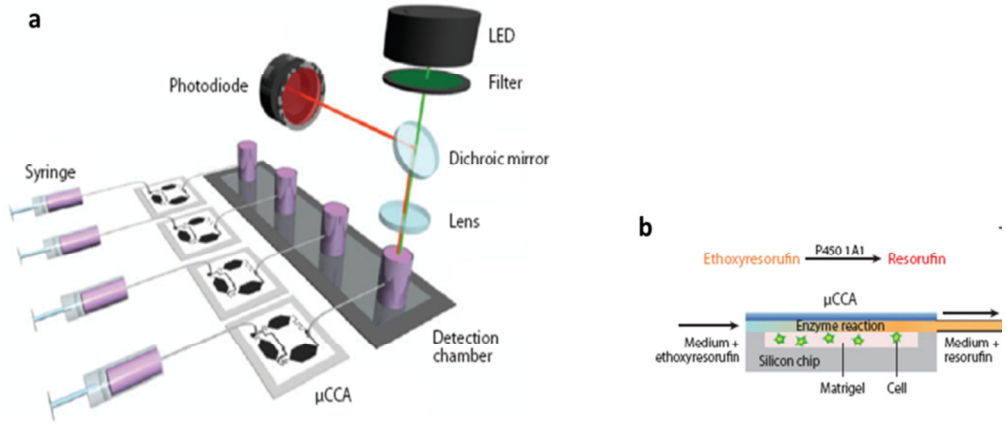

Fig. 3: Micro cell culture analog (µCCA) connected to an in situ fluorescence optical detection system (ISFODS). (*a*) The system consists of a syringe µCCA chips and the ISFODS. (*b*) Medium-containing substrate is perfused into a µCCA, above the liver cells, and the fluorescent product from P450 enzyme metabolism is detected at the detection chamber, where the detection of fluorescent signal is made. Adapted from [18].

The integration of ultraviolet-visible absorption spectroscopy with microfluidic cell culture chips has been used, for example, to study acetaminophen metabolism and cytotoxicity [19].

Many electrical measurement methods such as amperometry with enzymatic bioelectrodes and cellular impedance can be integrated into µCCA devices [20]. Electrical impedance measurements are a particularly attractive option for determining cell viability in microfluidic cell culture devices because they are real time, label free, and non-invasive [21-23].

Another advanced technique in cells culture is the use of scaffolds. More authentic cellular behaviour is facilitated by making a three-dimensional structure that can be a simple hydrogel encapsulation of cells or mixtures of cell types [24] or preformed scaffolds that may represent a high level of authenticity, particularly for autocrine-like compounds. These systems also increase the concentration of cell in the chamber helping the analysis of metabolites and secreted molecules. Although most work with µCCAs has

utilized two-dimensional cell cultures, it has been demonstrated that a 3D culture enhance the cells vitality and growth [25]. The mechano-physical features of the scaffolds can favor cells adhesion and survival and lead to biological signals released [26].

Finally as noticed by Esch et al. in their review about body on a chip devices more useful devices should developed and included barrier tissue analogs. Barrier tissues such as the epithelium of the gastrointestinal (GI) tract, the lung epithelium, the skin, and the blood-brain barrier can significantly reduce the bioavailability of drugs that are taken up orally, through inhalation, or through application to the skin, leading to reducted doses to the target organs.

A study of Mahler et al. improve the μCCA device with a co-culture of intestinal epithelial cells (CaCo-2 cell) and HT-29 goblet-like cells so that the epithelium was covered with mucous [27]. Proof of concept experiments showed that acetaminophen (one of the most widely used analgesic and antipyretic drugs) passes through the epithelial layer where is firstly metabolized and then is further metabolized by liver cells, resulting in liver cell toxicity in a dose-dependent manner. The presence of the GI-tract barrier reduced liver cell death because acetaminophen diffused slowly across the mucous-covered CaCo-2/HT-29 cell layer, and, in addition, intestinal cells also converted some of the drug into nontoxic metabolites.

A future direction in advanced *in vitro* testing is individualized health care [28].

Since the level of enzymes and other metabolites can differ from person to person, everyone responds differently to drugs. Small tissue sample could be taken from a patient (biopsy) and tested for the efficacy of a mixture of drugs or for a range of different biological tests.

New advanced *in vitro* technologies are less expensive and ethically less questionable than experimenting with animals, moreover they allow a larger experimental space to be explored. The microfluidic format and the presence of possibility to study multiple-cell type in combination afford the devices several advantages compared to others *in vitro* drug screening models. A big challenge is recreating authentic cell behavior on the microfluidic platform and developing sensors that can monitor the physiology of cells within three-dimensional tissue constructs. These devices can be used as a preliminary screening to determine whether to invest effort and resources in a particular drug testing or biochemical pathway.

Chapter 2

Nanotoxicology: an emerging issue

Nanoparticles (NPs) are generally defined as engineered structures possessing at least one dimension sized from 1 to 100 nm. The science which studies and manipulates those nano-objects is nanotechnology, which consists essentially in a set of techniques that allows creating and using materials and devices at a very small scale.

Although nanoparticles are generally considered an invention of modern science, they actually have a very long history. Probably the earliest use being in glazes for early dynasty Chinese porcelain. A Roman cup, called the Lycurgus cup, used nanosized gold cluster to create different colors depending on whether it was illuminated from front or the back, obviously the cause of this effect was not known to those who exploited it [29].

Even these days, pottery from the Middle Ages and Renaissance often retain a distinct gold or copper colored metallic glitter. The luster was caused by a metallic film applied to the transparent surface of a glazing. The luster originated within the film itself, which contained silver and copper NPs dispersed homogeneously in the glassy matrix of the ceramic glaze. These nanoparticles were created by the artisans by adding copper and silver salts and oxides together with vinegar, ochre and clay, on the surface of previously-glazed pottery [3].

The first description, in scientific terms, of the optical properties of nanometer-scale metals was provided by Faraday in his classic 1857 paper [30]. In 1908, Turner points out that: "It is well known that when thin leaves of gold or silver are mounted upon glass and heated to a temperature which is well below a red heat, a remarkable change of properties takes place,

whereby the continuity of the metallic film is destroyed. The result is that white light is now freely transmitted, reflection is correspondingly diminished, while the electrical resistivity is enormously increased" [31]. Nowadays, the ability to see nano-sized materials has opened up a world of possibilities in a variety of industries and scientific endeavors.

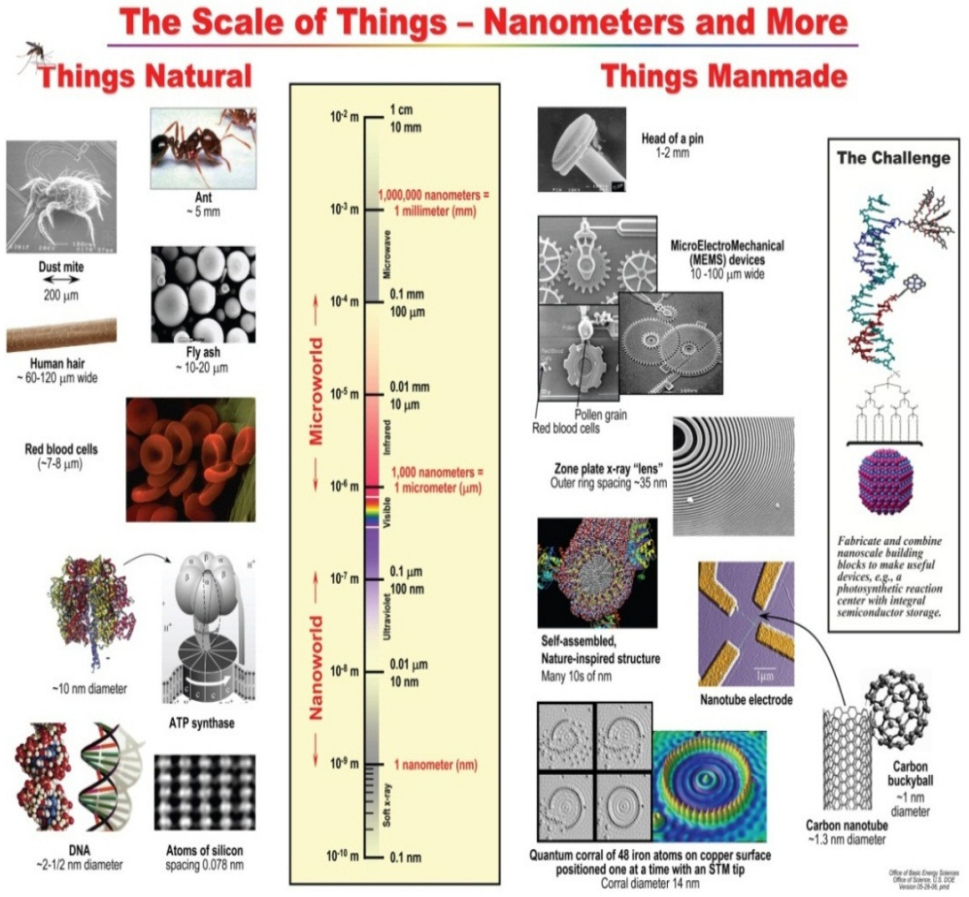

Fig. 4: Picture represents “The Scale of Things”, it provides a comparison of various objects to help understanding exactly how small a nanometer is. From objects that can be seen by human eye to objects about a nanometer or less in size, such as the ATP molecule used in humans to store energy from food. (Designed by the Office of Basic Energy Sciences (BES) for the U.S. Department of Energy using U.S.). Reproduced with permission from [32].

1. NANOPARTICLES: PROPERTIES AND APPLICATIONS

The large interest for NPs is due to the fact that the transition from microparticles to nanoparticles can lead to a number of changes in physical, chemical, electrical, optical, mechanical and magnetic properties. NPs are effectively a bridge between bulk materials and atomic or molecular structures. A bulk material should have constant physical properties regardless of its size, but at the nano-scale size-dependent properties are often observed. Thus, two of the major factors in this are the increase in the ratio of surface-area-to-volume, and size of the particle moving into the realm where quantum effects predominate. The increase in the surface-area-to-volume ratio, which is a gradual progression as the particle gets smaller, leads to an increasing dominance of the behavior of atoms on the surface of particle over that of those in the interior of the particle. For bulk materials larger than one micrometer, the percentage of atoms at the surface is insignificant in relation to the number of atoms in the bulk of the material. The interesting and sometimes unexpected properties of nanoparticles are therefore largely due to the large surface area of the material, which dominates the contributions made by the small bulk of the material.

High surface area is a critical factor in the performance of such technologies as fuel cells and batteries (see below). The large surface area of NPs also results in a lot of interactions between the intermixed materials in nanocomposites, leading to special properties such as increased strength and/or increased chemical/heat resistance [33]. The high surface area provides, also, a tremendous driving force for diffusion, especially at elevated temperatures. Sintering can take place at lower temperatures, over shorter time scales than for larger particles. Moreover, NPs have been found to impart some extra properties to various day to day products. For example the presence of titanium dioxide nanoparticles imparts what we call the self-cleaning effect, and the size being nano-range, the particles cannot

be observed [34]. In fact, the dimension below the critical wavelength of light renders them transparent, a property which makes them very useful for applications in packaging, cosmetics and coating (see below). Zinc oxide particles have been found to have superior UV blocking properties compared to its bulk substitute. This is one of the reasons why it is often used in the preparation of sunscreen lotions [35], and is completely photostable [36].

Clay nanoparticles when incorporated into polymer matrices increase reinforcement, leading to stronger plastics, verifiable by a higher glass transition temperature and other mechanical property tests. These nanoparticles are hard, and impart their properties to the polymer (plastic) [37]. Moreover, perfectly-formed silicon nanospheres, with diameters of between 40 and 100 nanometers, are not just harder than silicon but among the hardest materials known, failing between sapphire and diamond [38]. NPs are currently made out of a very wide variety of materials such as titanium, zinc, aluminum, iron oxide and silicate NPs. Those new materials are used, or being evaluated for use, with different applications in several fields. The list below introduces some of those fields of use:

- Electronic: to increase the capability of electronics devices, for example display screens, reducing their weight and power consumption; or increasing the density of memory chips and reducing the size of transistors used in integrated circuits [39].
- Energy: to improve the efficiency of energy generation or develop new methods to generate energy. Stronger and lower weight blades are made possible by the use of nanotube-filled epoxy, increasing the amount of electricity generated by each windmill [40]. Companies (Bloo Solar, Solamer Energy, Nanosolar, etc.) have developed nanotech solar cells that can be manufactured at significantly lower cost than conventional solar cells.
- Space: Mavroidis and co-workers from Northeastern University in collaboration with NASA Institute of Advanced Concepts Design

developed two macro-scale devices with important space application that will be using bio-nanocomponent assemblies to build bio-nano robots in spacesuits [41], [42].

- Environment: improve the environment, cleaning up existing pollution and improving manufacturing methods to reduce the generation of new pollution. Researchers at NASA Kennedy Space Center have shown that iron NPs can be effective in cleaning up organic solvents that are polluting groundwater [43], [44].
- Consumer Products: nano has already found its way into lots of products of everyday use, from clothing to tennis racquets. Skin care products use NPs to deliver vitamins deeper into the skin; sunscreens also use NPs to block UV rays without leaving white residue on the skin. Lithium ion batteries use NP based electrodes powering plug in electric cars. Fishing rods use silica NPs to fill spaces between carbon fibers, strengthening the rod without increasing the weight. A nanoporous material called ThermaBlok® Aerogel Insulation is an excellent insulator, needing about one third the thickness compare to conventional insulation [45]. Nanoparticles have also been attached to textile fibers in order to create smart and functional clothing [46].
- Chemical Sensors: nanotechnology can enable sensors to detect very small amounts of chemical vapors. Various types of detecting elements, such as carbon nanotubes, zinc oxide nanowires or palladium nanoparticles can be used in nanotechnology-based sensors. These detecting elements change their electrical characteristics, such as resistance or capacitance, when they absorb a gas molecule [47].
- Medicine: the main application of nanotechnology in medicine currently being developed involves employing NPs for drugs delivery [48], [49], [50]. Particles are engineered so that they are attracted to diseased cells, allowing direct treatment of those cells (e.g. cancer

cells [51], [52]). This technique reduces damage to healthy cells in the body and allows for earlier detection of disease. In therapy fullerene NPs (also known as buckyballs) may be used to trap free radicals generated during an allergic reaction and block the inflammation that results from an allergic reaction [53]. Z-Medica is producing a medical gauze that uses aluminosilicate NPs that can quickly reduce bleeding in trauma patients by absorbing water, causing blood in a wound to clot quickly [54], [55]. Nanotechnology is also used in diagnostic and imaging techniques [56], [57]: iron oxide NPs can be coated with a peptide that binds to a cancer tumor in order to enhance, once the NPs are attached to the tumor, the images from the Magnetic Resonance Imagining scan thanks to the magnetic property of the iron oxide [58], [59]. NPs can attach to proteins or other molecules, allowing detection of disease indicators in a lab sample at a very early stage. Finally, NPs are involved in anti-microbial techniques as nanocrystalline silver [60] or nanocapsules containing antibiotics [59].

- Food: Companies are developing nanomaterials that will make a difference not only in the taste of food, but also in food safety, and the health benefits that food delivers. The Sharper Image developed FresherLonger™ Miracle Food Storage Containers which keep foods fresher longer than conventional containers thanks to the antimicrobial silver nanoparticles in the polypropylene material that reduce the growth of microorganisms. Researchers are using silicate nanoparticles to provide a barrier to gasses like oxygen, or moisture in a plastic film used for packaging reducing the possibly of food spoiling or drying out [61]. Zinc oxide nanoparticles can be incorporated into plastic packaging to block UV rays and provide anti-bacterial protection, while improving the strength and stability of the plastic film [62]. Nanosensors are being developed detect bacteria and other contaminates, such as salmonella, at a packaging plant.

This point-of-packaging testing has the potential to dramatically reduce the chance of contaminated food reaching grocery store shelves.

All the applications and examples given are only a small part of the products and projects on emerging nanotechnologies; a longer list is available on the web site www.nanotechproject.org.

2. NANOTOXICOLOGY

Nanotechnology offers society the promise of major benefits, and the use of nanotech in consumer and industrial sectors is expected to increase significantly in the future. In parallel however, because NPs have unique properties different from conventional materials, concerns about safety have been raised. The same properties of nanostructured materials that make them so attractive for applications could potentially lead to unforeseen health or environmental hazards [63].

In fact, the high surface to volume ratio can make the particles very reactive or catalytic [64]. Moreover the ability of NPs to pass through cell membranes in organisms, and their interactions with biological systems make them of high potential hazard [65].

In Europe and in the USA, governments, non-governmental organizations, and others have expressed concern that, while the field of nanotechnology and the number of consumer products incorporating nanomaterials increase dramatically, in many cases, the safety of these materials has not been demonstrated and there are still a large number of unanswered questions. For example, little is known about the relationship between nanoparticles (NPs) physicochemical characteristics and their ability to cross biological barriers and to enter the general circulation, their fate within the body (toxico-kinetics), their subsequent toxic impact, or the ability of our bodies to defend against such toxic impact.

Fears over the possible dangers of some nanotechnologies may be exaggerated, but they are not necessarily unfounded. Recent studies examining the toxicity of engineered nanomaterials in cell cultures and animals have shown that size, surface area, surface chemistry, solubility and possibly shape all play a role in determining the potential for engineered nanomaterials to cause harm [66].

First increased surface area enhances contact with their surrounding exposing catalytic or other active sites on the particle surface [67], in some cases inducing the formation of reactive oxygen species (ROS) [68].

Second, due to their small size, NPs are retained in many cells and organs to a larger extent at the intracellular more than at the extracellular level due to solubilization or degradation that takes place inside cells. Toxic effects have also been demonstrated to depend on the uptake mechanism (see below) [69], presumably due to differences in fate, for example, being stored in intracellular vesicles or secreted.

Another propriety to take in account is the shape of NPs that can play a crucial role in determining responses. Geometric effects have been highlighted by the example of high toxic needle-shaped carbon nanotubes, which impale entire cells [70], [71].

Physico-chemical NP properties of relevance for toxicology	
Size (airborne, hydrodynamic) Size distribution Shape Agglomeration/aggregation Surface properties Area (porosity) Charge Reactivity Chemistry (coating, contaminants)	Properties can change: • With method of production, preparation process, storage • When introduced into physiological, media, organism

Defects Solubility (lipid, aqueous, *in vivo*) Cristallinity	

Tab. 3: List of some physico-chemical properties of NPs that impact on their biological/ toxicological activity. Adapted from [72].

Rivera Gil and collaborators provided the main points that are important for nanotoxicological screening approaches [73], pre-testing criteria that should be kept in mind include:

(1) the need for defined and well-characterized NPs as model systems
(2) knowledge of NP properties and potential for exposure during all stages of their life cycle
(3) the need for knowledge about biokinetics
(4) the need for validated *in vitro* models that are predictive of outcomes following *in vivo* exposures
(5) the need for evidence that *in vitro* outcomes are NP-specific *via* appropriate benchmarking (*i.e.*, does a solute produce the same response? Do larger particles of the same composition produce the same response?)
(6) the need for ranking new NPs against well-validated benchmark NPs.
Moreover the concepts of dosimetry, dose metrics, exposure assessment, hazard identification, and risk characterization need still to be assessed.
The challenge for both health and environmental protection is to ensure that as nanomaterials are developed and use, any unintended consequences of exposures to humans are prevented or minimised. In addition, knowledge concerning how best to apply nanotechnology to detect, monitor, prevent and control is needed.

3. NANOPARTICLES EXPOSURE AND BIOKINETIC

Numerous applications of nanomaterials lead to many possible routes through which synthetic and free nanoparticles can get into the human body.

With the expected increased intentional (*e.g.*, in the field of medical diagnostics) and unintentional (*e.g.*, in occupational settings and chemical waste streams) exposures to NPs nanotoxicology has now become a critical element in safety assessments of nanomaterials. In the beginning interest in the potential toxicity of very small particles starts from studies of workers exposed to metal fumes [74] and inhalation studies with ultrafine particles [75]. As matter of fact the portal of entry for nano-objects firstly and mostly studied is the pulmonary tract.

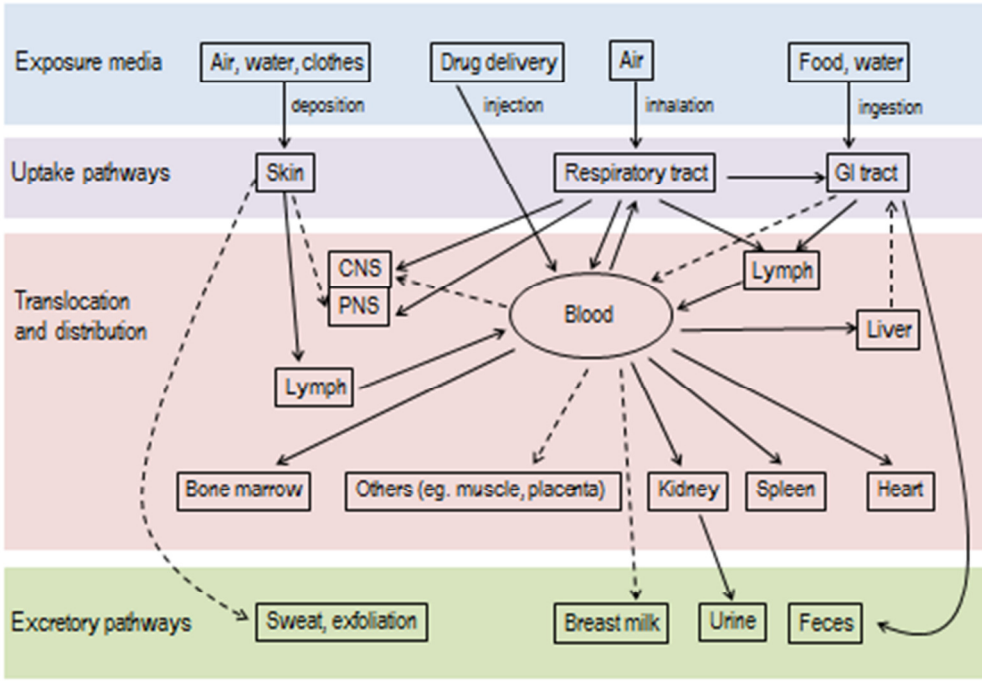

Fig. 5: A schematic overview of biokinetics of NPs. The arrows connect the routes, in dashed arrows the potential routes. Adapted from [66].

Inhaled particles smaller than 2.5 µm have access to the alveolar structures of the deep lung and may induce inflammation. Most of the particles that deposit into the lung are removed by mucociliary transport or, at alveoli level, through macrophage disposal. It was shown that high doses of nanoscale particles are, also capable of crossing the thin air–blood barrier to transmigrate into the blood [76].

Another inhaled route going directly to the brain is the uptake via olfactory nerve, here the particles can reach the brain, even if in a really small amount, and by pass the blood-brain barrier [77].

The healthy skin instead represents an effective barrier against many NPs. The uptake of nanoparticles, especially of the non-lipophilic type involved in cosmetics and in sunscreen applications, is hampered by the anatomic structure of the human skin. The EU FP6 project NANODERM (NanoDerm, 2008) results showed that TiO_2 deposited only in the corneocyte layers of the stratum corneum or in the hair follicles but is not detected in the deeper regions of the skin; although it was found by another group that very small particles (<10 nm) are capable of penetrating through to the epidermis or dermis [78]. Particle surface coatings or functionalization which are often used to prevent agglomeration, may strongly influence the penetration [79]. The corneal layer of stressed or diseased skin is more permeable to all kinds of particles and must be regarded independently [80].

Since the use of nano-materials is continuously highlighted in food and packaging, a route of increasing importance is the gastrointestinal tract. The nutrients, as well as everything orally taken, are absorbed by the small and large intestines by the intestinal epithelium and can be distributed in the body via the bloodstream. 98% of the nanoparticles administered orally to the test animals were excreted in the feces, whereas the rest was eliminated via urine, indicating some uptake into the blood circulation. In the same study, but using NPs intravenously administered approximately 80% of the material was found to have accumulated in the liver after one week

[66]. As matter of fact, injected administration route has to be considered since nanomaterials are really promising in diagnostic and therapeutic medical applications [81].

Going to the cellular level, several uptake mechanisms for NPs have been proposed. In contrast with large particles (> 500 nm) which will be exclusively taken up by phagocytosis, NPs may use other different translocation routes into the cells. NPs transport can use receptor-binding mechanisms [82], [83], diffusion through the plasma membranes, as adhesive interactions [84], [85] and any vesicle transport pathway for particles with diameters below 100 nm [86], [87].

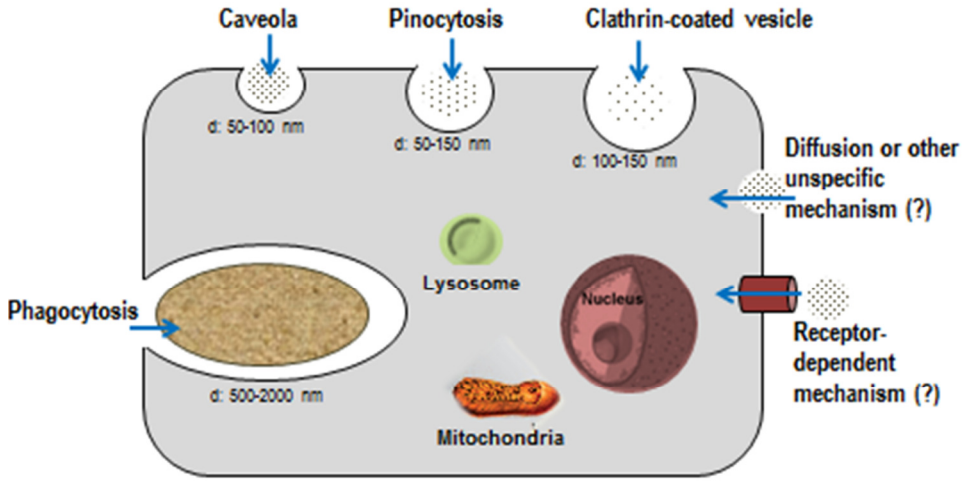

Fig. 6: Proposed uptake mechanisms for nanoparticles with different size. Adapted from [88].

The subsequent effects observed are influenced by the different uptake mechanisms: in the case of uptake by vesicular processes, particles are sheathed by membranes (for example, caveolae). Free transport through the membrane, however, would be assumed to be more critical, as it allows particles to achieve direct contact with the plasma proteins and with other molecules of the cell. The uptake of nano-particles may well have fatal consequences for the cell if the material consists of, for example, an incompatible metal and/or is removed owing to physiological conditions.

Moreover, NPs that do not dissolve but remain stable for a long time (biopersistent) or accumulate in cells may become “active” in another way while obeying the surface principle: as there are considerably more atoms available on the particle surfaces, they can interact with the environment much more efficiently. Finally, for biological systems coming into contact with such objects, the materials constituting the nanofractions are also relevant even with uniform shapes and sizes [89], [90].

Size, shape, surface, and composition can significantly cause biological effects and must be considered separately for each material to evaluate its potential toxicity.

4. NANOPARTICLES TESTING AND RISK ASSESSMENT

New properties and behavior of NPs with respect to bulk materials leads to the need for a systematic risk research as information about safety and potential hazards is required. Toxicology tests and the resulting database would provide information for material safety data sheets for NPs as well as a basis for potential NP risk assessments and risk management.

Toxicity assays will identify the potential hazard by establishing dose-response relationships or stress and inflammatory responses. However, because a risk of adverse effects associated with NPs is a function of hazard and exposure, the generally accepted approach is to incorporate both components into a risk assessment paradigm, consisting of Hazard Identification, Hazard Characterization, Exposure Assessment and Risk Characterization [91] so that appropriate risk management decisions can be made.

Whereas first investigations concerning the toxicity of NPs were based on *in vivo* experiments (i.e., inhalation studies, etc.), due to the huge amount of a large variety of different NPs it is desirable to develop and validate simple non *in vivo* assays in order to reduce and avoid extensive testing using laboratory animals. *In vitro* studies enable the identification of conceptual

models for interactions of NPs with cells [73]. An important issue to take in account within *in vitro* models is the interference of the NPs with well-established toxicity assays in order to avoid confounding or even conflicting data. Each test should be characterized in advance considering the presence of NPs, moreover it is recommended to perform two different tests for each biological end point to exclude cross-reactions [88].

Cytotoxicity assay	Detection principle	NP interference	Altered readout	Particle studied
Cell viability				
MTT	Colorimetric detection of mitochondrial activity	Adsorption of substrate	Reduced indication of cell viability	Carbon nanoparticles
LDH	Colorimetric detection of LDH release	Inhibition of LDH enzyme	Reduced indication of necrosis	Trace metal-containing nanoparticles
Annexin V	Fluorimetric detection of Phosphatidylserine exposure (apoptosis marker)	Ca^{2+} depletion	Reduced indication of apoptosis	Chitosan nanoparticles
Propidium Iodide	Staining of DNA (necrosis marker)	Dye adsorption	Reduced indication of necrosis	Carbon nanoparticles
Neutral red	Colorimetric detection of intact lysosomes	Dye adsorption	Reduced indication of cell viability	Carbon nanoparticles
Caspase	Fluorimetric detection of Caspase-3 activity (apoptosis marker)	Inhibition of Caspase-3 enzyme	Reduced indication of apoptosis	Trace metal-containing nanoparticles, especially Zn^{2+}

Stress response				
DFC	Fluorimetric detection of ROS production	Fluorescence quenching	Reduced indication of oxidative stress	Carbon nanoparticles
Inflammatory response				
ELISA	Colorimetric detection of cytokine secretion	Dye adsorption	Reduced indication of cytokine concentration	Metal oxide nanoparticles

Tab. 4: Nanoparticles interference with cytotoxicity assay. Adapted from [92].

In vitro high-dose toxicology and mechanistic studies should be viewed as proof-of-principle studies, though, that ultimately require validation *in vivo*. A major issue that needs to be carefully considered is the relevancy of the doses applied *in vitro* for predicting *in vivo* outcomes. At very high doses assays can certainly identify a NP as hazardous but how realistic is the study for *in vivo* exposure conditions?

Therefore, it is desirable to develop and validate simple non *in vivo* assays for the purpose of predicting *in vivo* responses.

In parallel, efforts should be made to obtain data on exposure levels occurring for workers at NP manufacturing sites despite best occupational hygiene conditions, as well as for anticipated consumer exposures to nano enabled products [72].

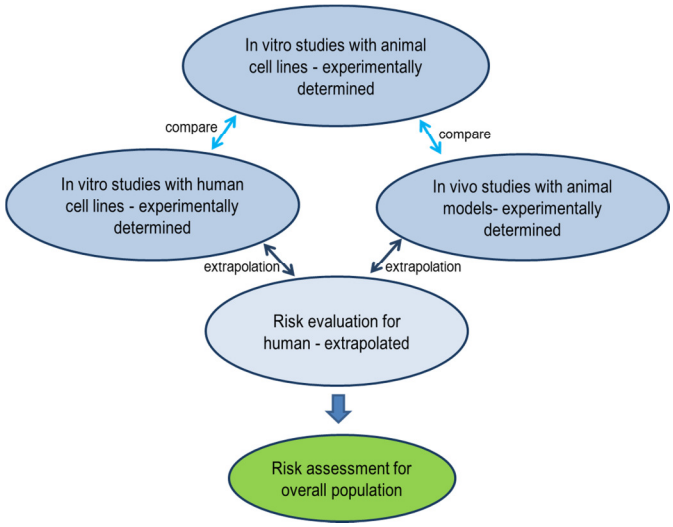

Fig. 7: The evaluation process of toxicity of NPs. In the diagram are shown the *in vitro-in vivo* relationship and its extrapolation to humans. Adapted from [88].

Chapter 3

Bioreactor design and improvement for investigating absorption, biotransformation & biodistribution

1. BIOREACTOR: MCmB

The request of more physiological tests that do not involve animals was underlined in chapter 1. Given the concerns regarding animal testing many groups have developed systems that are more representative of human physiology (as described in paragraph 4, chapter 1).

Our group at the Interdepartmental Research Center "E.Piaggio", developed a "system on a plate" modular MultiCompartmental Bioreactor (MCmB) array [93] commercialized as Quasi-Vivo® (by Kirkstall Ltd). Its main advantage is its size: with no need to change multiwell plate/petri dish culture protocols. The microscale dimensions that make body-on-a-chip devices (described in paragraph 4, chapter 1) so attractive lead also to the need of translating experimental methods to be feasible in the micro-range. The MCmB offers the possibility to use the same protocols as multiwell plates improving them with mechanical, flow and biochemical stimuli, or cross-talk by adding other cell types so as to recreate the physiological environment. It was designed as an easy-to-assemble modular lego-type device according to finite element methods and allometric scaling in order to

have low shear stress, high nutrient turnover, and physiologically relevant cell numbers and fluid residence times. Many cues should be controlled *in vitro* using engineering and design as shown in figure 8.

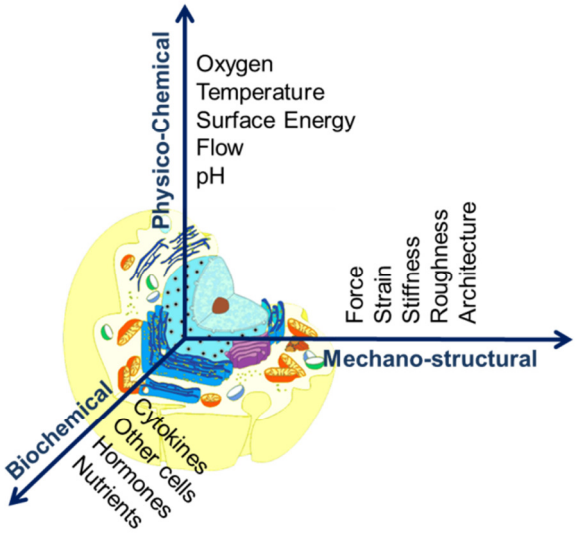

Fig. 8: A representation of the more important biochemical, physio-chemical and mechano-structural cues presented in the cellular microenvironment and the parameters that can be controlled. Adapted from [94].

The level of cross-talk is likely to depend strongly on dynamic stimuli such as flow and concentration gradients. The flow rate and volume will determine the residence and passage times of molecules and oxygen, as well as the shear stress on the cells. The goal of dynamic culture device design is the balance between high oxygen mass transfer and low wall shear stress to cells. Shear stress is given by a fluid moving along a solid boundary, this tangential flow constantly stimulates cells [95] by a low velocity convective motion but in contrast most type of cells cannot support high levels of shear which compromises their function.

The MCmB is fabricated in PDMS (polydimethylsiloxane), a biocompatible elastomer. The modular chamber is similar in size to that of a 24 well plate with a volume of 2 mL. The choice to design a modular device is justified by the possibility to allow any tissue or organ model to be simulated and performed simply by connecting the chambers in a desired configuration. The bioreactor unit is composed of two self-sealing (male-female joint) parts, of which top piece has smart design that allows bubbles (one of the biggest problem in microfluidic device) to be conveyed to the outlet tube. Varying the flow rate it is possible to set oxygen and nutrient residence time and low shear stress of the order of 10^{-5} Pa at the bottom of the chamber where cells are housed.

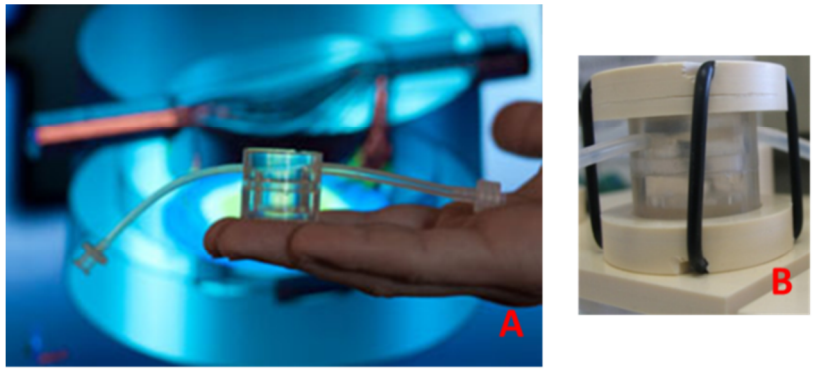

Fig. 9: Pictures of MCmB showing the size and the shape (A). In the right, bioreactor is shown within his closure system (B)

MCmB is well characterized in Mazzei et al. [93] and has been already tested using different high throughput multi compartmental bioreactor experiments [94-101].

Hepatocytes were firstly used to test the MCmB because they are the difficult cells to culture for their rapid loss of phenotypic expression in-vitro and because of their sensitivity to oxygen concentration, with high metabolic demands.

The high importance of flow rate has been shown, with a decrease in viability below 180 µL/min, due to lower oxygen concentration, and above 500 µL/min as result of too high shear stress. Albumin production, analyzed as marker of function, confirmed the vitality of cells as the albumin concentration under flow condition was higher with respect to controls till 500 µL/min [93].

In Guzzardi et al. a study on metabolic regulation in dynamic culture conditions in the MCmB was performed and compared with static models. In this work cross talk between hepatocytes and adipocytes was explored. Significant differences in metabolic and functional profiles between static and dynamic settings, and in the mono- versus the connected cultures were found [96].

In Vinci et al. it was shown that the combination of 3-D scaffolds and dynamic flow conditions enhances hepatocyte culture with an increase in cell density compared with monolayer controls and a three-fold increase of metabolic function in dynamic culture compared with static monolayer cultures [97].

In a second work, it was demonstrated that the presence of flow significantly modifies cellular metabolism of hepatocytes, adipocytes and endothelial cells [98]. Hepatocytes, endothelial cells and adipocytes were connected together each in a MCmB chamber to investigate metabolic cross-talk between them in regulating glucose and lipid metabolism [99].

Another work from the same author used the MCmB for primary human hepatocyte culture, showing that medium flow stimulates the expression and activity of detoxification genes [95]. Those results were confirmed by Vozzi et al. [100] who detected diclofenac (arylacetic non-steroidal anti-inflammatory drug -NSAID-) toxicity in the MCmB system at concentrations significantly lower than conventional hepatocyte cultures, similar to what has been observed in-vivo.

2. ALLOMETRY

A modular device allows the possibility of designing experiments according different models. In our work we choose to develop a system according to allometric rules.

Allometry is the science of scaling and deals with changes in body size and relationships amongst different parameters and processes in all organisms as a function of body mass M. The basic allometric equation can be used to correlate physiological variables between organisms of different sizes.

$$Y = a \bullet M^b$$

Y is the physiological parameter (for example time, length, metabolism) and *M* is the mass of the organism, *a* is a proportionality factor and b is the allometric exponent [94].

In simpler words, allometry is used to calculate the biological dimensions and parameters of *in vitro* systems to ensure that the most important features (cell numbers, cell ratios, flow rates) with respect to those of the human body.

This scaling model ensures that the same relationships between cells and organs in the human body are going to be maintained even in the bioreactor environment. Varying the number of bioreactors it is possible to vary cell surface, cell number, cell volume relationships to get closer to the physiological body relationship.

The simplest scaling model considers the cell ratios. It was estimated that ratio between endothelial weight and hepatic tissue weight in the abdominal region is 1:10 [101], so in order to reproduce this relationship 10 fold more hepatocytes with respect with HUVECs should be used. Translated to the MCmB this means one bioreactor each cell type, since the HUVECs have a surface area almost 10 fold more respect with hepatocytes so in the same confluent surface there will be 10 fold less cells.

Sbrana and Ahluwalia [94] studied allometric scaling within the MCmB considering different models such as biotransformation, gas exchange, skin and intestinal adsorption, glucose metabolism, excretion and nutrient transport using exchange surface areas and metabolism rather than cell numbers. Their results are summarized in the table 5.

MCmB physiological model	Cells	Modules (chambers)	Relationship
Biotransformation	Hepatocytes	1 liver	
Gas Exchange and Biotransformation	Hepatocytes, Lung epithelial cells	4 lung epithelia (confluent layer), 1 liver	Lung mass, b=1 (800 g) Lung area, b=2/3 (80 m^2)
Absorption and Biotransformation	Hepatocytes, Skin epithelia	12 liver, 1 skin epithelia (confluent layer)	Skin mass, b=0.87, (4-8 kg) Skin area, b=2/3 (1.8 m^2)
Nutrient absorption and Biotransformation	Hepatocytes, Intestinal epithelial cells	1 liver, 9 intestinal epithelia (confluent layer)	Intestinal bed, b=2/3 (200 m^2)
Biotransformation and Nutrient transport	Hepatocytes, Endothelial cells	4 liver, 1 endothelial cell (confluent layer)	Capillary bed, b=11/12 Total capillary bed area=500 m^2
Biotransformation, Nutrient transport and Nutrient absorption	Hepatocytes, Endothelial cells, Intestinal epithelial cells	4 liver, 1 endothelial cell, 32 intestinal epithelia	

Tab. 5: An example of allometric-based MCmB configurations for some physiological models, considering surface area and metabolic scaling. Adapted from [94].

The relationship between endothelial cells and hepatocytes was tested experimentally [101] as will be described in chapter 4.

3. INLIVETOX BIOREACTOR SYSTEM

The MCmB was the starting point to develop a dedicated device for the InLiveTox project. The aim of the device was to simulate the processes of intestinal absorption, endothelial biodistribution and hepatic biotransformation using 3 tissues. The final system, ILT, therefore consisted of 2 MCmB chambers with HUVECs and hepatocytes respectively and also included a specially designed chamber with a semi-permeable membrane (figures 10 and 11).

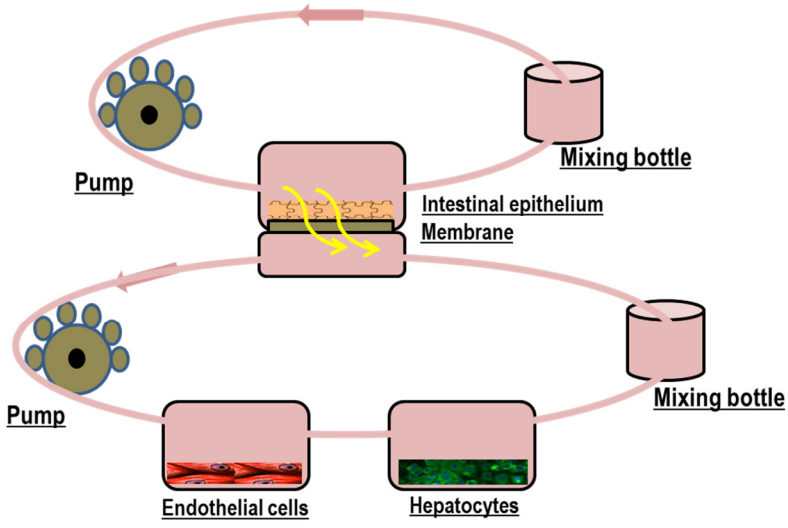

Fig. 10: ILT system diagram showing the two circuit and the cell types involved

The first circuit represents the gastrointestinal tract, only intestinal epithelial cells are housed in this circuit; a membrane with intestinal cells on it separates the upper from the lower circuit which is composed of the lower part of intestinal bioreactor connected to two bioreactors housing endothelial and hepatocyte each.

The intestinal bioreactor was designed in a two step way in order to have a first version (ILT 1) to test and a second improved version (ILT 2) which would solve all any problems with the first design version. Only ILT2 version was used for the experiments described in this thesis. Target cell bioreactors are two unmodified MCmB modules (named in the project and this thesis ILT 0).

3.1. ILT 2 intestinal bioreactor

The ILT 2 intestinal bioreactor consists of a microfabricated membrane, a membrane holder and a silicon chamber designed on the basis of ILT 0 bioreactor. Special ILT 2 closures were fabricated in order to allow the insert of electrodes that take contact with the electrical surface of the membrane. This electrical contact is needed for the continuous measurement of the TEER (Trans-epithelial electrical resistance) which gives, constantly, the value of the integrity of the epithelial layer. ILT 2 bioreactor is shown in fig. 11.

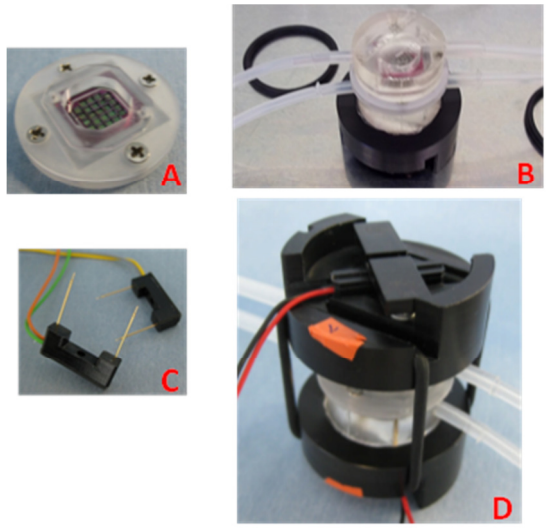

Fig. 11: ILT 2 bioreactor: a membrane into its holder (A), holder into the chamber (B), the electrode sticks (C) and the complete intestinal bioreactor with closure and electrodes inserted (D).

Two bubble traps were added before each ILT2 circuit (upper and lower) to avoid bubbles that can lead to inconstant measurement.

3.2. ILT complete system

The complete ILT system consists of 1 ILT 2 intestinal bioreactor (with a membrane in the holder) and 2 ILT 0s connected after the lower part of ILT 2. Moreover 2 bubble traps were added before each ILT 2 inlet tube to avoid bubble formation that interferes with the flow measurement.

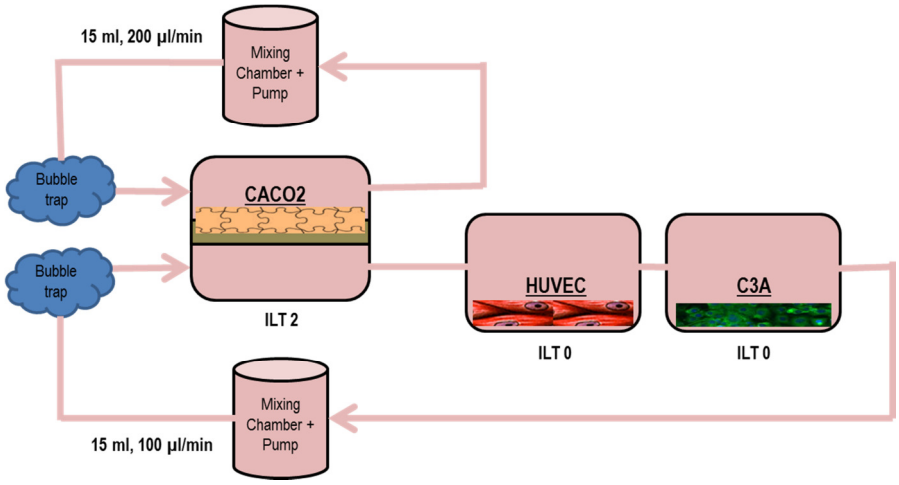

Fig. 12: Scheme of complete three tissue ILT system

The final system looks as in figure 13.

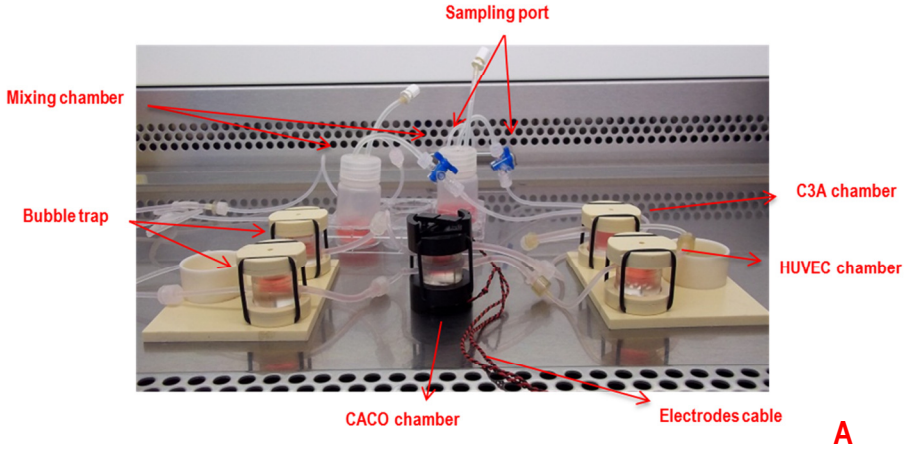

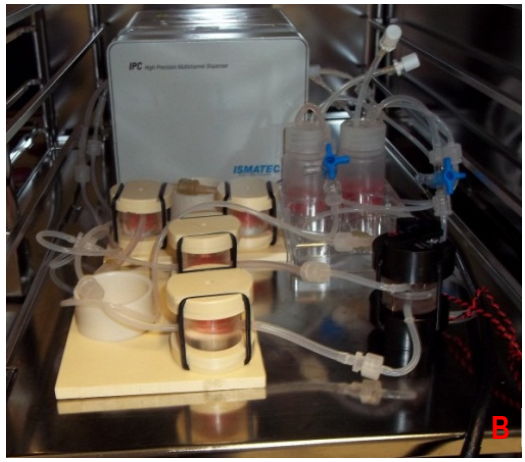

Fig. 13: The final ILT system: complete assembled system (A) and in the incubator connected to the pump (B).

Section II

Experimental design, materials and methods

Chapter 4

Experimental design

The main part of this thesis was carried out within the European Union FP7 InLiveTox project. Its focus was on the setup of the ILT system both from the technical and biological testing side. It also involved the study of the toxicity of some nanoparticles of industrial and environmental interest. NP toxicity was assessed on HUVEC in static conditions, while both HUVEC and C3A were tested in dynamic conditions using an optimized allometric configuration. Finally, after the "healthy" baseline was established, the complete three tissue ILT system was tested with two types of NP and positive control, to assess the system's performance.

In detail, the experimental plan was divided into 6 steps to achieve the objectives outlined in the abstract.

1. **ESTABLISHMENT OF NPs TESTING ON HUVEC STATIC CULTURE**

Firstly NP toxicity was evaluated in static conditions to establish a dose-response curve for each particle using standard *in vitro* methods. Moreover we can compare the results to those observed in ILT system.

HUVEC (as well all the other cell types) were tested with each nanoparticle (Polystyrene-FITC 50nm, Polystyrene-FITC 200nm, Ag, TiO2, Au 15nm and Au 80 nm) in order to establish lethal and sub-lethal effects within a range of concentrations.

It was decided to perform different assays, some of them evaluating the same function at different levels or with two different methods. The aim was to reduce mismatching and false positive/negative outputs due to NP interference.

All the assays performed are listed in the table below (Tab. 6):

FUCTION	ASSAY	OTHER ASSAY
Viability	Metabolic activity (Alamar Blue)	Membrane integrity (LDH assay)
Oxidative stress	GSH assay	
Apoptosis	Fas Ligand Bead Assay	
Inflammation	Cytokine Bead Assay	
vWF marker	mRNA expression	Immunostaining

Tab. 6: Assays chosen for NP toxicity evaluation

Each assay was checked for the NP interference in absence of cells and where necessary the value was subtracted from the sample data.

2. IDENTIFICATION OF COMMON DYNAMIC CULTURE CONDITIONS

To perform a dynamic multiple cell type culture, all cell types need to be connected to each other by a flow of medium. Standard culture medium for the 3 cell types are 3 different ones, so a common medium was required and testing of different media was performed.

HUVEC, C3A and CaCo-2 cells were tested in different media and the best one was chosen as a common medium for the ILT system (named ILT medium). Moreover, both HUVEC and C3A were separately tested in ILT medium at different flow rates in order to establish a range of flow feasible for the cells in the lower circuit. The testing concerned viability evaluation as well as some marker analysis.

All the technical parameters such as volume, flow rate, position of the pump with respect to the bioreactors as well as protocols for seeding cells onto coverslips and their handling were established.

3. ALLOMETRIC SCALING

A remarkable aspect of the system is the modular design so that each model can be assessed independently and then together. Allometric scaling enables a physiologically relevant model to be property designed. Two different scaling models were tested; one was studied considering the cell number ratio between cells, so proportional scaling, and the other based on metabolic rates. According to table 5 in chapter 3, the nutrient absorption-nutrient transport-biotransformation model, should have 32 intestinal epithelia, 1 endothelial and 4 liver bioreactors. However, because of the limit in membrane availability, 32 intestinal epithelia bioreactors could not be employed. Therefore we used a simpler model with only 1 intestinal bioreactor with increased flow circulation to increase passage through the membrane.

The allometric scaling models were then used for studying the relationship between HUVEC and C3A in the body. It was decided to experimentally study the simplest scaling model that considers the cell ratios (named cell number scaling model or CNSM), already mentioned in chapter 3 paragraph 2, and the model of biotransformation and nutrient transport described in table 5, chapter 3 (named surface and metabolic scaling model or SMSM).

Briefly a system with 1 HUVEC and 1 C3A bioreactors represents the CNS model (ratio between endothelial weight and hepatic tissue weight in the abdominal region 1:10) while 1 HUVEC connected to 4 C3A represents the SMS model (see tab. 5, chapter 3). Both the models were tested for viability and markers of functionality; moreover the cross-talk between the two tissues was studied and discussed. The best allometric scaling, leading to more physiological result, was chosen as a "lower circuit" for the ILT system.

4. NP DYNAMIC TESTING WITH SINGLE TISSUE CONFIGURATION

Having set up all the parameters for the dynamic system and established the dose-response curve in static conditions, it is possible to start checking whether the toxicity of those particle changes under flow conditions. The most toxic nanoparticle, Ag, was chosen for this test. HUVEC and C3A were firstly checked respectively for negative and positive baselines (healthy and dead cells) in the dynamic set up. Then some concentrations of Ag NP (a range from 5 µg/mL to 100 µg/mL) were analyzed.

Those results enabled the assessment of NP toxicity under flow conditions in the absence of cell cross-talk.

5. EVALUATION OF ILT SYSTEM BASELINE

In this step a baseline for functional markers and viability of the 3 cell types in the connected abdomen-mimic system, the ILT complete system, was established. All the assays were checked for sensitivity of measuring markers in ILT volumes and baseline values were defined. Moreover, a "dead cell" baseline using TRITON X-100 (non-ionic surfactant able to permeabilize and destroy cell membranes) in order to have even the high toxic marker values was also performed.

6. NPs TESTING IN ILT SYSTEM

In the final part of the thesis the complete system was tested with nanoparticles. Polystyrene-FITC NP was firstly chosen to measure the NP passage across the intact epithelial barrier. Then again, the most toxic NP, Ag, was assayed in order to have detectable end-points. The results were compared with the other *in vitro* testing models to determine the physiological relevance of cell response in the ILT system.

Chapter 5

Materials and methods

1. CELL CULTURE

Eagle's Minimum Essential Medium (EMEM), Dulbecco Modified Eagle's Medium High Glucose (DMEM-HG), Penicillin/Streptomycin/Amphotericin B, L-Glutamine was purchased from Lonza Bioscience (Basel, Switzerland). Fetal bovine serum (FBS) was purchased from PAA (Pasching, Austria); all other reagents were purchased from Sigma-Aldrich (St. Louis, USA) if not otherwise specified.

1.1. HUVEC extraction and culture

HUVEC (Human Umbilical Vein Endothelial Cell) were extracted using a modified protocol collagenase solution treatment from Baudin et al. [102]. Two donated umbilical cords were sufficient for all the experiments.

The medium for culturing HUVEC was EMEM supplemented with 10% FBS, 1% Penicillin/Streptomycin/Amphotericin B, 2 mM L-Glutamine; 1% non-essential amino acids 100X; 1% MEM vitamins solution; 10 µg/mL Endothelial Cell Growth Supplement (ECGS), 10 ng/mL Human Epidermal Growth Factor (hEGF); 3 ng/mL basic Fibroblast Growth Factor (bFGF); 1 µg/mL Hydrocortisone, 10 µg/mL Heparin Sodium Salt (named ILT medium). The endothelial cells were routinely trypsinized and used between passage 3 and 8.

HUVEC were seeded 24 h before the experiment, on a surface (well plate, or plastic coverslip (NUNC, Denmark)) coated with 1% Gelatin from porcine skin with a concentration of 20,000 cells/cm^2.

1.2. C3A culture

Human hepatoma-derived cell line C3A (ATCC Culture, USA) were cultured in EMEM with 10% FBS, 1%Penicillin/Streptomycin/Amphotericin B, 1% L Glutamine 200 mM; 1% non-essential amino acids 100X and 1% MEM vitamins solution (named complete EMEM). C3A were seeded in a 300,000 cells/cm^2 concentration. Only if seeded on glass coverslip a collagen coating is added: 200 µL of 0,2 mg/mL of type I collagen was pipetted and let cross link for about 30 min at 37°C. Collagen was prepared by extracting acid-soluble collagen from rat tail tendons [103].

1.3. CaCo-2 culture

Human epithelial colorectal adenocarcinoma cells, CaCo-2 (ATCC Culture, USA) were cultured in DMEM High-Glucose medium with 10% FBS, 1%Penicillin/Streptomycin, 1% non-essential amino acids 100X (named complete DMEM). Cells were seeded in a 60,000 cells/cm^2 concentration.

When CaCo-2 are seeded on ILT membranes, 21 days are needed for differentiated and confluent layer cells before using for the experiment.

ILT membranes were fabricated by CSEM (Neuchatel, Switzerland) with a structure of silicon-nitride (SiN) wafer with 1 µm porous membrane. Each membrane was cleaned and activated with Piranha water (sulfuric acid H_2SO_4 (96%), hydrogen peroxide H_2O_2 (30%) @ 50°C) treatment. Before seeding CaCo-2, membranes were housed in ILT membrane holder with biological-compatible tape which insures the electrodes holes remain dry and sterile during the culture.

1.4. Dynamic cell culture

Dynamic experiments were carried out in ILT 0 bioreactor system (described in chapter 3) when endothelial cells and/or hepatocytes were used. A flow rate of 100 µL/min was chosen with 15 mL volume of ILT medium (if not differently specified). If epithelial cells were used, the experiment was carried out in the ILT 2 bioreactor system (described in paragraph 3.1, chapter 3). In this case the upper circuit flow rate was set at 200 µL/min while the lower at 100 µL/min and the volume was 15 mL of ILT medium each circuit. Bioreactors can be connected to each other in order to have a more complex system for different kinds of experiment.

1.4.1. Assembling of ILT 0

Coverslips from HUVEC and/or C3A culture were moved to the bottom of the ILT chamber. Each bottom part of the chamber was filled with 500 µL of media in order to avoid drying of cells during assembly of the system. The rest of the volume was added to the mixing bottle. In general the total circuit volume is 2 mL per chamber plus 3 -5 mL for the mixing chamber and tubing. However it may vary if bubble traps or long term cultures are used.

Chambers were closed and connected to the system and let run with the pump (Ismatech IPC-4, Zurich, Switzerland) into a 37°C/5% CO_2 incubator for the experimental time.

1.4.2. Assembling of ILT 2

The membrane with fully differentiated cells was taken from the culture well; the external part of the holder was dried with sterile gauze. Tape was taken off from the holes with tweezers and the membrane was inserted between the two parts of the ILT 2 bioreactor. Then the bioreactor was closed and electrodes were pushed till electrical contact was made with the membrane. ILT 2 was connected to each circuit system (upper and lower circuit) and

filled with the medium previously added to each mixing bottle. The complete system with the pump (Ismatech IPC-4, Zurich, Switzerland) was placed in the 37°C/5% CO_2 incubator for the desired time.

2. NANOPARTICLES

Nanoparticles tested are shown in table 7.

Nanoparticle	Source
Polystyrene-FITC Fluoresbrite® Microparticles 50 nm (PS 50) Polystyrene-FITC Fluoresbrite® Microparticles 200 nm (PS 200)	Polysciences Inc. (Germany)
Ag NM 300	Ras GmbH
TiO_2 rutile-anatase, thermal, 7 nm	Hombikat UV100
Phosphine-Au NP 15 nm (Au 15) Phosphine-Au NP 80 nm (Au 80)	Kind gifted from Dr W.G. Kreyling (Helmholtz Zentrum Munich)

Tab. 7: List of the tested nanoparticles and their sources

For each NP, aliquots of 2 mL solution were prepared with a concentration of 1 mg/mL in ILT medium. Stock solution was sonicated in a water bath (Bandelin electronic, Berlin, Germany) before each use.

3. EXPERIMENTAL PROTOCOLS

Each experiment was performed under sterile conditions and was run at least in triplicate.

3.1. Establishment of NPs testing on HUVEC static culture

6,200 HUVEC cells in 200 µL were seeded in gelatin coated 96 multiwell plates 24 h before the experiment. Then medium was replaced with 200 µL of fresh medium containing different concentrations of NP as in the scheme below (Table 8), for each NP type.

	NP	Conc (µg/cm²)
HUVEC	Polystyrene-FITC 50 nm	625
	Polystyrene-FITC 200 nm	312,5
	Ag NM 300	156,3
	TiO_2	78,1
	Ph-Au NP 15 nm	39,1
	Ph-Au NP 80 nm	19,5
		9,8
		4,9
		2,4
		1,2

Tab. 8: List of concentrations used for NP tests

After 24 h medium and cells were analyzed.

Control samples were seeded and analyzed in the same condition and time of treated samples. They were untreated HUVEC (negative control) and Triton™ X-100 treated HUVEC (positive control). For each particle concentration the interaction with the assay was also tested in the absence of cells in order to avoid false negative or positive result due to particles interference (as discussed in chapter 2, paragraph 4).

3.2. Identification of common culture conditions

Three different media were tested in order to choose an optimum common medium:

- ILT medium (as described above)
- ECGM medium plus supplement kit (Promega, Madison, USA)
- Complete EMEM (as described above)

Cells were seeded in a 24-well plate at the same concentration in each medium and analyzed over 3 days for viability.
Then, HUVEC and C3A cells were seeded on coverslips to be analyzed in single-cell dynamic conditions at different flow rates in the chosen medium to determine the best range of flow rates. As controls, the same type and number of coverslips were placed in a Petri dish with the same amount of medium as the dynamic experiment (8 mL of ILT medium).

Morphology was observed for HUVEC and metabolic markers such as albumin, urea and glucose were analyzed for C3A.

3.3. Allometric Scaling

HUVEC (25 000 cells/coverslip) and C3A (250 000 cells/coverslip) were seeded on coverslips as described in paragraph 1. A system with 5 connected ILT 0 bioreactors was used, as shown in figure 14.

For the Surface and Metabolic Scaling Model (see paragraph 3, chapter 4) 1 HUVEC slide was placed in the bottom of the first chamber and 4 C3A slides were transferred to each of the other chambers of the system. The Cell Number Scaling Model (see paragraph 3, chapter 4) consisted in 1 HUVEC slide placed in the bottom of the first chamber and 1 C3A slide in the second chamber, the other three chambers were left empty of cells (Figure 14 B). The circuits were closed and filled with 15 mL of ILT medium and run at 100 µL/min in the incubator for 72 h.

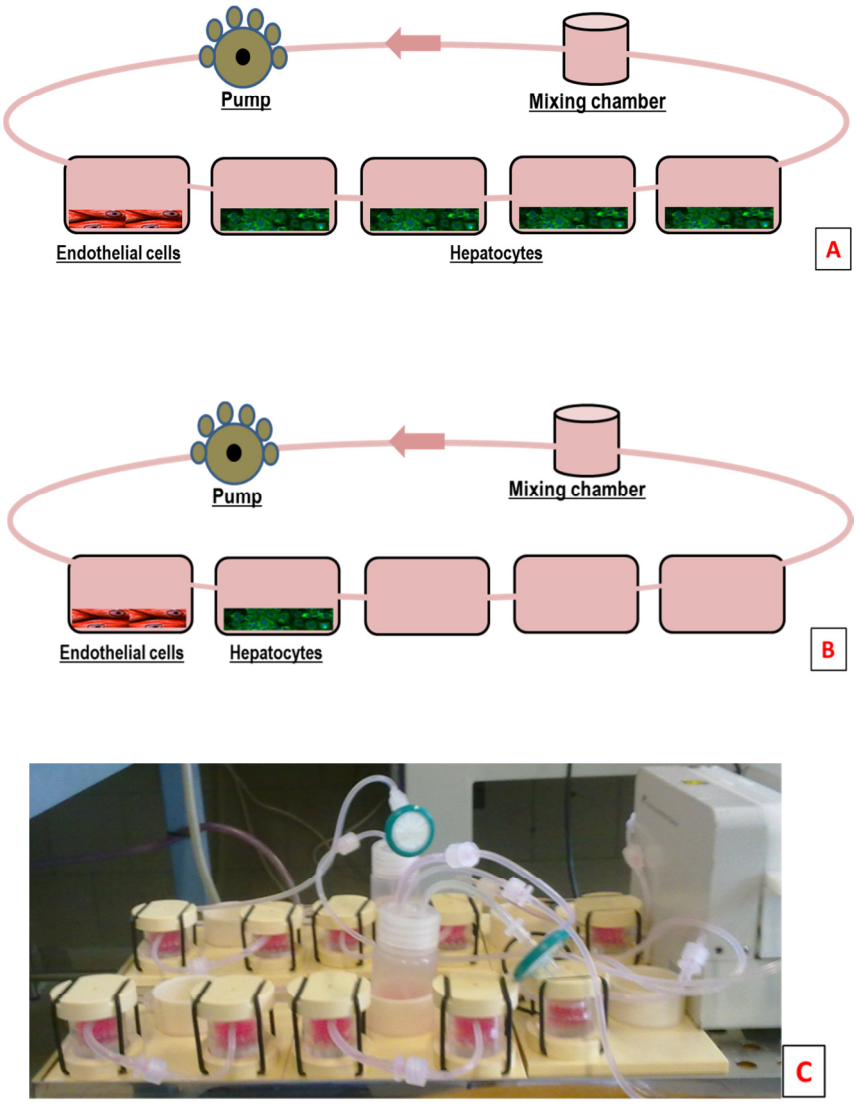

Fig. 14: The configuration of the two allometric models: the scheme of the Surface and Metabolic Scaling Model (SMSM) (A) and the Cell Number Scaling Model (CNSM) (B), and as they appear in reality (C).

As control, the same type and number of coverslips were placed in a Petri dish with 15 mL of ILT medium.

At the end of the experiment cells were analyzed for viability, morphology (HUVEC) and cytochrome activity (C3A) and medium was analyzed for

glucose, urea, D-lactate, glycerol, triglycerides (TG) and free fatty acids (FFA).

3.4. NP dynamic testing with single tissue configuration

HUVEC and C3A were tested for toxicity under dynamic conditions with different concentrations of Ag. The system used consisted in a 2 bioreactor-connection, with HUVEC or C3A in the first or the second chamber as in figure 15.

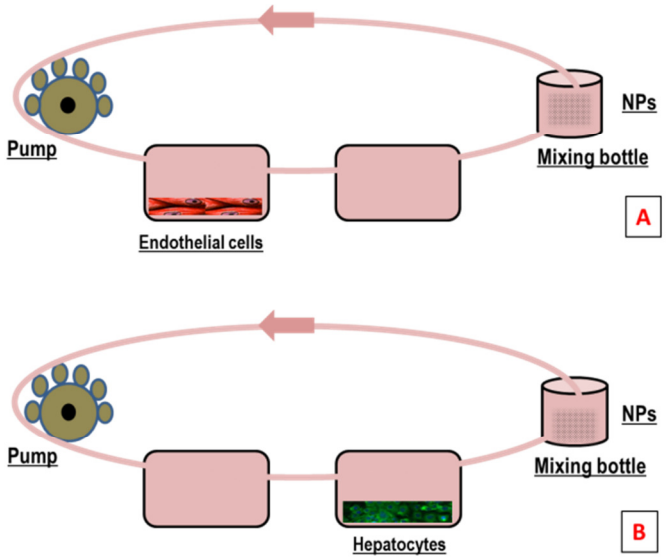

Fig. 15: The configuration of the two one tissue models: HUVEC experiment (A) and C3A experiment (B).

15 mL of medium with Ag NP at different concentrations was used in order to match the volumes in the complete ILT system (paragraph 3.5).

Cells were tested for viability, HUVEC were tested for vWF and C3A for α-actin. Moreover soluble markers of inflammation and apoptosis were analyzed.

3.5. Evaluation of ILT complete system baseline

A complete ILT system consists of one ILT 2 with CaCo-2 and two ILT 0 respectively with HUVEC and C3A cells (as described in paragraph 3, chapter 3); each circuit has also a bubble trap before ILT 2 (Fig. 16) and sampling ports before the mixing bottles. Bubble traps are placed to avoid bubbles in the bioreactor that could affect both the flow and the TEER (Trans Epithelial Electrical Resistance) measurement while sampling ports are useful for sampling medium during the experiment in sterility without open the mixing chambers.

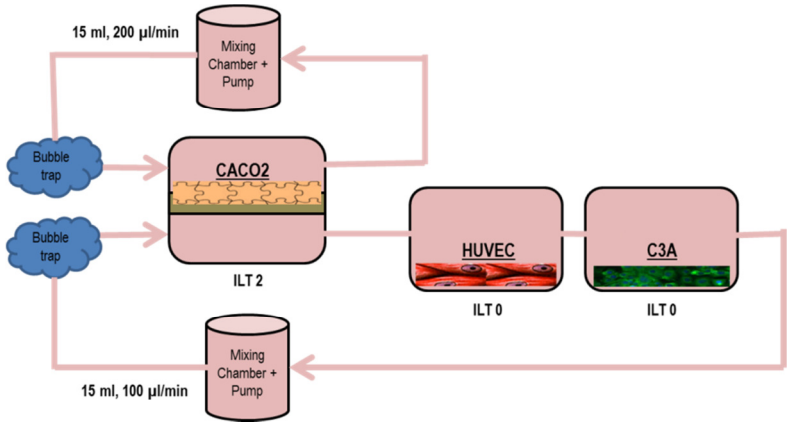

Fig. 16: Scheme of complete three tissue ILT system

Finally, the system was assembled as described in paragraph 1 and let run in the incubator for 24 h. A continuous measurement of TEER was taken using a modified EVOM 2 (WPI Inc, Sarasota, USA) that sends data to a dedicated software developed using LabVIEW (National Instrument, Austin, USA).

Samplings were at definite time points (1 h, 3 h, 8 h, endpoint 24 h) and each experiment was analyzed with the assays listed in table 9.

SAMPLE		ASSAY
Cells	on all	Alamar
	CaCo-2	ZO-1 (tight junction) staining
	HUVEC	vWF staining
	C3A	Phalloidin staining
Medium	from all	LDH Cytokine ELISA Apoptosis ELISA
	from C3A	Albumin ELISA

Tab. 9: List of assays performed within ILT system experiments

Baseline values were determined both for positive and negative controls. The positive control was the three tissues ILT dynamic culture and the negative control was the three tissues ILT dynamic culture with Triton™ X-100 added to the medium (in both mixing chambers).

3.6. NPs testing in ILT system

Polystyrene-FITC 55 nm NP (PS 50 nm) 1 mg/mL was firstly used to study the passage across the epithelial layer in the ILT complete system. Then, Ag was tested. The same protocol to assemble ILT system as for the baseline experiment was used (paragraph 3.5). 1 mg/mL of PS 50 nm or different concentrations of Ag NP were added only to the upper circuit (apical side with respect to CaCo-2 cells).

The same assays listed for the baseline were performed for the PS and Ag NP experiment (Table 9).

4. ASSAYS

4.1. Assays on cells

Alamar viability Assay (Metabolic activity evaluation)

Viability was tested at the end of the experiment using CellTiter™Cell Viability Assay (Promega, Madison, USA). Experimental medium was replaced with fresh medium and the reagent was added to the well in a volume correspondent to the tenth of the medium volume (e.g. for a 24-well plate 400 µL of medium were used and 40 µL of reagent were added), then the plate was placed in the incubator. Measurements of fluorescent emission with a fluorescent plate reader (Fluostar Optima, BMG Labtech, Aylesbury, UK) were after 30 minutes and after 2 hours and 30 minutes at 590 nm. The slope of fluorescence increase was calculated (representing the specific metabolic activity) and expressed as percentage of control viability (untreated cells).

Immunostaining and chemical staining (Function of cells)

Immunostaining was performed to detect key role molecules in cells: von Willebrand Factor (vWF) for HUVEC and tight junction protein ZO-1 for CaCo-2. A chemical staining using fluorescent labeled phalloidin was also used to investigate the distribution of F-actin in C3A cells.

After the experiment cells were fixed in iso-propanol 70 % over night. Then, washed cells were stained with the first antibody suspended in 2% BSA solution (Monoclonal Mouse Anti-Human Von Willebrand Factor, Dako, Glostrup, Denmark) for 1 h and after 3 washing steps the second antibody was added (AlexaFluor®, Invitrogen, Paisley, UK) to the cells. DAPI (4',6-diamidino-2-phenylindole) staining was also performed to fluorescent label the nuclei.

Analysis of fluorescence was carried out using an optical microscope (AX70, Olympus Italia, Milan) with a 20X and 40X objectives or with a confocal microscope (Zeiss LSM 510 confocal microscope with the software LSM510 package). Captured images were analyzed and the stained proteins were semi-quantified using ImageJ software (National Institutes of Health, USA).

Gluthation depletion assay (Oxidative stress evaluation)

Experiments were run at different time points (2 h, 6 h, 24 h) as oxidation can occur very quickly and last for some hours. At the end of each experiment cells were scraped off and the acid extract was analyzed for GSH/GSSG content as described in Senft et al [104]. Briefly, 10 µL of acid extract from the trichloracetic acid (TCA) extraction were incubated 5 min with the Redox Quencing Buffer. Then, 29 µL of o-phtalaldehyde (OPT) solution were added and let react for 30 min. The fluorescence emission at 420 nm of the reaction product was used to calculate the GSH value with respect to the standard curve values. A pre-step with dithionate was added to a second set of samples to reduce GSSG to GSH and then indirectly measure the GSSG content so to calculate the GSH/GSSG ratio.

RNA extraction and quantification of vWF gene expression (HUVEC, function of cell)

RNA from confluent wells of treated HUVEC was isolated using RNeasy® Mini Kit (Qiagen, Milan, Italy) and its content were verify measuring (Biophotometer, Eppendorf, Hamburg, Germany) the absorbance at 260 nm. mRNA purity was evaluated calculating the ratio between absorbance value at 260 nm and the value at 280 nm (A260/A280). 1 µg of RNA was reverse transcribed using QuantiTect® Reverse Transcription (Qiagen, Milan, Italy).

Real time PCR analysis was performed using DyNamo™ Flash SYBR® green qPCR kit (Finnzymes, Vantaa, Finland) for 39 cycles (95 °C for 10 s, 60 °C for 30 s, 72°C for 30 s) using cycler specific pair of Primer (Forward primer VWF (exon 3) 5'-AGA AAC GCT CCT TCT CGA TTA TTG-3'; Reverse primer VWF (exon 4) 5'-TGT CAA AAA ATT CCC CAA GAT ACA-3'). PCR products were identified by their melting curve. β-Actin was the housekeeping gene for HUVEC.

Cytochrome P 450 activity (C3A, metabolism evaluation)

At the end of the experiment C3A cells were tested for Cytochrome P 450 (CYP 450) activity. Vivid® CYP450 3A4 Screening Kit (Invitrogen, Paisley, UK) was used to measure the cytochrome metabolism, the increase of fluorescence emission at 585 nm after substrate adding represents the fluorescent signal of produced metabolites.

Transepithelial Electrical Resistance (CaCo-2, monolayer integrity)

Transepithelial Electrical Resistance (TEER) was assessed with EVOM 2 (World Precision Instruments, Sarasota, USA). When performed an ILT 2 experiment TEER values were detected every 15 min and registered with a dedicated software developed using LabVIEW (National Instrument, Austin, USA).

Morphology

Cells morphology before and after experiments, was observed using an optical microscope (Olympus, AX70, Olympus Italia, Milan) with a 10X and 20X objective.

4.2. Assays on medium

Medium from every experiment was stored in order to measure soluble molecules concentration. From static culture and dynamic cells culture only endpoint media were stored. Sampling and endpoint media were, instead, analyzed in ILT complete system experiments.
Each assay was carried out in accordance with the manufacturer's instructions and at least a duplicate was measured for each sample.

Media from NP testing on HUVEC static culture (paragraph 3.1) were analyzed for cytotoxicity Detection Kit (LDH, Roche, Germany), Fas-Ligand, ICAM-1, IL-8, and TNF-alpha with BD™ FLEX kit bead based ELISA (BD Biosciences, Franklin Lakes, USA). NP interference was evaluated in each assay.

Media from allometric models experiments (paragraph 3.3) were analyzed for glucose, urea, D-lactate, glycerol, triglycerides (TG) and free fatty acid (FFA) concentrations using colorimetric and fluorimetric commercial kits (Glucose Test Kit, Megazyme International Ltd, Ireland; Urea Kit, Sigma-Aldrich, St.Louis, USA; D-Lactate, Free Glycerol Assay kit, Triglyceride quantification kit, Free Fatty Acid Quantification Kit all from Biovision Inc., Milpitas, USA). Human albumin concentration was determined by an ELISA immunochemical assay (Bethyl Laboratories, Montgomery, USA).

Media from one (paragraph 3.4) and three tissues (paragraphs 3.5 and 3.6) ILT experiments were analyzed for the same assays as for the NP testing on HUVEC static culture, moreover human albumin ELISA quantification was performed (not for HUVEC dynamic ILT experiment).

5. STATISTICAL ANALYSIS

Results were calculated from at least three different experiments and expressed as means ± standard deviation of the mean. Data were analyzed

by Student's t-test. Statistical significance was set at $p<0.05$ (indicated with *) and high significance was set at $p<0.01$ (marked with **). LC_{50} was calculated using Sigma Plot 11.0 (Systat Software, Inc., Erkrath, Germany).

Section III

Results and Discussion

Chapter 6

Results

1. ESTABLISHMENT OF NPs TESTING ON HUVEC STATIC CULTURE

NP toxicity on HUVEC cells was tested in order to determine the LC_{50} and investigate sub lethal effects such as loss of function or inflammation analyzing 3 relevant doses for each NP.

1.1. Cell viability

Dose dependent toxicity was assessed both for metabolic activity (Alamar Assay) and membrane integrity (LDH Assay). The Alamar assay evaluates the mitochondrial capacity to reduce the reagent to a fluorescent product, while the LDH assay measures the total amount of lactate dehydrogenase (LDH), a cytoplasmic enzyme in the medium, released from cells when the cellular membrane is damaged.

In both assays high toxicity was shown for Ag and TiO_2 NP treated HUVEC with an LC_{50} of 24.6 µg/cm^2 (Alamar Assay) and 1 µg/cm^2 (LDH Assay) for Ag NP and 28 µg/cm^2 (Alamar Assay) and 53 µg/cm^2 (LDH Assay) with TiO_2 (Figure 17).
High Ag interference was found with the LDH assay using the same amount of cell lysate with different concentrations of particles. A reduction in absorbance was measured for treatment with Ag NM 300 NP at concentrations higher than 20 µg/cm^2. This interference is characteristic of

enzymatic assays and is thought to be due to the adsorption of the enzyme onto the particle surface, reducing the enzyme activity [105]. However, when corrected for the particle interference a very strong cytotoxic effect was revealed as shown in figure 17 B.

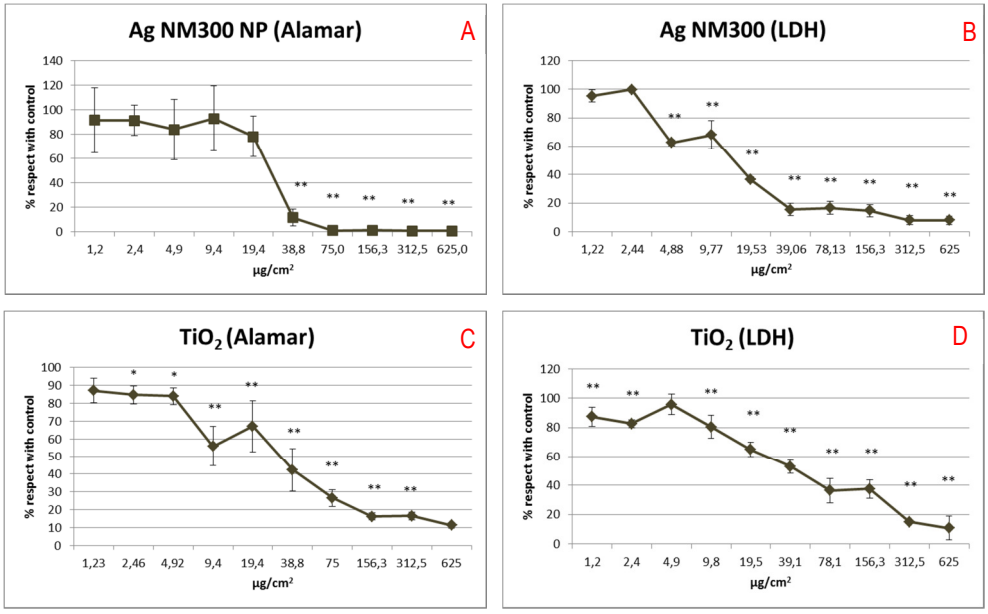

Fig. 17: Viability dose response curve for Ag (A and B) and TiO_2 (C and D) exposed HUVEC. Viability was assessed both at the level of metabolic activity level (A and C) and membrane integrity (B and D). Data are expressed as percentage of untreated HUVEC viability; mean ± SD, * $p<0.05$ and ** $p<0.01$, n=3

The Ag dispersant was also checked, and no toxicity at relevant concentrations was observed (Figure 18).

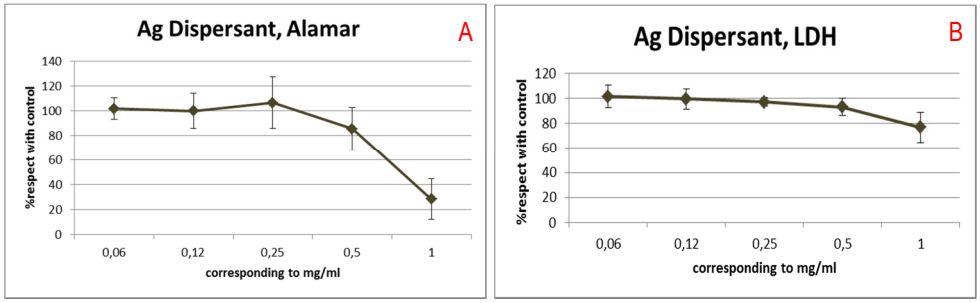

Fig. 18: Viability dose response curve for Ag Dispersant treated HUVEC. Viability was assessed both at the level of metabolic activity (A) and membrane integrity (B). Data are expressed as percentage of untreated HUVEC viability; mean ± SD, n=3

No significant toxicity with Polystyrene 50 nm (PS 50 nm) and Polystyrene 200 nm (PS 200 nm) was observed (Figure 19), while low toxicity was shown for both Au particle sizes at higher concentrations (Figure 20).
The outliers which showed significant higher viability with respect to control values are thought to be due to particle interference as already discussed.

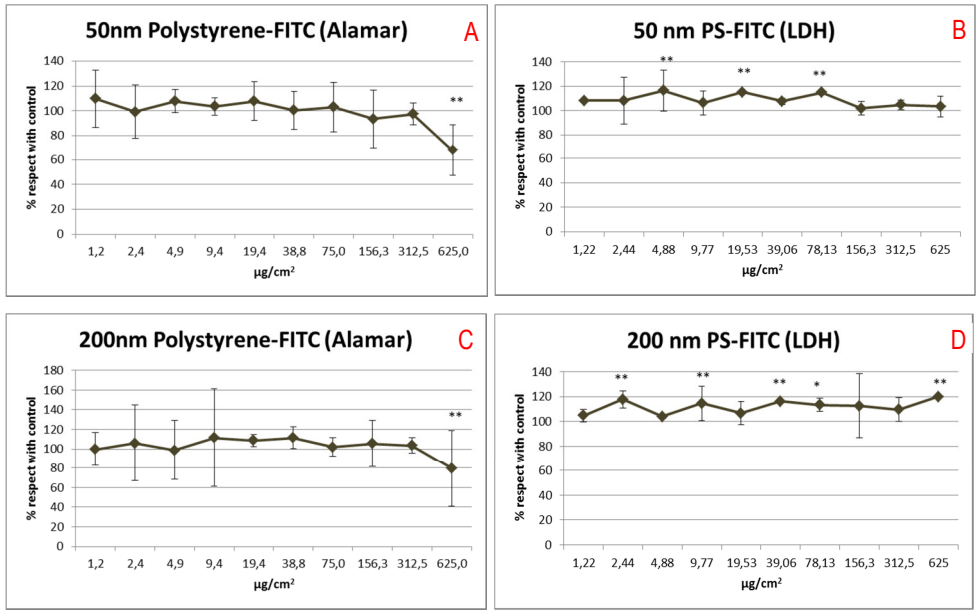

Fig. 19: Viability dose response curve for Polystyrene-FITC 50 nm (A and B) and 200 nm (C and D) treated HUVEC. Viability was assessed both at the level of metabolic activity (A and

C) and membrane integrity (B and D). Data are expressed as percentage of untreated HUVEC viability; mean ± SD, * p<0.05 and ** p<0.01, n=3.

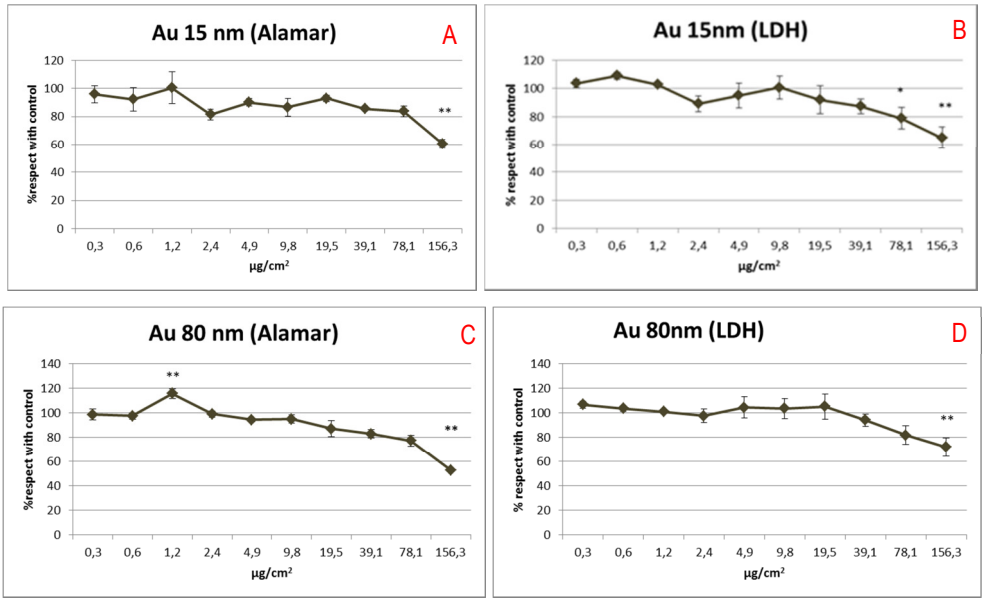

Fig. 20: Viability dose response curve for Au 15 nm (A and B) and 80 nm (C and D) treated HUVEC. Viability was assessed both at the level of metabolic activity (A and C) and membrane integrity (B and D). Data are expressed as percentage of untreated HUVEC viability; mean ± SD, * p<0.05 and ** p<0.01, n=3.

1.2. Oxidative stress

When cells are subjected to an oxidative stimulus reduced glutathione GSH (γ-glutamylcysteinylglycine) is converted to GSSG, its oxidized form. The accumulation of GSSG determines a decrease in the GSH/GSSG ratio which is a signal of increased levels of oxidative stress. Ideally, the evaluation of GSH/GSSG ratio should be performed at early time points as oxidative stress can occur in the early steps of the cell response to the stimulus.

The glutathione depletion assay was performed on HUVEC cultured in 12 well-plates and treated with NPs at different time points (2 h, 6 h, 24 h). Unfortunately no detectable GSH was found as all the samples were out of

the range of detection. Increasing the amount of cells it is possible to measure some GSH as shown in figure 5. However, a suitable value is only reached when a large number of cells are used, so this assay was found to be not feasible for the evaluation of oxidative stress on HUVEC cells in the ILT system.

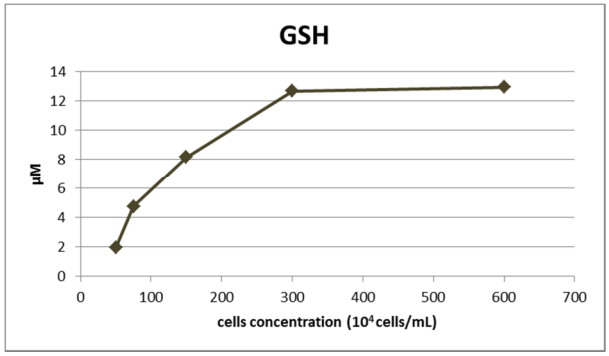

Fig. 21: GSH concentration with respect to the cell concentration (untreated cells). More than 3 x 10^6 cells/mL are needed to reach a suitable value for GSH evaluation, n=1.

1.3. Inflammation

Inflammation was assessed measuring HUVEC cytokine release after NP treatment. Three concentrations for each NP type were tested, from 160 to 5 µg/cm^2 for low-toxicity NPs and from 20 (or 40) to 1 µg/cm^2 for high-toxicity ones.

1.3.1. Interleukin 8 (IL-8)

IL-8 is a pro-inflammatory protein stored in the Weibel-Palade bodies and released in case of stress and inflammation.

PS NPs of both sizes had IL8 expression comparable to controls with a slight decrease at highest concentration. Ag, TiO_2 and Au of both size showed instead, a significant increase with respect to the controls (untreated). The increase was also found to be concentration dependent in all these particles.

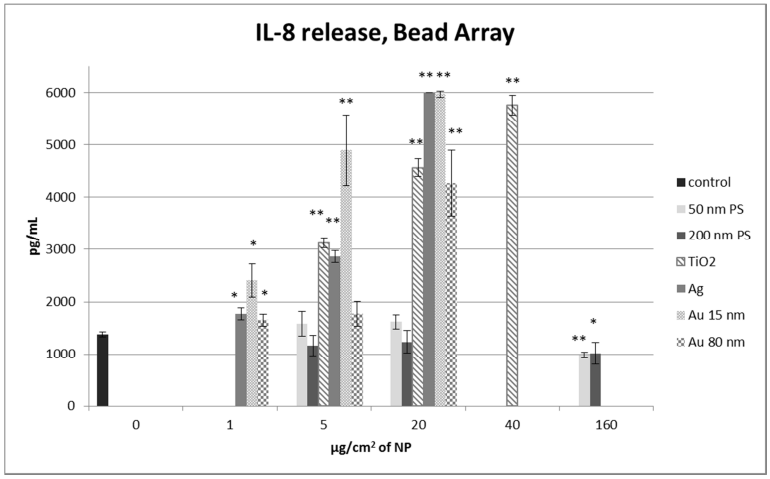

Fig. 22: IL-8 release at different concentrations of NPs treated HUVEC. Data are expressed as concentration (pg/mL) in the medium; control sample is untreated HUVEC; mean ± SD, * $p<0.05$ and ** $p<0.01$ with respect to control, n=3.

1.3.2. Intercellular Adhesion Molecule-1 or CD54 (ICAM-1)

ICAM-1 is a transmembrane protein associated with intercellular adhesion. ICAM-1 signaling seems to produce a recruitment of inflammatory immune cells and as a consequence initiation of the inflammatory cascade.

ICAM was only detected at a high concentration of polystyrene 50 nm. TiO_2 and Au showed highly significant ($p<0.01$) increase of ICAM with a peak at 20 µg/cm^2 of Au 80 nm. This concentration was able to stimulate ICAM release 28 fold more that in the controls.

No ICAM release was observed from any Ag treated cells.

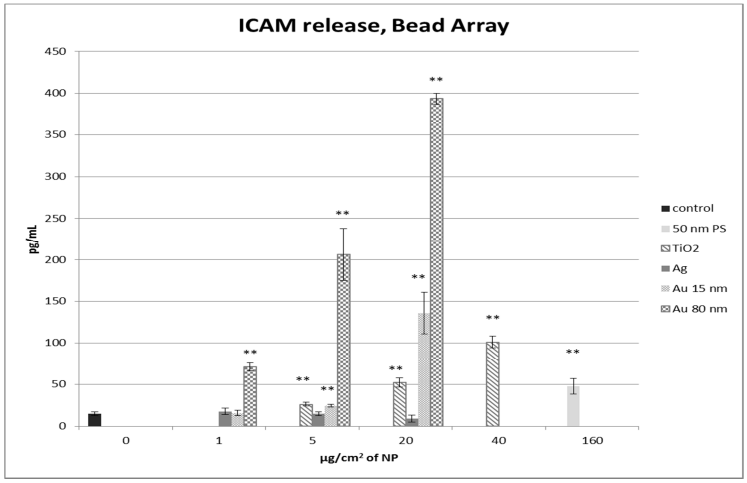

Fig. 23: ICAM-1 release at different concentrations of NPs treated HUVEC (ELISA Array). Data are expressed as concentration (pg/mL) in the medium; control sample is untreated HUVEC; mean ± SD, * $p<0.05$ and ** $p<0.01$ with respect to control, n=3.

1.3.3. Tumor Necrosis Factor-α (TNF-α)

TNF-α is a cytokine involved in systemic inflammation and is involved in the acute phase reaction. No detectable TNF-α was found in any of the samples. It is likely that the TNF-α concentration in the samples was too low to be detected.

1.4. Apoptosis

1.4.1. Fas-Ligand

Fas ligand (CD95L) is a transmembrane protein. When the receptor binds it activates the caspase cascade with a consequent induction of apoptosis.
Only in a few analyzed samples was Fas-L detectable. Ag treated HUVEC showed concentration dependent high apoptosis marker levels; surprisingly polystyrene beads 50 nm had the highest increase at a concentration of 160 µg/cm^2. This concentration did not show toxic effects in Alamar and LDH Assays.

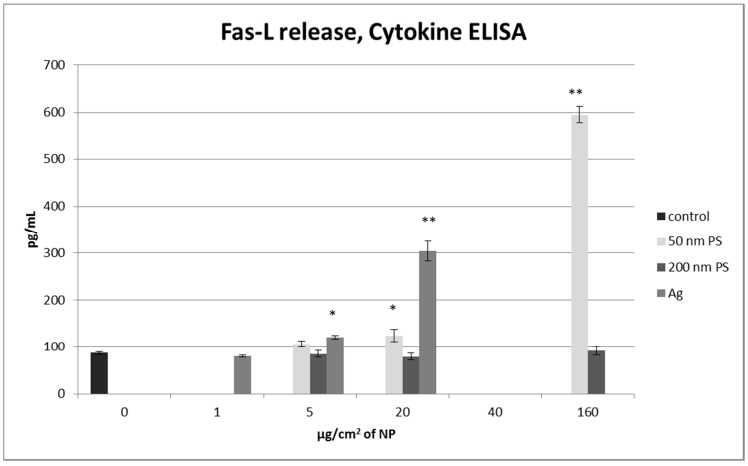

Fig. 24: Fas-L release at different concentrations of NPs treated HUVEC (ELISA Array). Data are expressed as concentration (pg/mL) in the medium; control sample is untreated HUVEC; mean ± SD, * $p<0.05$ and ** $p<0.01$ with respect to control, n=3.

1.5. Function of cells: von Willebrand Factor expression

vWF is a glycoprotein present in blood plasma and produced constitutively in the Weibel-Palade bodies of endothelium. Its primary function is to bind other proteins and has an important role in the platelet adhesion pathway and coagulation cascade.

High levels of vWF expression could mean an inflammation status.

vWF expression was analyzed both at mRNA and protein expression levels for significantly toxic NPs (Ag and TiO_2) and non-toxic ones (PS-FITC 50 nm and 200 nm)

1.5.1. vWF mRNA quantification

mRNA from NP treated HUVEC was extracted and real time PCR was performed in order to quantify the vWF mRNA expression .

Au NPs of both sizes were found to increase vWF production indicating compromised HUVEC function. Polystyrene 50 nm (not the highest

concentration) and Ag NP at lower concentrations, instead, lead to high levels of vWF expression indicative of a relevant inflammatory status.

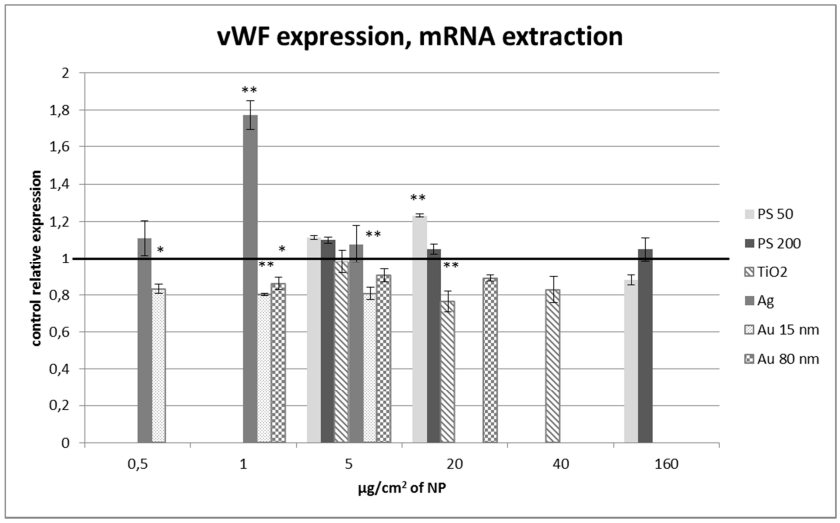

Fig. 25: vWF mRNA expression at different concentrations of NPs treated HUVEC. Data are expressed as samples/control (untreated HUVEC) ratio; mean ± SD, * $p<0.05$ and ** $p<0.01$ with respect to control, n=3.

1.5.2. vWF protein expression

vWF protein levels were also assessed for some NP (PS of both sizes, Ag, TiO_2). NP treated HUVEC were fixed, stained for vWF and analyzed with a microscope. The immunocytochemical images of vWF staining were quantified using image processing.
All images were taken at the same luminous intensity to ensure a constant background. The data were obtained from three wells per concentration and averaged using at least 3 regions of interest (ROIs) per well.

PS-FITC NP of both sizes had a strong interference with the visualization of secondary antibody as the FITC absorption spectra (green) overlapped with the fluorescent spectra (red) of the antibody used to stain HUVEC. Image

processing was thus performed in order to discern the vWF signal from that of FITC as shown in figure 26.

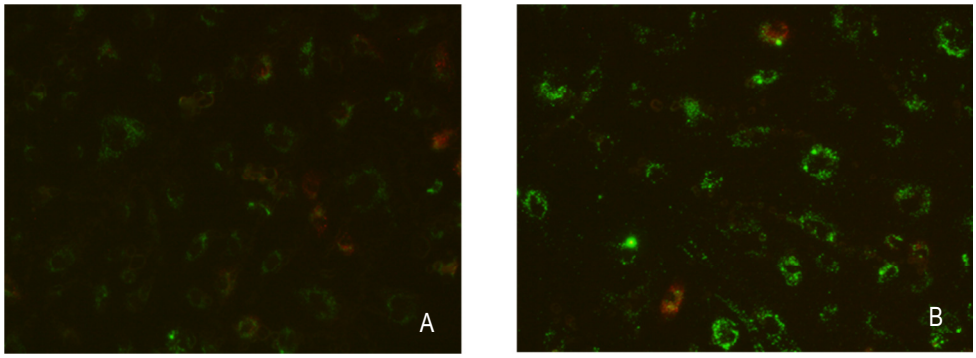

Fig. 26: Processed images showing co-localization of vWF and FITC (in green) and ROIs corresponding only to vWF (in orange) after 5 µg/cm^2 50nm Polystyrene-FITC (A) and 5 µg/cm^2 200 nm Polystyrene-FITC (B), X20 objective.

Results from image processing showed a constant and concentration independent expression of vWF in PS treated cells with respect to untreated samples.

vWF expression from Ag treated HUVEC showed a peak of more than 250% fluorescence at 3 µg/cm^2 with respect to controls, while at higher concentrations the fluorescence dropped, either because there were fewer stained cells due to detachment of dead ones or because the vWF expression machinery was compromised (Fig. 27).

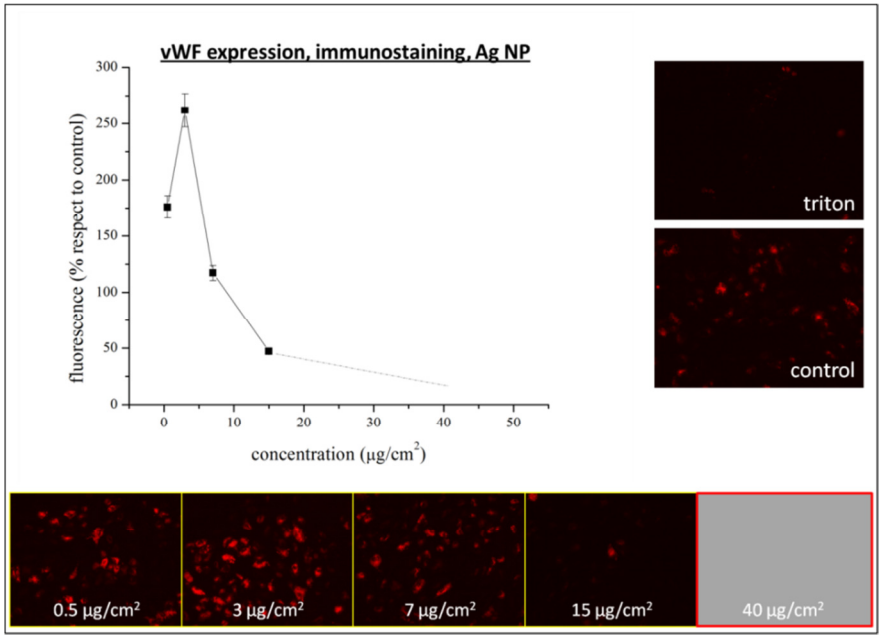

Fig. 27: Dose response curve of HUVEC treated with Ag NP at different concentrations. vWF expression is represented as the % of control red pixels after processing fluorescent micrographs; mean ± SD, n=3. A fluorescent micrograph (20X objective) for each concentration and control is also shown.

The same even if lower increased expression trend was found with TiO_2 treated HUVEC.

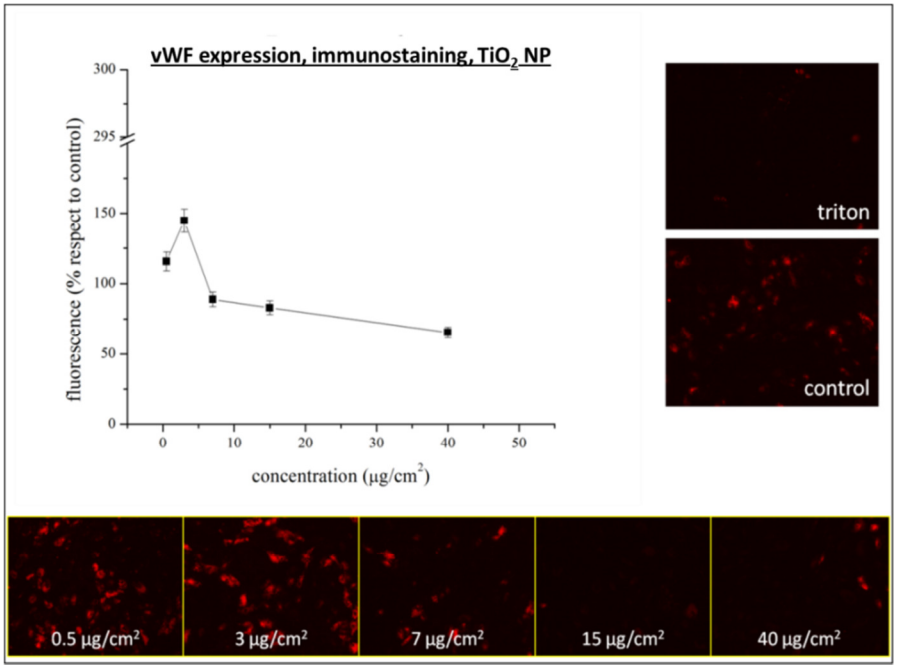

Fig. 28: Dose response curve of HUVEC treated with TiO_2 NP at different concentrations. vWF expression is represented as the % of control red pixels after processing fluorescent micrographs, mean ± SD, n=3. A fluorescent micrograph for each concentration and control is also shown.

2. IDENTIFICATION OF COMMON DYNAMIC CULTURE CONDITIONS

In order to perform a dynamic multiple cell type culture all the protocols need to be optimized. First of all a common medium suitable for all the 3 cell types need to be established. Then dynamic culture at different flow rates was tested in the new medium.

2.1. Media testing

Cells were tested in three different media (ECGM, EMEM, ILT medium) in standard static conditions analyzing viability every day for 3 days with Alamar Assay. Results were expressed with respect to the standard

(recommended medium for the cell type) medium value of the same day and with respect to the viability on the first day in order to evaluate the eventual difference in growth rate.

2.1.1. HUVEC viability

The standard medium for HUVEC is ECGM medium, so all the media were analyzed with respect to the ECGM daily value (Fig. 29 A) or with respect to ECGM viability value on day 1 (Fig. 29 B).

Data showed that HUVEC were more metabolically activate in ILT medium with respect to control medium, while cells started dying after 3 days in EMEM. This trend was confirmed when cell growth was evaluated with respect to the control medium viability on day 1. HUVEC were proliferating in ILT medium even more than in ECGM medium, while in EMEM there was a decrease in proliferation.

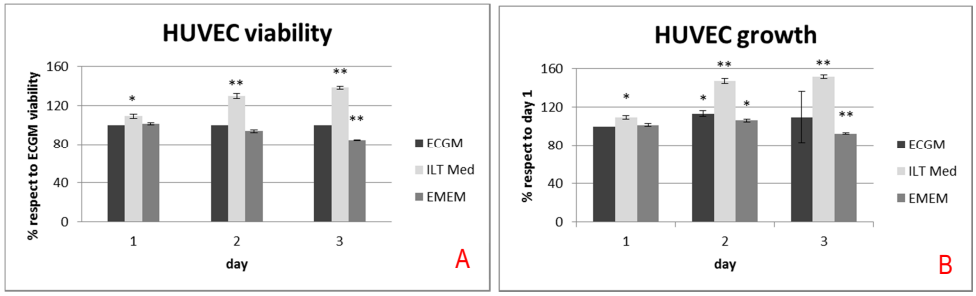

Fig. 29: Viability of HUVEC in different media; data plotted with respect to daily ECGM value (A) and with respect to ECGM value of day 1 in order to evaluate cell growth; mean ± SD, * $p<0.05$ and ** $p<0.01$, n=2.

The viability data were confirmed by morphological analysis of HUVEC using a microscope, where cultivated in EMEM lose their typical cobblestone shape (as in fig. 30 A) and start detaching from the confluent layer (Fig. 30 B).

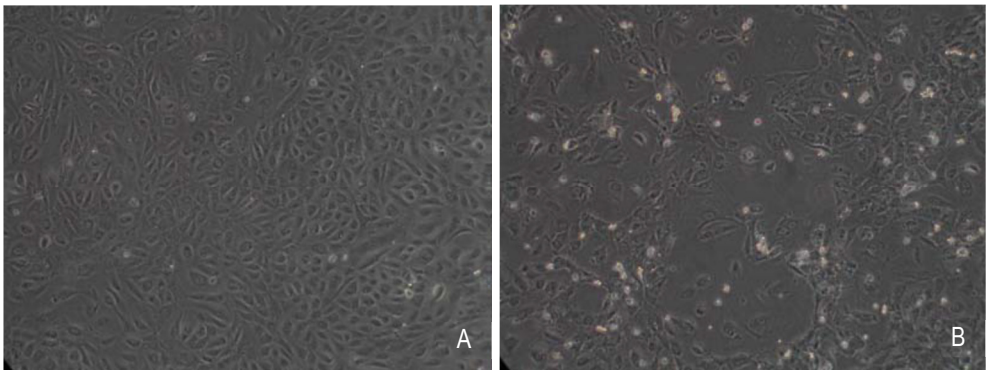

Fig. 30: HUVEC morphology after 24 h ECGM (A) and EMEM (B). 20 X objective.

2.1.2. C3A viability

The recommended medium for C3A is EMEM. Viability data for the different media were plotted with respect to controls either using the daily value (Fig. 31 A) or with respect to EMEM viability value on day 1 (Fig. 31 B). Both viability and proliferation in ECGM or ILT medium were not significantly different from the control medium values. Cells reacted to each medium in a similar manner.

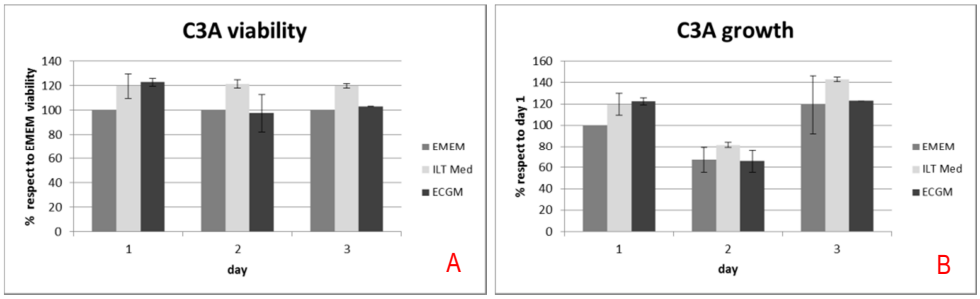

Fig. 31: Viability of C3A in different media; data plotted with respect to the daily EMEM value (A) and with respect to the EMEM value of day 1 in order to evaluate the cell proliferation; mean ± SD, n=2.

2.1.3. CaCo-2 viability

The standard medium for CaCo-2 is DMEM but EMEM is also suitable medium for only 3 days of culture, so viability data were compared with respect to the EMEM value. No change in viability was found (Fig. 32 A) and a slight increase in growth was present for each medium (Fig. 32 B).

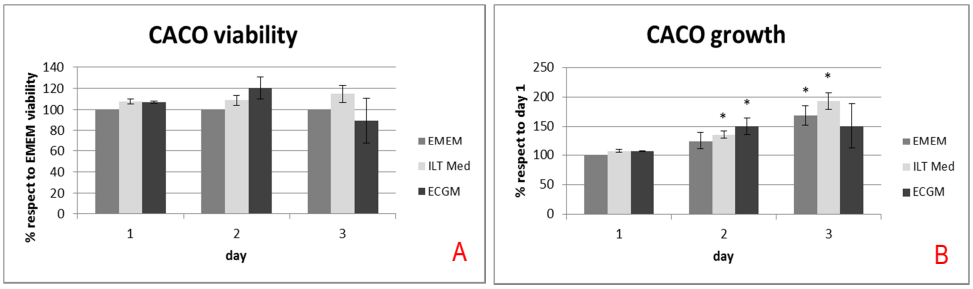

Fig. 32: Viability of CaCo-2 in different media; data plotted with respect to the daily EMEM value (A) and with respect to EMEM value of the day 1 in order to evaluate cell growth; mean ± SD, n=2.

2.2. Dynamic condition set up

Dynamic conditions suitable for all the cell types were tested. HUVEC and C3A were checked for viability (Alamar Assay) at different flow rates (CaCo-2 was tested by another group) in ILT medium. Moreover functional marker analysis was performed.

2.2.1. Viability

Flow rates from 0 µL/min (cells in the ILT0 system with pump switched off) to 1000 µL/min were tested. Both cell types showed a good viability under flow rates below 500 µL/min.

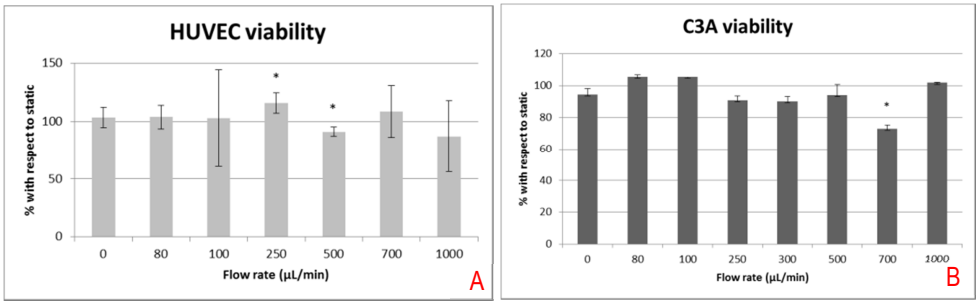

Fig. 33: Viability of HUVEC (A) and C3A (B) at different flow rates; control samples were cells cultivated in the same conditions but maintained in a petri dish; 0 µL/min refers to cells in the dynamic system without the pump switched on. Mean ± SD, * $p<0.05$ with respect to control, n=2.

2.2.2. Functional marker of HUVEC

HUVEC from dynamic experiments were immunostained for vWF expression.

A slight flow rate dependent increase was observed as described in Galbusera et al. [106].

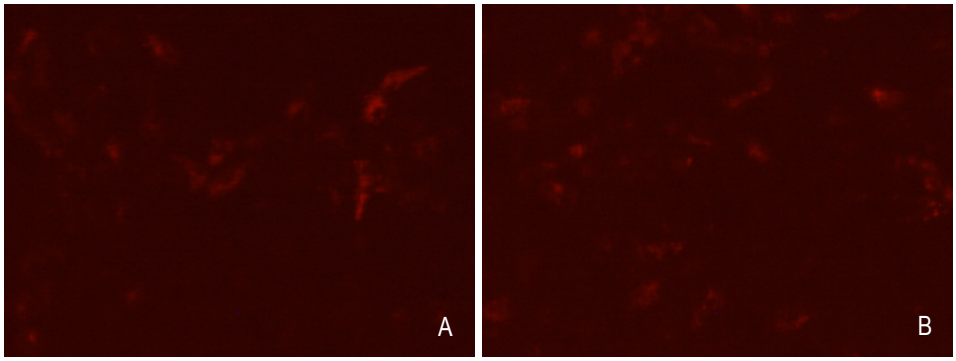

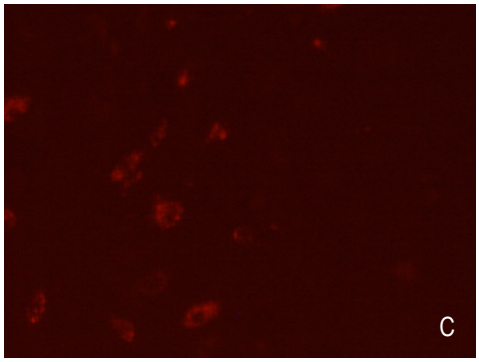

Fig. 34: Fluorescent micrograph of vWF stained HUVEC after 24 h in static conditions (A) and dynamic conditions with 100 µL/min (B) and 1000 µL/min flow rate (C). 20X objective.

2.2.3. Functional markers of C3A

C3A glucose uptake was analyzed to see whether cell metabolism depends on flow rates, moreover albumin and urea release in the medium were measured in order to check for the hepatocytes ability to produce metabolites.

We did not observe significant differences in glucose and urea concentrations for the different flow rates. However there was a significant ($p<0.01$) increase in albumin release at 200 µL/min with respect to the 0 µL/min control (Fig. 35 B).

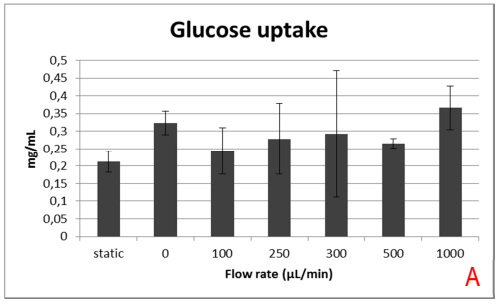

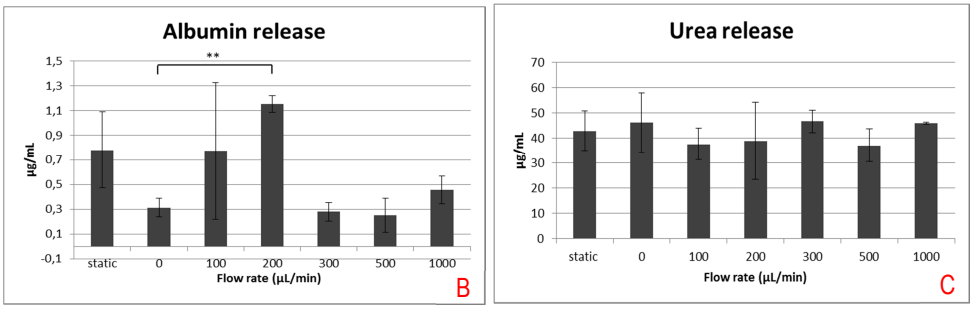

Fig. 35: Markers of C3A function: glucose uptake (A), albumin release (B) and urea release (C) at different flow rates; static samples were cells cultivated in a petri dish; 0 µL/min were cells in the dynamic system without the pump switched on. Mean ± SD, ** $p<0.01$, $n=2$.

3. ALLOMETRIC SCALING

Two scaling models were studied experimentally. The “Surface and Metabolic Scaling Model” (SMSM) evaluates the surface area of liver and vascular endothelium considering physiological ratio while the “Cell Number Scaling Model” (CNSM) determines the cell number ratio scaling the total amount of hepatocytes and endothelial cells in the gastrointestinal tract.
Media and cells from experiments were analyzed for cell metabolism and markers of hepatic function.

3.1. Viability

HUVEC and C3A cells were checked for viability with Alamar Assay. Both cells in the two experimental models showed good viability, to within 80% of static controls.

3.2. Carbohydrate metabolism

Carbohydrates are the primary source of energy and metabolic intermediates. Glucose is the main carbohydrate used by the cell in both aerobic and anaerobic respiration. Hepatocytes are able to store or release glucose through glycogen synthesis or glycolysis pathways.

D-Lactate levels seem to be function of both glycolysis and gluconeogenesis in hepatocytes [107]. D-Lactate participates in the glyoxalase pathway which is thought to help release the stress of elevated glucose intake, enhancing glycolysis and producing more lactate. Abnormally high concentrations of lactate have been related to disease states such as diabetes and lactate acidosis [108].

3.2.1. Glucose

Glucose dosing in the media showed a higher uptake in the SMSM configuration. Anyway in both static and dynamic conditions the higher consumption of glucose can be attributed to the higher amount of cells with respect to the CNSM model (4 fold more). Significant ($p<0.01$) differences were observed between the two models in static conditions (Fig. 36).

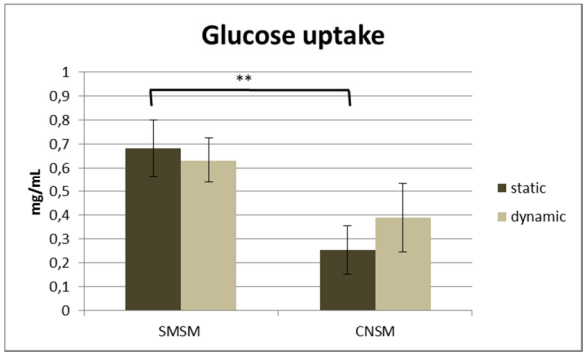

Fig. 36: Glucose uptake from cells in the two allometric model configurations. Static samples were the same type and number of cells cultivated in a petri dish. Mean ± SD, * $p<0.05$ and ** $p<0.01$, n=3.

3.2.2. D-Lactate

A significant ($p<0.05$) decrease of lactate release in dynamic conditions was observed. No difference was found between the two models even when relating D-Lactate release with glucose uptake (Fig. 36), similar

concentrations of lactate were found in both configurations despite the lower uptake of glucose in the CNSM (Fig. 37).

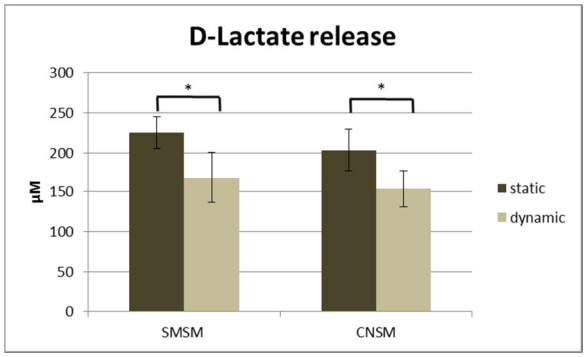

Fig. 37: D-Lactate release from cells in the two allometric model configurations. Static samples were the same type and number of cells cultivated in a petri dish. Mean ± SD, * $p<0.05$ and ** $p<0.01$, n=3.

3.3. Fat metabolism

The liver has a major role in the regulation both of glucose metabolism and fat metabolism. It can either oxidize and synthetize fatty acids and triglycerides sending them to energy production or to storage.
Free fatty acids (FFA) and glycerol provided by ingestion or by drawing on triglycerides are used as substrates for ATP production.

3.3.1. Triglyceride

Triglyceride dosing showed that cells in the CNSM configuration took up about twice as much triglyceride content as the SMSM even though the total amount of cells present in the system was four time less. No significant change was observed between the static and dynamic set up in both models.

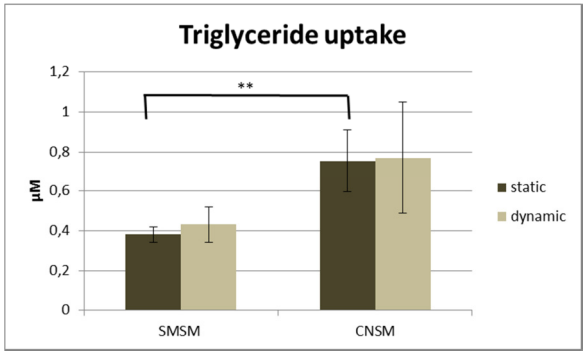

Fig. 38: Triglyceride uptake from cells in the two allometric model configurations. Static samples were the same type and number of cells cultivated in a petri dish. Mean ± SD, n=3.

3.3.2. Free Fatty Acid

Free Fatty Acid (FFA) data showed a variable trend between the two configurations. All data comparisons were highly significant ($p < 0.01$).

In the SMSM configuration, high FFA uptake was observed for the static set up with a relevant lower uptake in the dynamic set up. In the CNSM the slight uptake in static conditions was contrasted by a highly significant release in the dynamic configuration (Fig. 39). This inversion of the trend is likely caused by HUVEC, which have a low level of FFA release in static conditions, while really high levels of free FFA are observed in dynamic conditions. HUVEC FFA motion was more prevalent than that of C3A which takes up FFA uptake in both static and dynamic conditions [98].

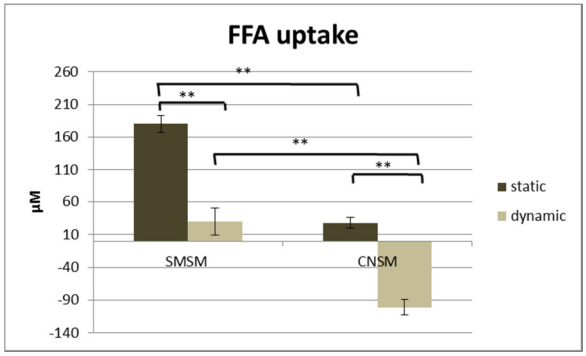

Fig. 39: Free fatty acid uptake from cells in the two allometric model configurations. Static samples were the same type and number of cells cultivated in a petri dish. Mean ± SD, * p<0.05 and ** p<0.01, n=3.

3.3.3. Glycerol

The same level of glycerol was taken up by cells both static and dynamic states in the two configurations. A lower uptake was shown in the CNSM with respect to SMSM (Fig. 40).

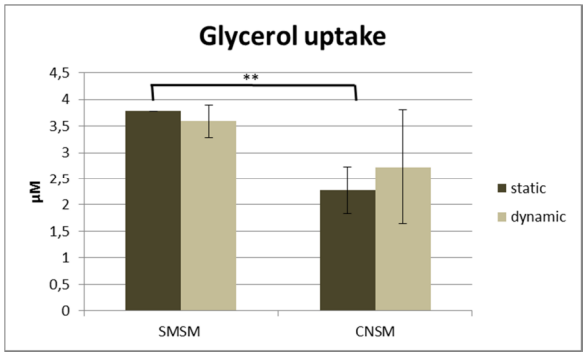

Fig. 40: Glycerol uptake from cells in the two allometric model configurations. Static samples were the same type and number of cells cultivated in a petri dish. Mean ± SD, * p<0.05 and ** p<0.01, n=3.

3.4. Function

The liver is the key orchestrator of metabolism, many enzymatic reactions occur in this organ Healthy hepatocytes are able to perform carbohydrate,

lipid and xenobiotic metabolism, the synthesis of many molecules including albumin, and convert ammonia into urea.

3.4.1. Cytochrome P450 subfamily 3A4

The cytochrome P450 subfamily 3A4 (CYP3A4) is the main enzyme for drug metabolism and synthesis of cholesterol, steroids, and other lipid.
Even if cell lines are thought to be less metabolically active and express low cytochrome enzyme levels [109], data showed a constant activity of CYP3A4 in both SMSM configurations while a lower but not significant level was observed in the CNSM dynamic model with respect to static set up (Fig. 41).

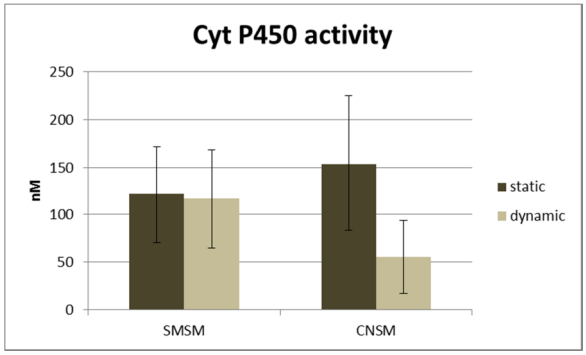

Fig. 41: CYP450 activity in the two allometric model configurations. Static samples were the same type and number of cells cultivated in a petri dish. Data expressed as metabolized product concentration, mean ± SD, n=3.

3.4.2. Albumin

Significant increase in albumin release was detected in the CNSM configuration where cells release twice more albumin than in SMSM. The content of albumin in each configuration was similar in static and dynamic conditions.

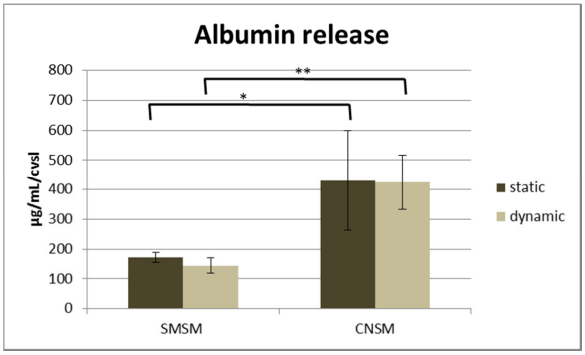

Fig. 42: Albumin release from cells in the two allometric model configurations. Static samples were the same type and number of cells cultivated in a petri dish. Data reported as concentration per coverslip; mean ± SD, * p<0.05 and ** p<0.01, n=3.

3.4.3. Urea

Urea release had the same trend as albumin. Significantly higher amounts of urea were released from cells in CNSM configuration (p<0.01) and even more in the dynamic set up (p<0.05).

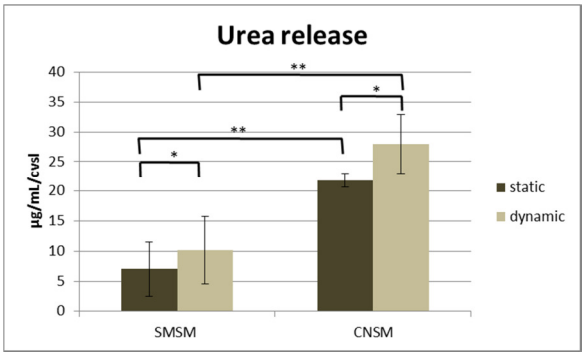

Fig. 43: Urea release from cells in the two allometric model configurations. Static samples were the same type and number of cells cultivated in a petri dish. Data plotted as concentration per coverslip; mean ± SD, * p<0.05 and ** p<0.01, n=3.

4. NP DYNAMIC TESTING WITH SINGLE TISSUE CONFIGURATION

Different concentrations of Ag were studied with HUVEC and C3A, respectively, in dynamic conditions.
The same assays as for the static NP testing, described in paragraph 1, were performed.

4.1. HUVEC

4.1.1. Cell viability

Once more, cells were analyzed for viability with Alamar and LDH assays. Unfortunately the interference of Ag NP with LDH assay the (already observed in paragraph 1.1) made the data difficult to analyze since the amount of Ag NP in the samples from dynamic experiments is unknown (adsorption of NP on the bioreactor system walls and cell uptake can influence the NP concentration in the media) so it was not possible to subtract the zero background medium/Ag NP from the experimental samples.

According to the Alamar data Ag was highly toxic to HUVEC cells under dynamic conditions from a concentration of 25 µg/mL, showing an LC_{50} of 12.13 µg/mL.

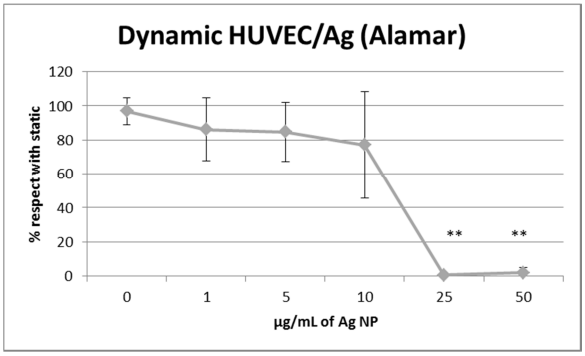

Fig. 44: Viability dose response curve for Ag treated HUVEC under dynamic conditions. Viability was assessed in terms of metabolic activity. Data are expressed as percentage of untreated-static condition HUVEC viability; mean ± SD, * $p<0.05$ and ** $p<0.01$ with respect to static control, n= at least 3.

4.1.2. Inflammation

IL8, ICAM-1 and TNFα release were analyzed as markers of inflammation. A significant increase in IL8 release was found in Ag NP treated HUVEC under dynamic conditions at a concentration of 10 µg/mL. Higher concentrations showed almost no release, perhaps due to cell death. No ICAM-1 and TNFα was detected.

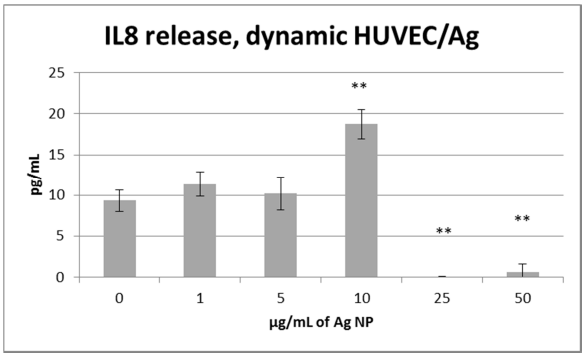

Fig. 45: IL-8 release at different concentrations of Ag NP treated HUVEC under dynamic conditions. Data are expressed as concentration (pg/mL) in the medium; control sample is untreated dynamic HUVEC; mean ± SD, * $p<0.05$ and ** $p<0.01$ with respect to control, n=3.

4.1.3. Apoptosis

Fas Ligand was measured in media sample from dynamic experiments. The results had high standard deviations because the concentrations measured were close to detection limits. A slight increase with increasing Ag NP concentration can be observed till 10 µg/mL Ag; at higher Ag levels Fas-ligand appears to decrease.

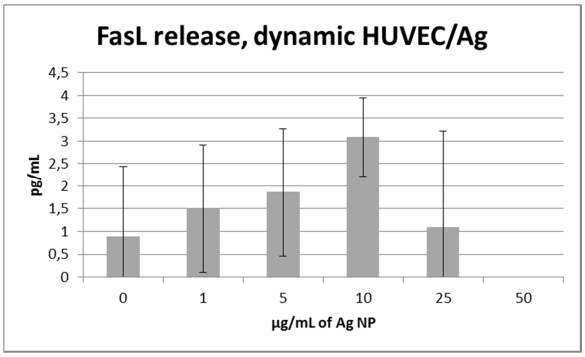

Fig. 46: Fas-L release at different concentrations of Ag NP treated HUVEC under dynamic conditions. Data are expressed as concentration (pg/mL) in the medium; control sample is untreated dynamic HUVEC; mean ± SD, n=3.

4.1.4. Cell function: von Willebrand Factor expression

vWF expression was significantly ($p<0.01$) lower than control at the highest concentration of Ag NP, likely due to cell death as explained in paragraph 1.5.

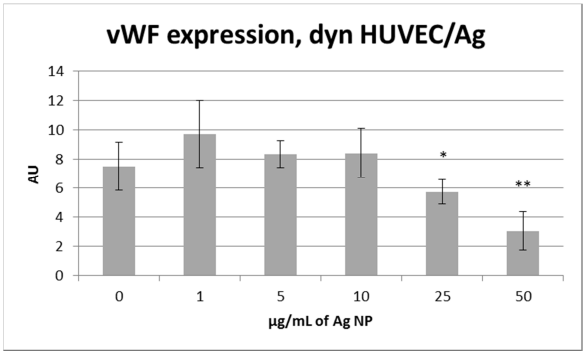

Fig. 47: vWF expression at different concentrations of Ag NP treated HUVEC under dynamic conditions. Data are expressed as arbitrary units; control sample is untreated dynamic HUVEC; mean ± SD, * $p<0.05$ and ** $p<0.01$ with respect to control, n=3.

4.2. C3A

4.2.1. Cell viability

C3A cells from dynamic experiments were analyzed with Alamar and LDH Only the Alamar assay is shown as Ag strongly interferes with the LDH assay as explained for HUVEC in paragraph 4.1.1.

NP treated C3A under dynamic conditions showed an LC_{50} of 12.37 µg/mL.

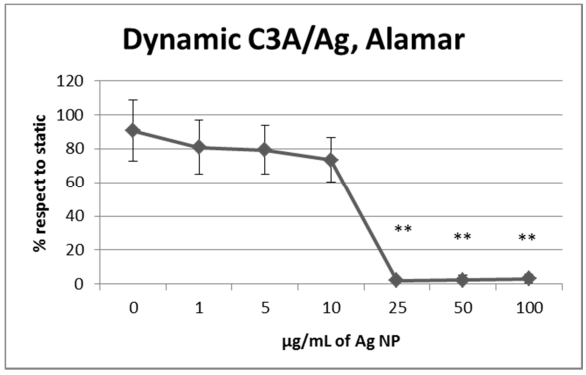

Fig. 48: Viability dose response curve for Ag treated C3A under dynamic conditions. Viability was assessed in terms of metabolic activity. Data are expressed as percentage of untreated C3A viability under static conditions; mean ± SD, * $p<0.05$ and ** $p<0.01$ with respect to control, n= at least 3.

4.2.2. Inflammation

Significant ($p<0.05$) IL8 increase at low Ag NP concentrations was found while ICAM-1 had an increasing trend proportional to Ag NP concentration, before decreasing again due to cell death. No TNFα release was detected.

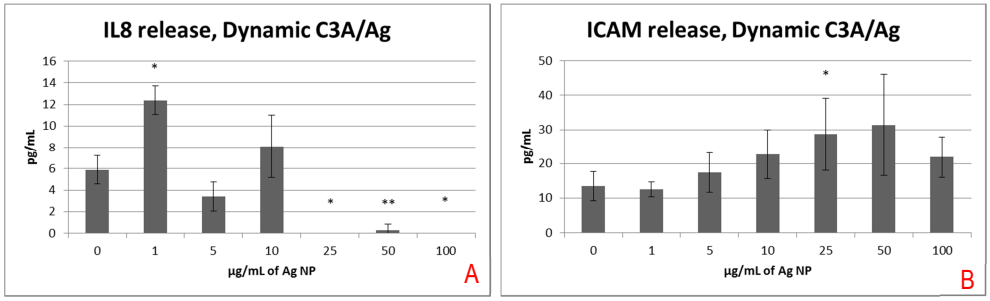

Fig. 49: IL-8 (A) and ICAM (B) release at different concentrations of Ag NP treated C3A under dynamic conditions. Data are expressed as concentration (pg/mL) in the medium; control sample is untreated C3A (dynamic); mean ± SD, * $p<0.05$ and ** $p<0.01$ with respect to control, n=3.

4.2.3. Apoptosis

Significant amounts of Fas-Ligand were released by C3A cells when exposed to low concentrations of Ag NP in dynamic conditions ($p<0.01$ with respect to control). Fas-Ligand was undetectable at higher more Ag toxic concentrations.

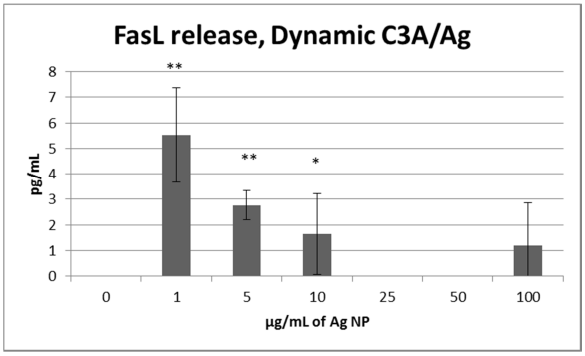

Fig. 50: Fas-L release from C3A under dynamic conditions as a function of Ag NP concentration. Data are expressed as concentration (pg/mL) in the medium; control sample is untreated C3A (dynamic); mean ± SD,* p<0.05 and ** p<0.01 with respect to control, n=3.

4.2.4. Cell function: albumin release and phalloidin expression

Albumin concentrations dropped significantly (p<0.01) when Ag NP concentrations greater than 10 µg/mL were administered, indicating damage in protein synthetic function cell state at these concentrations.

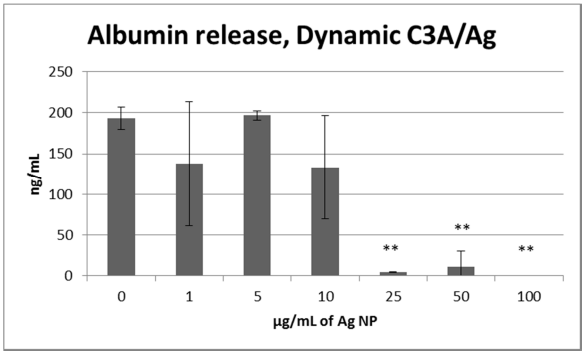

Fig. 51: Albumin release at different concentrations of Ag NP treated C3A under dynamic conditions. Data are expressed as concentration (ng/mL) in the medium; control sample is untreated dynamic C3A; mean ± SD, * p<0.05 and ** p<0.01 with respect to control, n=3.

Phalloidin expression also dropped above the same Ag concentrations as did albumin.

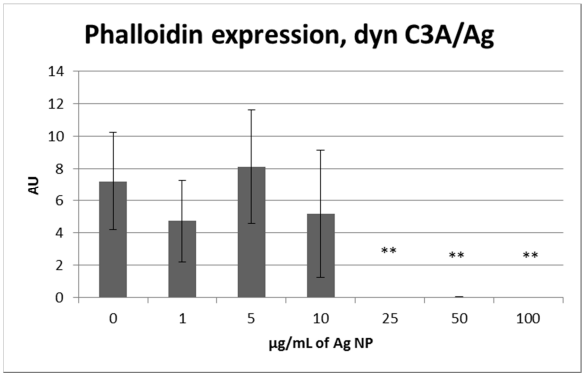

Fig. 52: Phalloidin expression at different concentrations of Ag NP treated C3A under dynamic conditions. Data are expressed as arbitrary units; control sample is untreated dynamic C3A; mean ± SD, * $p<0.05$ and ** $p<0.01$ with respect to control, n=3.

5. EVALUATION OF ILT SYSTEM BASELINE

ILT complete system was firstly checked for baseline. Negative, untreated connected dynamic culture, and Positive, TRITON X (surfactant) spiked medium connected dynamic culture, controls were used.
The same assays as for the static NP testing, described in paragraph 1, were performed.

5.1. Cell viability

Viability was tested directly on cells using Alamar Assay and media from the same experiments was used to assay LDH released from cells. When the Alamar Assay was performed a viability value for each cell type was obtained; while evaluating LDH in the media two values were measured, one from the upper circuit medium representing LDH released from CaCo-2, and the other from the lower circuit medium which is the LDH released from HUVEC and C3A.

CaCo-2, HUVEC and C3A cells showed a good viability in the connected system set up. The positive control (dead cells), as expected had a huge decrease in viability according to the Alamar Assay.

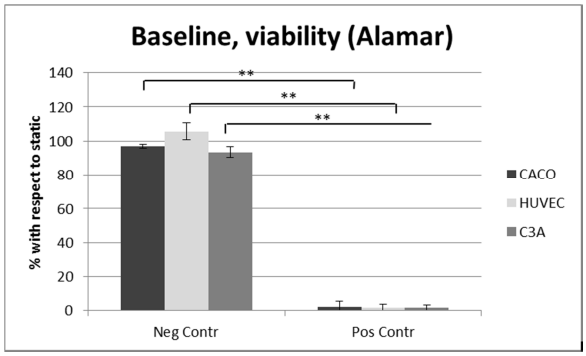

Fig. 53: Viability of cells (CaCo-2, HUVEC and C3A) in the ILT system connected culture. Negative control is the untreated cells in the ILT system and Positive Control is Triton X treated cells. Data are expressed as percentage of static cell culture viability, mean ± SD, * $p<0.05$ and ** $p<0.01$, n=4.

Media sampled from upper and lower circuits showed an increased in LDH release in the positive control (TRITON X spiked medium) while values close to the detection limit in the negative control resulted in high standard deviations. Plotting the LDH trend with respect to time (Fig. 55) showed that healthy cells (values lower than 1) were clearly different from dead cells values (higher than 1).

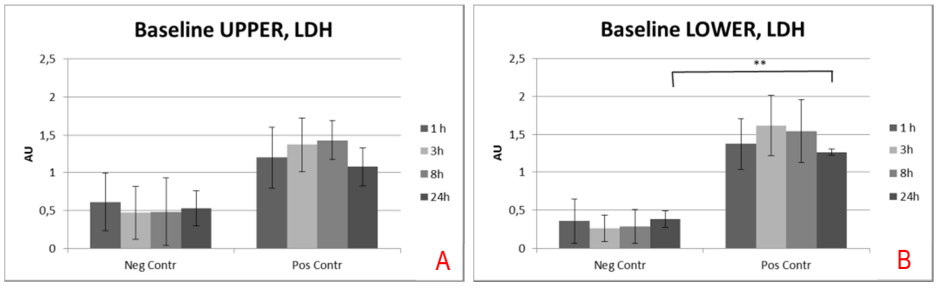

Fig. 54: LDH release from cells in the ILT system connected culture from media sampled in the upper (A) and the lower circuit (B). Negative control is the untreated cells in the ILT

system and Positive Control is Triton X treated cells in the ILT system. Data are expressed as arbitrary units, mean ± SD,* p<0.05 and ** p<0.01, n=3.

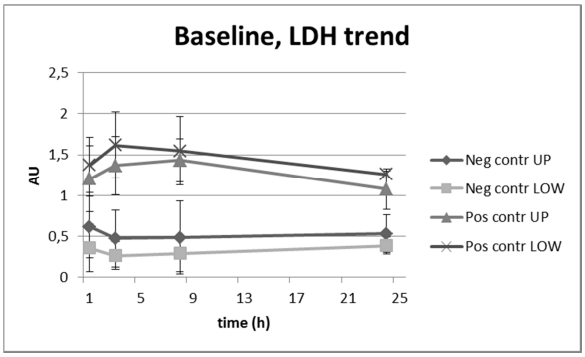

Fig. 55: LDH release from cells in the ILT system connected culture from the upper and the lower circuit medium sampling. Negative control is the untreated cells in the ILT system and Positive Control is Triton X treated cells. Data are expressed as arbitrary units, mean ± SD, n=3.

5.2. Inflammation

No IL8 release either from negative or positive controls was found (TRITON X did not stimulate IL8 release). High release of ICAM, instead, was found in the positive (TRITON X) control media.

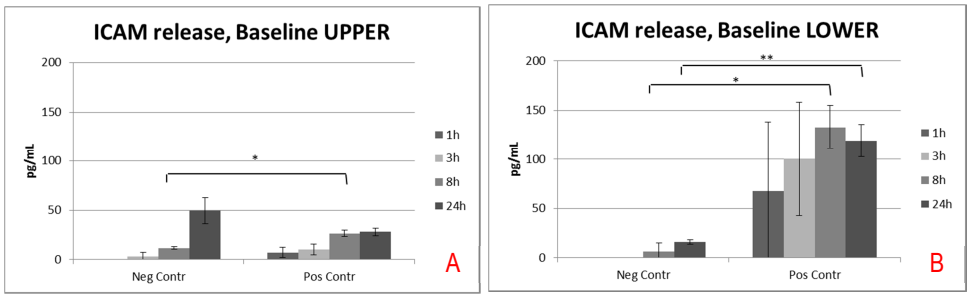

Fig. 56: ICAM release from cells in the ILT system connected culture from the upper (A) and the lower circuit (B). Negative control is the untreated cells in the ILT system and Positive Control is Triton X added medium in the ILT system. Data are expressed as concentration (pg/mL), mean ± SD,* p<0.05 and ** p<0.01, n=3.

5.3. Apoptosis

No detectable Fas-Ligand release was found in any of the analyzed samples.

5.4. Function of CaCo-2: TEER

Trans epithelial electrical resistance (TEER) was measured in order to monitor the integrity of the epithelial barrier. The expression of tight junctions within the epithelial cell layers, also give a measure of cell integrity and functionality.
CaCo-2 maintained their membrane properties during the baseline control experiment showing a constant TEER value of about 1800 Ω.

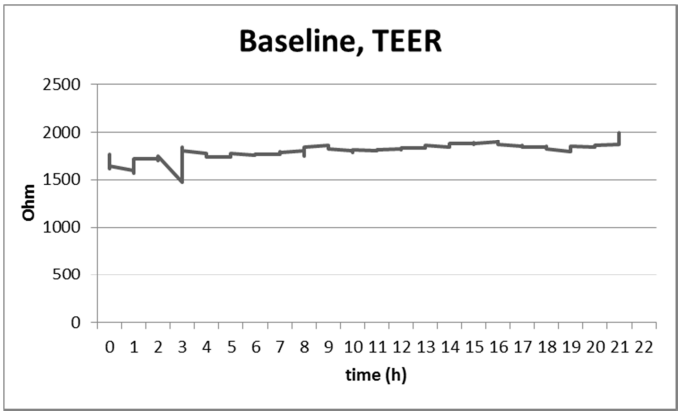

Fig. 57: CaCo-2 TEER trend in the ILT system connected culture in the negative control baseline experiment. Data are expressed as resistance (Ohm) during the experiment.

Rapid loss of barrier function was observed in the positive control (data not shown).

5.5. Function of HUVEC: von Willebrand Factor expression

HUVEC cells were stained for vWF (as described for the static protocol) after each experiment. Digital images of cells were analyzed by quantifying

the total intensity of red pixels using ImageJ. The analysis showed a significantly ($p<0.01$) higher fluorescence in the negative control with respect to positive control.

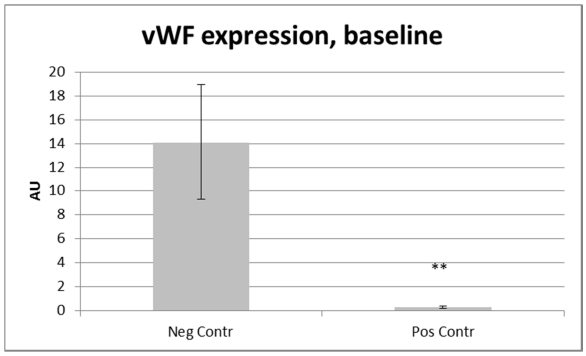

Fig. 58: vWF expression in the ILT system connected culture. Negative control is the untreated HUVEC culture in the ILT system and Positive Control is Triton X spiked medium in the ILT system. Data are expressed as arbitrary units, mean ± SD,* $p<0.05$ and ** $p<0.01$, n=3.

5.6. Function of C3A: albumin release and phalloidin expression

C3A hepatocytes release high amounts of albumin in the lower compartment in baseline conditions. On the other hand when the negative control experiment was performed, lower release was found in the positive control where the cells were exposed to Triton surfactant. No albumin was found in the upper circuit in the negative control experiment while some really low concentration can be detected in the positive control where the epithelial barrier was clearly damaged, allowing the passage of molecules from the lower to upper circuit.

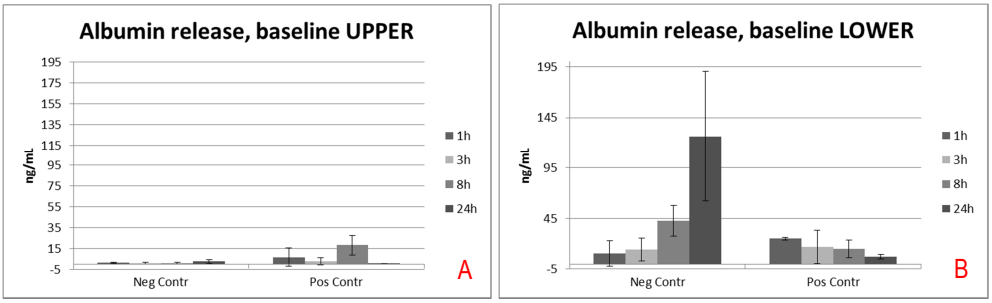

Fig. 59: Albumin release from C3A in the ILT system connected culture from the upper (A) and the lower circuit (B). Negative control is the untreated cells in the ILT system and Positive Control is Triton X spiked medium in the ILT system. Data are expressed as concentration (ng/mL), mean ± SD, n=3.

Microscopic analysis of hepatocytes stained for phalloidin showed a highly significant ($p<0.01$) difference between the two experimental protocols with almost no expression in the positive control.

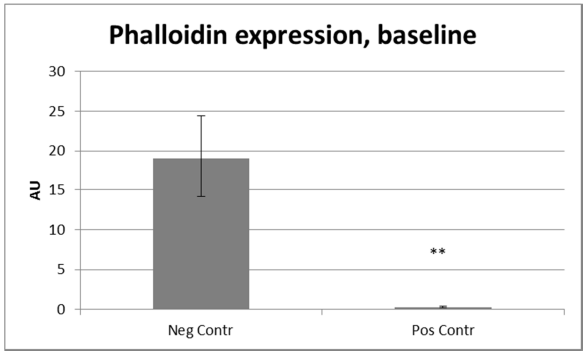

Fig. 60: Phalloidin expression in the ILT system connected culture. Negative control is the untreated cells in the ILT system and Positive Control is Triton X spiked medium in the ILT system. Data are expressed as arbitrary units, mean ± SD, * $p<0.05$ and ** $p<0.01$, n=3.

6. NPs TESTING IN ILT SYSTEM

In this section the NP testing within the ILT system was reported. Polystyrene-FITC 55 nm NP was used to characterize the system, and then preliminary results from Ag NP testing were shown.

6.1. Polystyrene-FITC 55 nm NP

In order to evaluate the passage across the intact epithelial barrier, polystyrene-FITC 55 nm NP (PS NP) were used. A high upper circuit concentration (1mg/mL) was chosen in order to have a detectable lower circuit concentration. Moreover viability, inflammation, apoptosis and cell function were tested.

6.1.1. Viability

Cells showed a good viability with respect to controls, comparable to the static condition toxicity analysis.

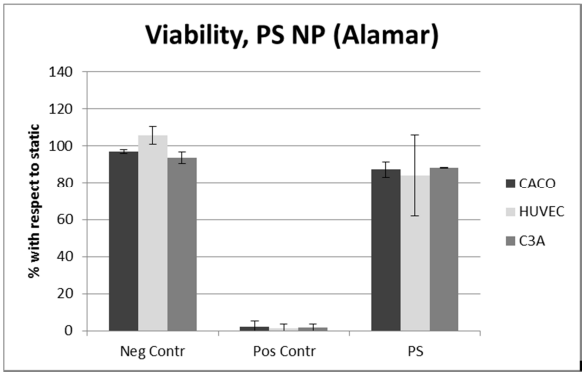

Fig. 61: Viability of cells (CaCo-2, HUVEC and C3A) in the ILT system connected culture. Negative control is the untreated cells in the ILT system and Positive Control is Triton X treated cells in the ILT system. Data are expressed as percentage of static cell culture viability mean ± SD, n=3.

6.1.2. Inflammation

A significant ($p<0.01$) IL8 release was found in the lower circuit, while almost no ICAM was released from both circuits.

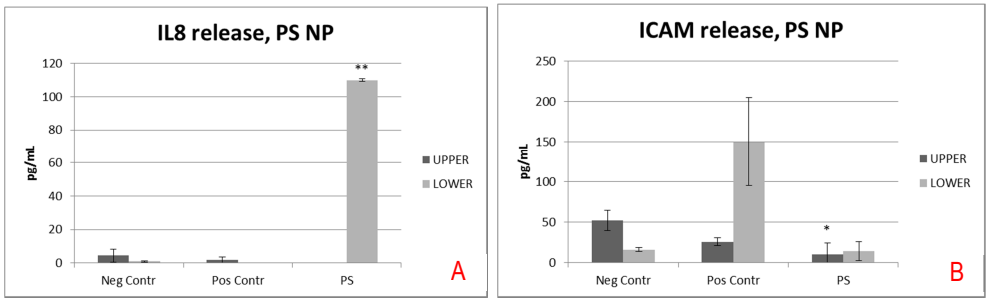

Fig. 62: IL8 (A) and ICAM (B) release from cells in the ILT system connected culture from the upper and the lower circuit medium sampling. Negative control is the untreated cells in the ILT system and Positive Control is Triton X spiked medium in the ILT system. Data are expressed as concentration (pg/mL), mean ± SD, * $p<0.05$ and ** $p<0.01$ with respect to negative control, n=3.

6.1.3. Apoptosis

No Fas-L release was observed in the PS NP experiment.

6.1.4. Function of CaCo-2: TEER

A constant TEER value of 1934.24 ± 109.17 Ω was maintained during the PS NP experiment (data not shown).

6.1.5. Function of HUVEC: vWF expression

Expression of vWF from HUVEC in the lower circuit of PS-FITC 50 nm experiment was found to be slightly lower than the control sample.

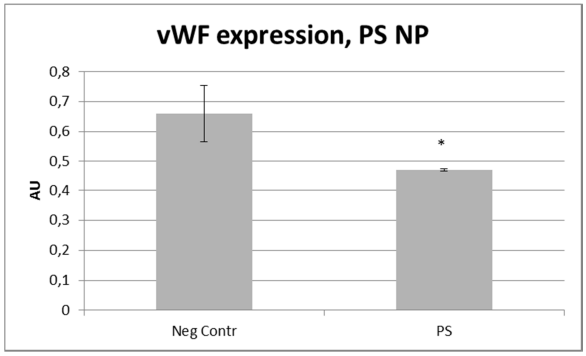

Fig. 63: vWF expression from HUVEC in the ILT system connected culture. Negative control is the untreated cells in the ILT system. Data are expressed as arbitrary units, mean ± SD, * $p<0.05$ and ** $p<0.01$ with respect to control, n=3.

6.1.6. Function of C3A: albumin release

Albumin levels were comparable to negative controls in both circuits in the PS NP experiments.

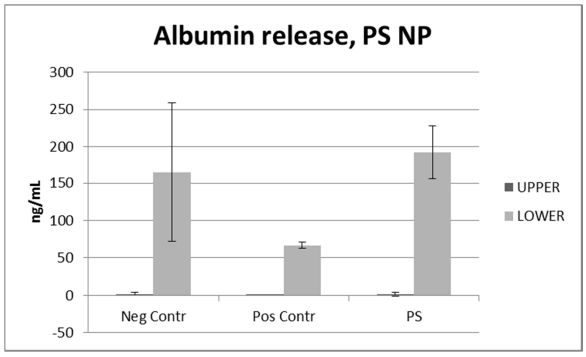

Fig. 64: Albumin release from C3A in the ILT system connected culture from the upper and the lower circuit. Negative control is the untreated cells in the ILT system and Positive Control is Triton X medium in the ILT system. Data are expressed as concentration (ng/mL), mean ± SD, n=3.

6.1.7. PS-FITC 50 nm NP passage evaluation

100 µL of medium sampled from lower circuit at 1 h, 3 h, 8 h, 24 h were measured. All samples were found to be under the limit of detection (0.01

mg/mL). However subsequent confocal analysis showed fluorescent PS NPs on HUVEC and C3A coverslips after 24 h of PS NP circulating in the upper circuit of the ILT complete system (Fig. 65 and 66). This indicates that the NPs did cross the epithelial barrier.

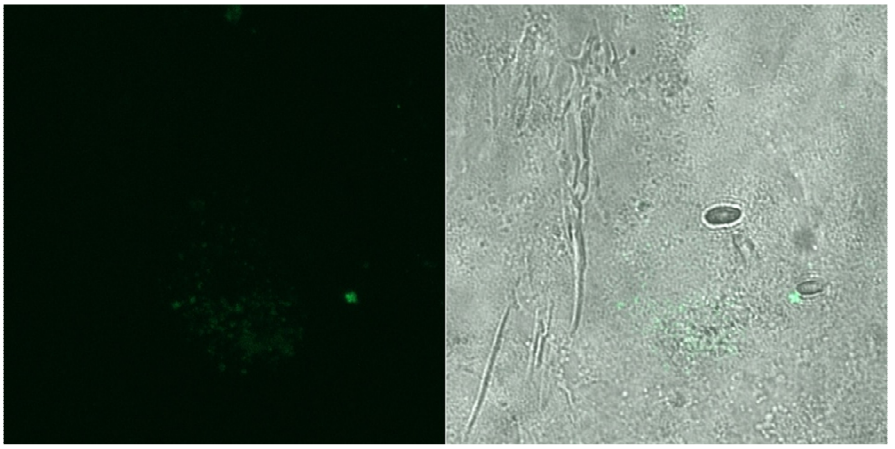

Fig. 65: PS-FITC NP (green dots) on HUVEC cells after passage across the intestinal epithelium in the ILT complete system. Fluorescent micrograph (on the left) and its overlapping with white light image (on the right). Magnification 63 X plus zoom 20.

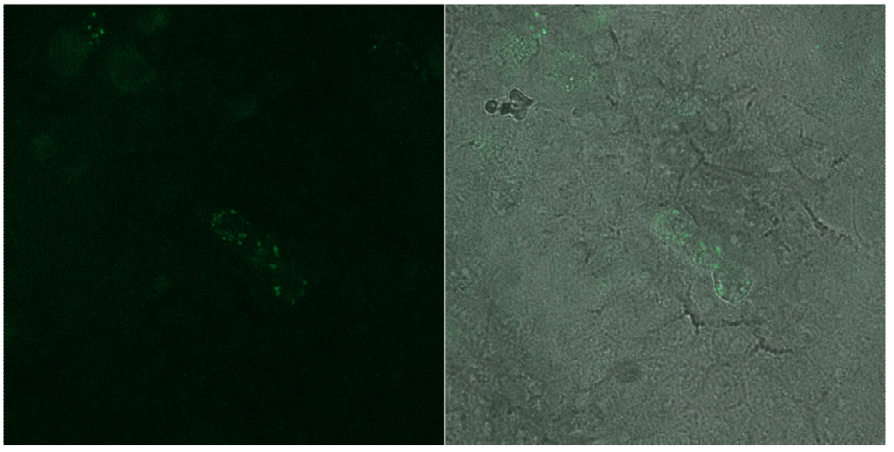

Fig. 66: PS-FITC NP (green dots) on C3A cells after passage across the intestinal epithelium in the ILT complete system. Fluorescent micrograph (on the left) and its overlapping white light image (on the right). Magnification 63 X.

6.2. Ag NP preliminary results

Two concentrations (50 µg/mL and 200 µg/mL) of Ag NP were tested in the ILT complete system and standard analyses were performed. Preliminary results are shown.

6.2.1. Viability

CaCo-2 viability decreased with increasing concentrations of Ag NP (50 to 200 µg/mL), while cells in the lower circuit maintained a good viability.

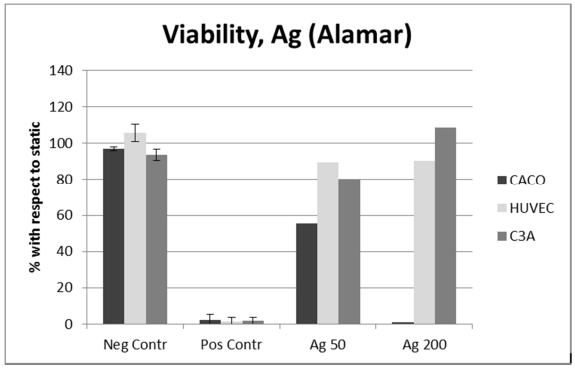

Fig. 67: Preliminary viability results (CaCo-2, HUVEC and C3A) from Ag NP experiments in the ILT connected culture system. Negative control is the untreated cells in the ILT system and Positive Control is Triton X treated cells in the ILT system. Data are expressed as percentage of static cell culture viability mean ± SD, n=3 for controls, n=1 for Ag NP.

6.2.2. Inflammation

High inflammation through the IL8 pathway but not ICAM was found in the lower circuit of samples from Ag NP experiments. Slightly higher ICAM concentrations with respect to controls were found in the upper medium.

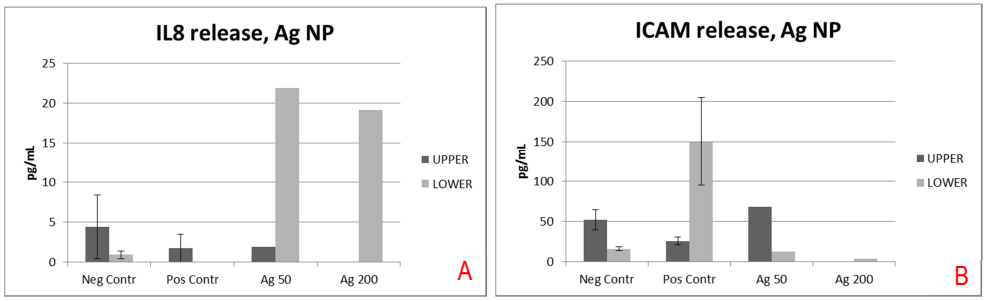

Fig. 68: Preliminary IL8 (A) and ICAM (B) release results from Ag NP experiments in the ILT connected culture system from the upper and the lower circuit. Negative control is the untreated cells and Positive Control is Triton X treated cells in the ILT system. Data are expressed as concentration (pg/mL) ± SD, n=3 for controls, n=1 for Ag NP.

6.2.3. Apoptosis

No apoptosis marker was found in the analyzed samples.

6.2.4. Function of CaCo-2: TEER

A constant decrease in the TEER value was measured in CaCo-2 cells exposed to Ag 50 µg/mL during the experimental time.

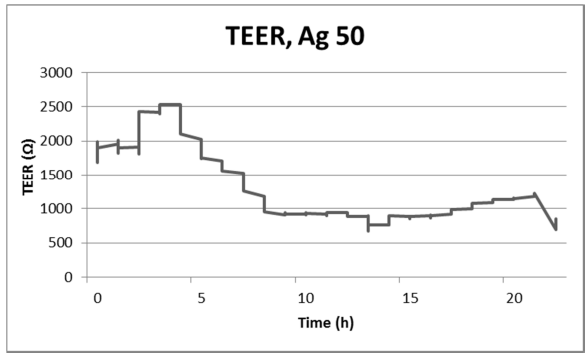

Fig. 69: CaCo-2 TEER trend in the connected culture ILT system in the Ag 50 µg/mL experiment. Data are expressed as resistance (Ohm) during the experimental time

In the Ag 200 µg/mL experiment a quicker drop down in the TEER value was observed (data not shown).

6.2.5. Function of HUVEC: vWF expression

No change in HUVEC vWF expression was observed in the Ag 50 µg/mL experiment (upper circuit only), while a slight decrease was detected when adding Ag 200 µg/mL to the upper circuit of the ILT system.

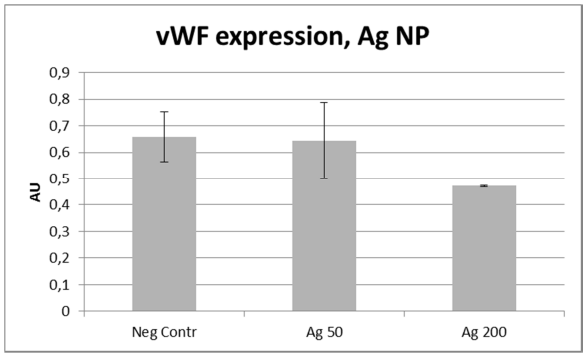

Fig. 70: vWF expression from HUVEC in the connected culture ILT system. Negative control is the untreated cells in the ILT system. Data are expressed as arbitrary unit ± SD, n=3 for controls, n=1 for Ag NP.

6.2.6. Function of C3A: albumin release

A concentration dependent decrease in albumin release was found with respect to control sample.

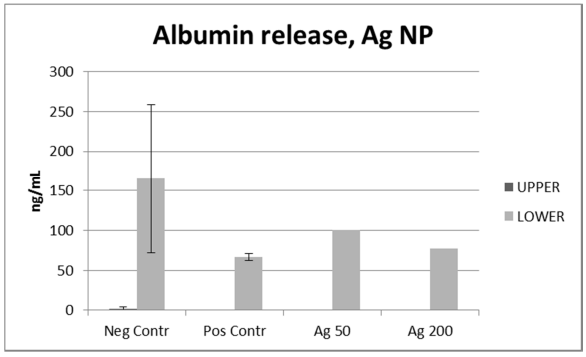

Fig. 71: Preliminary Albumin release results from Ag NP experiments in the ILT system connected culture from the upper and the lower circuit. Negative control is the untreated cells in the ILT system and Positive Control is Triton X treated cells in the ILT system. Data are expressed as concentration (ng/mL) ± SD, n=3 for controls, n=1 for Ag NP.

Chapter 7

Discussion

The aim of this thesis is the validation of a new *in vitro* method to assess NPs toxicity so as to gain new insights into the nano-world and its safety.
Development of a new method means creating a new system and new optimized protocols to use it. Further, the more integrated is the system, the more simplifications are needed to deal with the process step by step (from static culture to dynamic culture to connected dynamic culture) and be able to understand data from the most complex method.
Finally in order to validate a new method comparison with standard protocols is required, to see whether improvements come out from the new approach.

1. ESTABLISHMENT OF NPs TESTING ON HUVEC STATIC CULTURE

The standard *in vitro* method accepted by the scientific community is certainly the petri dish/multiwell cell culture. Besides providing comparative data, the standard cell culture experiments definitely represent a first, if somewhat simplistic, insight into NP toxicity on HUVECs. Knowing the effect of chosen the NPs on a simple culture also serves to better orient the ILT system approach.
NPs toxicity and sub lethal effects on HUVEC were checked at different levels, with different assays. The reason for this choice was due to the NP interference with assays as already mentioned in paragraph 1.1, chapter 6.

When data from two different assays are concordant with each other the probability that we have reliable data is really high [110].

Both Alamar Assay and LDH Assay confirmed that Ag NP and TiO_2 NP were highly toxic for HUVEC (Fig. 17, chapter 6); although was not possible to overlap the LC_{50} values, maybe due to difference in the sensitivity of the two methods. In any case the LC_{50} values were both very low.

Polystyrene-FITC of both sizes (PS 50 nm and PS 200 nm) were not toxic while a slight toxicity can be ascribed to Au NPs (both sizes). Data from these NPs also confirmed that neither viability assay was subject to interference. As matter of fact these chosen assays have really different experimental protocols: the Alamar Assay has to be performed directly on cells and is based on their capability to metabolize a reagent (added to fresh medium without suspended tested NPs); the LDH assay is an enzymatic assay performed on medium samples to detect LDH release from damaged cells. Viability is the basic level to assess toxicity so it's really important to have meaningful data from more than just one assay.

Yet, NPs have many other effects besides cell death [111]. Often NPs induces oxidative stress or inflammation and can lead to apoptosis or necrosis [112-114]. Based on this principle other markers were assayed. Oxidative stress due to free radical formation in the presence of NPs is one of the most important sub-lethal reactions to occur in cells after NP treatment [115], [116]. Unfortunately, no detectable marker of oxidation was found using the GSH assay. This was attributed to the relatively low number of cells which did not produce a suitable GSH concentration for detection (Fig. 21). As the number of cells is even lower in ILT system than in the standard, leading anyway to undetectable comparable data the GSH assay was eliminated from the test list.

Continuing with sub lethal analysis, inflammation was studied evaluating either IL8 and ICAM-1, and TNFα as markers. No detectable TNFα was measured in any of the samples. High IL8 levels were found in all samples

except for PS NPs, which showed a small decrease at the highest concentration (Fig. 22). Only PS 50 nm at highest concentration had a slight increase in released ICAM (Fig. 23), suggesting that relevant concentrations of these particles do not induce inflammation, and only high amounts of the smaller PS (50 nm) initiate pro-inflammatory signals. The most toxic NPs, Ag and TiO_2, released a huge amounts of IL8, but only in TiO_2 samples was ICAM release increased. This result was really interesting, hinting the point that inflammation can be triggered at different levels and involve different markers (ICAM-1 is known to be stimulated by IL1 and TNFα [117-119]) depending of the type of NPs. In fact, Au NPs showed both high release of IL8 and ICAM-1 (Fig. 22 and 23), higher ICAM for Au 80 nm with respect to Au 15 nm while higher levels of IL8 were observed for the smaller Au NPs. These NPs seem to activate both pathways, but in a size dependent manner.

In summary, Ag trigged inflammation through an IL8 involved pathway and did not have any effect on ICAM. Both TiO_2 and Au 15 nm triggered inflammation by IL8 and ICAM pathways, but principally the one involving IL8, while Au 80 nm evidently activates the ICAM signaling pathway to a greater extent than the IL8 one.
Whatever the pathway is, the data showed as almost every NP induces inflammation, even at low concentrations.
It is possible to theorize for Ag NP, for example, a first state of inflammation that can lead to some apoptosis (Fig. 24) and cell death. A different process, not ending in cell death, was found with PS 50 nm NP, which induced slight (Fig. 23) or no inflammation (Fig. 22) but had an interesting increase in Fas-L, the apoptosis marker. It seems that these NPs induce at most a slight inflammation by a non-IL8 pathway that then induces the initiation of apoptotic processes.

Looking at the functional marker, von Willebrand Factor, a nice correlation in the trend of its two expression levels in Ag treated cells is shown. After an

increase in the vWF expression around a few µg/mL of Ag NP, the signal dropped down at both mRNA (Fig. 25) and protein level (Fig. 27). This decrease can be ascribed to cell death which resulted in fewer cells being stained or processed for mRNA extraction. However, no correlation in the TiO_2 treated cells between mRNA and protein expression was observed for vWF. A similar to Ag trend was present in the vWF staining for the TiO_2 treated HUVEC (Fig. 28) even if a lower increase at 3 µg/mL of concentration was found; on the other hand mRNA expression decreased with TiO_2 concentration. This inconsistency was maybe caused to the high interference of the particles with the extraction (purity of mRNA content for TiO_2 treated cells was always low, in a concentration dependent manner). As matter of fact, considering the high level of inflammation through different pathways and the high interference with mRNA extraction, it is likely that even vWF expression was increased, in accordance with the vWF immunostaining data.
mRNA expression data showed that Au 15 nm but not Au 80 nm was able to slightly compromise HUVEC functionality of vWF production (Fig. 25).
No relevant vWF expression from PS NPs was observed, confirming that these NPs do not trigger inflammation.

Those data all together (summarize in table 10) represent a first insight into NP toxicity on HUVEC cells.

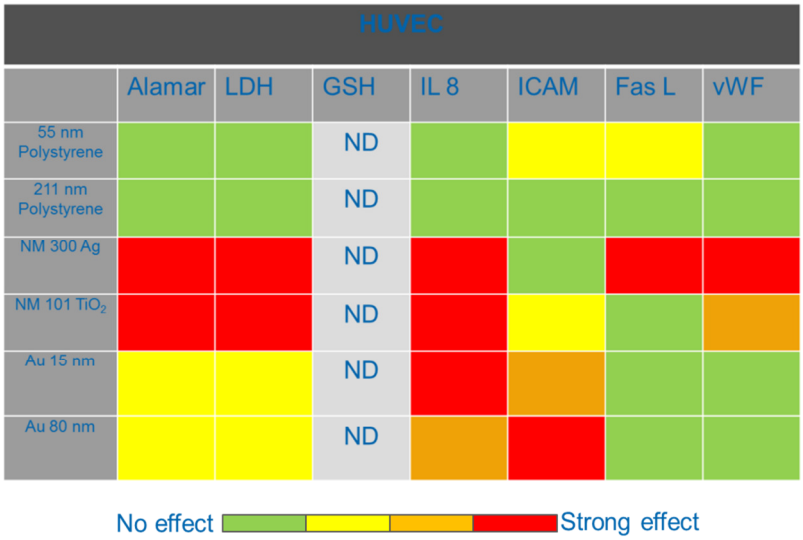

Tab. 10: Summary of determined toxicity levels of tested nanoparticles on HUVEC cells; ND = not determined; green = not toxic over the determined concentration range; yellow = slight toxicity at high concentrations; orange= medium toxicity and red = high toxicity

The data showed that some NPs like Ag and TiO_2 were more toxic than others. Moreover, sub-lethal effects showed that other outcomes besides the impairment in viability can occur in NP treated cells. In fact, low toxicity PS 50 nm NP was shown not to induce any inflammation, but did induce the apoptotic pathway, which may underlie a low level in cell death. Were only data on inflammation to be recorded, it could lead to a wrong safety classification.

In addition a high dependency on NP type (Ag, TiO_2 and Au) and even sizes (Au 15 and Au 80 nm NPs) in the induced effects is evident.

Finally, different pathways can be involved behind the high levels of inflammation observed in most cases, once more depending on the type and size of NPs.

2. IDENTIFICATION OF COMMON DYNAMIC CULTURE CONDITIONS

The first step in an *in vitro* co-culture is to find the optimum conditions for the common culture. Different media from the simplest to the most enriched one were tested. HUVEC cells were found to be the most sensitive cells to different media (Fig. 29); this result was not surprising since these were the only primary cells to be used in the experiments (CaCo-2 and C3A are cell lines). C3A did not appear to be influenced by medium content variations (Fig. 31) while CaCo-2 proliferation was stimulated to by all the media but it had a constant trend in the ILT medium (Fig. 32). According to these data the ILT medium was chosen as the best one for co-culture.

As the ILT approach involves not only connected culture but also flow conditions, it is necessary to find the optimum range of flow rates.
It is known from Mazzei et al. [93] that the limit for the ILT0 bioreactor to have laminar flow and suitable oxygen concentration is 1 mL/min; several flow rates below this limit were tested both with HUVEC cells (more sensitive as primary cells but more resistant to shear stress) and C3A cells (more resistant as cell line but sensitive to shear stress).
Good viability was found at flow rates lower than 500 µL/min, while C3A had a peak of viability at 80-100 µL/min, HUVEC did better at slight higher flows between 100-250 µL/min (Fig.33).

Looking at the functionality markers, HUVEC showed constant or slightly increased expression of vWF from 100 to 1000 µL/min (Fig. 34), while C3A had a slightly higher uptake of glucose under flow with respect to static conditions (Fig. 35 A), a significant increase from 0 to 200 µL/min of albumin release (more healthy cells accordingly to the viability data) and a constant urea release (Fig. 35 B and C).
An important point is that all the samples were compared with respect to a control which was not only same cells and culturing day with respect to the

dynamic ones but also same type and volume of medium in order to avoid problems like concentration dependent release.

It is clear from the viability and cell function results that the best flow rate for HUVEC and C3A cells, that is for the lower ILT system circuit, was 100 µL/min. Results from flow rate testing of CaCo-2 (testing was performed by another research group) showed a good viability at any flow rate below 1 mL/min, so 200 µL/min was chosen as the flow rate for the upper circuit (intestinal barrier) in order to increase the passage of NPs (thanks to a higher upper flow rate with respect to the lower) and the number of times the medium circulates during a single experiment, so mimicking a bigger surface area for intestinal epithelia.

3. ALLOMETRIC SCALING

In order to recreate the most physiological *in vitro* system for the intestinal tract, two different allometric scaling models were tested.
The reader is reminded that SMSM is the acronym for “Surface and Metabolic Scaling Model” containing 25 000 HUVEC cells and 1 000 000 C3A cells; while CNSM is the “Cell Number Scaling Model” with 25 000 HUVEC cells and 250 000 C3A cells.
Focusing on the metabolic compartment we studied relationship between hepatocytes and endothelial cells, their cross-talk and tried to identify which of the two models better represents physiological state.

With this aim we analyzed metabolic and functional markers. As viability data were good in both models, the study was focused on hepatocytes which are multi-functional cells able to perform both carbohydrate and fat metabolism and storage. The model closer to the *in vivo* situation will be the one to be use in the ILT system.

Starting from the simplest and main metabolic analysis, glucose concentration was significantly lower in the SMSM configuration than the

CNSM (Fig. 36), meaning a higher uptake of sugar from the medium. This data anyway could be due to the higher number of cells in the SMSM (about 4 fold more) with respect to CNSM. In fact considering the concentration per cell, in the CNSM cells consumed more glucose in the dynamic set up with respect to the SMSM. In face of a higher uptake of glucose, higher D-lactate amounts per cell were released in CNSM, reaching total D-lactate values similar to the SMSM configuration (Fig. 37). It is known that *in vivo* high glucose uptake corresponds to increased production of D-lactate through the glyoxalase pathway; a similar mechanism may have occurred in the CNSM configuration. In fact in this model we observed more glucose intake per cell and also a higher D-lactate release that reached the level of the in SMSM (due to higher amount of cells). This could indicate that CNSM was more able to equilibrate the stress of high cytoplasmic glucose concentrations.

The second most important mechanism for energy production in humans is fat metabolism.
Relevantly higher triglyceride uptake was shown in the CNSM where the triglyceride concentration per cell in the dynamic set up was 8 fold less with respect to the concentration per cell in the SMSM (Fig. 38). This result means that cells in the CNSM were undergoing higher triglyceride turnover than in the SMSM, so indicating that in the CNSM cells were producing energy by fat metabolism at a higher level than in the SMSM.

The FFA uptake results are interesting and significant ($p<0.01$) (Fig 39).
It is known from Vinci et al.[98] that FFA uptake in hepatocytes does not differ between the static and dynamic set up; in contrast HUVEC cells are highly sensitive to flow and the FFA turnover is inverted: the cells uptake FFA in static conditions and release it in high amounts under flow conditions.
Keeping this in mind, the data in figure 39, chapter 6, can be interpreted as a sort of additive effect from static to dynamic, performed by HUVEC and hepatocytes. In static condition HUVECs slightly helped the FFA uptake of

C3A, which had the predominant role being considerably more cells with respect to HUVEC. The amount of cells also explains why the uptake in SMSM model was higher (6 fold more) than that in CNSM with lower cells content. The most interesting behavior in FFA motion was surely represented by the dynamic condition. In this configuration HUVEC competed with hepatocytes in the direction of FFA movement: lower uptake was shown in SMSM as the few amount of HUVEC (40 fold less cells) releasing FFA cannot overpass the high uptake of hepatocytes.
A complete overturn in the FFA trend was carrying out by HUVEC in the dynamic CNSM configuration, where high FFA release from HUVEC hided the C3A uptake, resulting in a final release. This high secretion of FFA can be due to the higher metabolism of triglyceride as confirmation that this molecule was not only up taken but also metabolized.

Glycerol data showed no difference between static and dynamic (Fig. 40); in SMSM uptake was slightly more than in CNSM, anyway there is reason to believe that a higher uptake of glycerol in CNSM configuration was hidden by some glycerol released from the high triglyceride metabolism. In CNSM, triglyceride and FFA analysis demonstrated as triglycerides were highly took up and also consumed. From each metabolized triglyceride molecule 3 FFA and one glycerol is released, so there should be a high release of glycerol together with the uptake measured in the samples. This consideration led to a theoretical higher intake of glycerol in CNSM with respect to SMSM, meaning again a higher metabolism.

In conclusion metabolism analysis showed a closer to *in vivo* physiology for CNSM model with an *in vivo* D-lactate trend, high fat metabolism with higher amount of products.

At this point, functional marker analysis is really important to see whether these results correspond to a higher functional state of cells in CNSM.

According to Cyt P450 evaluation lower metabolic activity was attributed to dynamic CNSM configuration. Anyway has to be underlining as cytochrome P450 3A4 is only one isoform of the hundreds housed in hepatocytes. Moreover, cannot be overlooked the fact that as cells line C3A cytochrome metabolic activity can be compromised with respect to physiological level [109].

Carrying on the functional marker analysis, albumin and urea release is surely one of the main functions of hepatocytes.

Albumin concentration per cells was more than twice increased in CNSM with respect to SMSM in both static and dynamic, indicating that a great key role was carrying out by cell cross-talk rather than the dynamic condition (Fig.42). Urea analysis demonstrated the both main role of co-culture and dynamic culture. Higher urea release was found in the dynamic set up, where cell are more stimulated by flow; but even higher is the concentration per cells in CNSM then in SMSM (Fig. 43).

These data confirmed the result obtained in the metabolism analysis, being also the marker of functionality closer to *in vivo* in the Cell Number Scaling Model.

This study demonstrated as high importance has to be given to the advanced *in vitro* model in order to find relevant physiological condition. Not only cross-talk and physical stimulus played an import role within the *in vitro* model, but also the exact relationship between cells is crucial to recreate the regular state of in-vivo in which cells feel suitable and equilibrate signals.

It has to be taken in account that most of the pathological state can be due to different relationship between cells numbers or signaling, like in hypertrophies or in several disease like Parkinson where less cells of the substantia nigra give failure in the signals lead to degenerative disorder.

Working with random number of cells in a co-culture could give rise to pathological state model rather than physiological.

In this part it was demonstrated as allometry improved the dynamic connected culture and orientated the choice for a suitable model of intestinal tract.

4. NP DYNAMIC TESTING WITH SINGLE TISSUE CONFIGURATION

The next level in the development of advanced models was to go a step further in complexity. From NP assessment in standard static cultures, once dynamic parameters were set, it was possible to increase the complexity and the resemblance to the *in vivo* scenario by first assessing NP toxicity in dynamic conditions.
Target tissues were tested separately under flow conditions and the most toxic nanomaterial, Ag NP was chosen as the first to be tested as significant toxic effects were expected.

Interestingly Ag toxicity under flow conditions both for HUVEC and C3A (Fig. 44 and 48) was higher with respect to static conditions (Fig. 17 A), showing an LC_{50} of 12.1 µg/mL instead of 25 µg/cm^2 for HUVEC and decreasing from 23 µg/cm^2 [120] of the static culture to 12.4 µg/mL for C3A in dynamic conditions. High IL8 release was found in both HUVEC static and dynamic set up at the Ag concentration close to the LC_{50} value, while again low ICAM-1 concentration was measured in the dynamic samples, mirroring the static behavior. The apoptosis levels were comparable too, even though the IC_{50} values were different.
Another interesting result was the vWF expression which was not significantly higher at low Ag concentration with respect to the control as observed for the static experiments. In order to understand this data it is important to underline that vWF is also a marker of shear stress in HUVEC: higher expression of this factor under flow with respect to static conditions is well known in the literature [106], so the flow stimulated vWF expression can hide the stimulation due to the presence of the particles.

Analysing C3A inflammatory markers, the results under flow were comparable to the static data, showing an increase in the release, up to the IC_{50}, after which it declined due to cytotoxicity [120].

In conclusion in dynamic experiments Ag NP triggered all the effects observed in the static culture but at lower Ag concentrations, demonstrating the important role of the flow in effecting the cells response to molecules and particles.
Physiologically no system is in a completely motionless state, cells are always subjected to some kind of dynamicity, from high vascular to interstitial flow.
These data demonstrates that dynamic conditions are an important feature to take into account when assaying the effect of drugs or molecules. In this case a higher (the lethal dose was about half) toxicity of Ag NP was shown, pointing out the importance of physiological relevance and more closely approximating the *in vivo* situation when the aim of the work is to test toxicology and create a safety report for new materials.

5. ILT COMPLETE SYSTEM BASELINE

The three tissue model for absorption, distribution and metabolism should first be able to maintain cells in a healthy and functional state.
With this aim the ILT complete system was tested to see whether is possible to distinguish between the healthy and highly toxic conditions. In these experiments the baseline control of healthy cells in the 3 tissues ILT system was referred to as "negative control", the static single cell culture was "static control" and the highly toxic conditions in the 3 tissues ILT was "positive ILT control".

The negative control untreated cells showed that viability under flow conditions in the three tissue configuration was comparable to the static

control. No inflammation or apoptosis was found, while markers for functionality were expressed at high levels.
In the positive ILT control (TRITON X) with dead cells, LDH from lower circuit was significantly ($p<0.01$) higher than baseline-negative control data in the 24 h (Fig. 54), while in the upper circuit the handling of CaCo-2 while assembling the system may have induced some stress on the cells but the difference between the static CaCo-2 control and the complete ILT system was insignificant ($p=0.056$). It was possible to ascribe this stress to the initial step of the experiment observing the 1 h data that was already quite high (Fig. 54 A). Anyway the low level of stress did not affect the function of the CaCo-2 as demonstrated by the TEER data in figure 57, chapter 6.
Strangely a slight decrease in LDH content in the 24 h with respect to earlier sampling for the positive control experiment can be noted; this might indicate an LDH adsorption to the tubing or the bioreactor walls or a TRITON associated degradation of LDH (Fig. 55).

Looking at the inflammation markers, the under detection limit data were expected both from baseline and TRITON-X samples. In fact, no inflammation should be present in the negative control, but neither is TRITON-X able to induce inflammation on cells.
Results concerning ICAM-1 concentration in the upper circuit seems to be due more to flow stimulation on CaCo-2 cells in the negative control, since the concentration increased in time (Fig. 56 A), while a constant amount of ICAM-1 was found in the positive control (Fig. 56), this time due to an initial high release, finding comparable values during the 24 h.

CaCo-2 function was demonstrated by the integrity of the cell layer: after a small period of adjustment in the resistance value, the trend was constant. Small variations in the measurement correspond to the sampling times (1 h, 3 h, 8 h), during which the system had to be manipulated slightly to allow the sampling (Fig. 57).

The expression of stained markers in HUVEC and C3A was significantly ($p<0.01$) higher in the negative control than in the positive control (Fig. 58 and 60).

Further relevant data were provided by the albumin analysis. As expected for the negative controls, no albumin was detected in the upper circuit (no hepatocytes there) while a high concentration was found in the lower circuit where functional hepatocytes released high amount of albumin (Fig. 59). Comparable low values were found, instead, in both circuits in the positive control where dead cells were not able to release significant amount of albumin, but also where the open barrier of a dying intestinal epithelium allowed the passage of some albumin from the lower circuit (Fig. 59).
This last result confirms the relevance of the ILT system: when an intact epithelial layer was present, barrier properties were shown, preventing even the passage of small molecules like albumin; when the barrier was compromised passage across the membrane was possible and basolateral molecules could be found in the CaCo-2 apical tract.

This data clearly show that an advanced *in vitro* system able to reproduce barrier properties as in the intestinal tract was developed. The system is also able to recreate a multi-organ environment so as to have cross-talk between cells and an environment which is closer to the physiological *in vivo* milieu.

6. NPs TESTING IN ILT SYSTEM

Having demonstrated that the ILT system worked, it was possible to start NP testing with the ILT method.
The last part of this thesis was addressed towards the evaluation of NP passage across the intact cell barrier.

From previous studies it is known that NP passage through the ILT membrane without cells is around 10-15%. To perform this study it was

chosen to use the fluorescent PS-FITC NP either for the easiness of measuring high-fluorescence NP either thanks to the low toxicity of this particle which were shown not to affect the barrier cell viability.
In fact, in order to reach detectable concentration in the lower circuit, there should be possible to use quite high concentration in the upper compartment, so low toxicity NP are required.

Viability of cells in the PS-FITC NP experiment (Fig. 61) confirmed that 1 mg/mL NP concentration was still not toxic for CaCo-2, while IL8 but not ICAM showed a high inflammation state of the target cell circuit (Fig. 62 A and B). Functionality of cells was comparable to control for CaCo-2 and C3A, while a small decrease in the vWF expression was found in the HUVEC cells (Fig. 63).

Looking at the lower circuit fluorescence measurement seemed that nothing was able to pass through. A lower than 10% of passage (correspondent to passage without cells) was expected; but CaCo-2 tight layer decreased NP transport to less than 1% (fix as detection limit) of the upper circuit concentration.
In order to understand if the value less than 1% meant that still some particles were able to translocate in a really low-undetectable concentration, fluorescent micrograph of target cells were taken using confocal analysis. The few particles (green dots in fig. 65 and 66) taken up by target cells in the lower circuit attested that PS-FITC NP was able to cross the barrier but in a less than 1% concentration. This data looks promising as low translocation (less than 0.4%) was already observed for nanoparticles *in vivo* [121].

Overall this concentration of particles cannot justify the modification in the marker concentration observed in the lower circuit.
IL8 release was huge and neither with higher concentration of PS-FITC NP this level was reached.

For this reason it is plausible to postulate an effect due to the cross-talk between cells, where messengers released from one cell type (maybe CaCo-2) can start the inflammation cascade on other cells (i.e. Target cells). Both viability of HUVEC and C3A and albumin release were comparable to controls, moreover vWF expression was found increased with low concentration of NPs (Fig. 63), so this loss of function seemed not to be ascribed to PS-NP.

Conversely, the preliminary data of Ag NP testing on cells were closer to the Ag NP sub-lethal effect induction.
Viability drops down only for CaCo-2 (directly exposed cells) to 50% and 1% respectively with 50 µg/mL and 200 µg/mL Ag NP concentration, while target cells still showed a viable cell metabolic activity (Fig. 67). Inflammation, instead, reflected the Ag NP toxicity showing high IL8 release but no ICAM-1 at low concentration (Fig. 68 A and B respectively). The effect of high Ag concentration led to slight decrease in the target cell function (lower vWF expression, fig. 70 and lower albumin release, fig 71, chapter 6) highlighting a higher Ag NP concentration in the lower circuit, since particles were able to cross the inefficient barrier of dead CaCo-2. When the particle concentration reaches a toxic level, barrier properties are lost leading to higher amount of particle translocation.

This study demonstrated the importance of barrier properties in the evaluation of molecule translocation across the intestinal epithelium.
An intact and tight epithelial layer represents a sort of protection for the body, preventing the direct passage of toxicants.

Anyway, as it happens in the multi-organ environment, consequences of direct stimulus on a cell type can be reflected on other organs even far away from the locus of action of the stimulus. Hence, direct effect of NPs on CaCo-2 cells can trigger inflammation on downstream cells that have no

direct exposure to the stimulus, but they can feel a perturbed state in the body-system so initiation of a concerted response from the whole body.

The multiorgan response is an important feature to take in account that standard methods often neglects. Pharmacology literature teaches us that frequently drugs designed to have effect on an organ also interfere with other pathways triggering for example side effects on other organ (i.e. hepatic toxicity of Nimesulide [3]).

The ILT system is an improved method that considers further levels involved in the response cascade. Moreover it integrates a biological barrier that usually is able to change the magnitude of a stimulus leading a more physiologically relevant situation.

Section IV

Conclusion

Chapter 8

Conclusion

Physiologically relevant methods are the frontier of future *in vitro* research.
This thesis is driven by the great interest that involves the development of new *in vitro* models able of investigating systemic and multiple pathway interactions. More convenient and ethically less questionable models capable of recapitulating inter-organ cross talk are particularly relevant in toxicology where the need of the complex response machinery of the body and the inadequacy of traditional *in vitro* methods have led to the massive use of the animal model.

A variety of *advanced* models have been proposed to overcome the simplicity of current methods. Unfortunately, 3D cell culture models, tissue slices or micro-scale cell culture device have had difficulty in gaining widespread acceptance and usage both because new model needs to be tested and validated each time and because new protocols are required. For this reason, in the current project, a body-on-a-plate able to translate standard protocols and cell handling techniques with minimal adaptation rather a microfluidic body-on-a-chip device was designed.
The principal goal of this thesis was to develop a new method to study on the effects of nanoparticles after ingestion using a 3 tissue connected culture system, the ILT.
The ILT system development embraced different disciplines (biology, engineer, toxicology, drug delivery etc.) to reach a high level of complexity integrating an epithelial bio-barrier with a vascular-hepatic connected culture

in order to recapitulate the processes of absorption, distribution and metabolism in the human body.

Firstly an allometric study demonstrated the key role of conserving cell proportions in the body when recreating the organ-system *in vitro*. This thesis showed different numbers of cells in a scaling relationship leads to different results due to differences cell-cell interaction mediated by soluble signals.

To validate and compare the ILT system with conventional techniques, a toxicological study on cells with both standard methods and advanced ones was performed. The results from this study were used to analyze and understand data from the new more complex models in order to gain new insights into NP toxicity at different levels.
In the study with conventional methods (static multiwell plate) a range of engineered nanoparticles of industrial interest was tested assaying various levels of toxicity, from sub-lethal to fatal levels.
It was shown that not only cell viability could be affected but also inflammation or function impairment could also be triggered. Silver NPs are found to be highly toxic even at low concentrations and surprisingly TiO_2 NPs also showed high toxicity on HUVEC cells while the literature describes it to be non-toxic on other cell cultures.
Furthermore, this thesis confirms the dependency of nanotoxicity on the size (Au 15 and Au 80 nm) and the type of NP (Ag, TiO_2, Au, PS NP).
Concrete evidence of how significant the use of an improved method is, comes out with studying NP toxicity within dynamic conditions: Ag NP was found to be twice as toxic under flow conditions, underlining the different behavior of cells and of their interaction with NP in the two models.
The dynamic conditions are closer to the *in vivo* environment as no physiological system is static: flow, movement and concentration gradients are present in all animals.

Another insight gained in this thesis was the central role of biological barriers. Comparison of the nanoparticle passage data in the two flow ILT system with the *in vivo* literature result showed a promising correlation between the NP translocation percentages across the intestinal epithelium. Bio barriers are fundamental to address the right dose that actually reaches the systemic circulation, so avoiding the testing of non-relevant doses.

In conclusion, in this thesis a new body-on-a-plate device (ILT) in which culture chambers are connected by the flow of a common medium was developed, tested and validated.
Data demonstrated that ILT system device is able to simulate an *in vivo*-like environment and to mimic ligand mediated cross-talk between different cells connected by the blood stream as occurs in the body.
The new method was tested assaying NP toxicity, but it could be used with a large range of molecules of industrial and scientific interest (drugs, toxics, proteins, antibodies) and even to study *in-vivo* targeting, molecular mechanisms and physiological and pathological interactions between organs.
This work will have a high impact on the advancement of *in vitro* models and the ILT system developed has been patented in order to continue the R&D on a large scale.

Glossary

ACRONYM	SIGNIFICATION
NP	Nanoparticle
Ag NP	Silver Nanoparticle
PS NP	Polystyrene-FITC Nanoparticle
Au NP	Gold Nanoparticles
TiO_2 NP	Titanium dioxide Nanoparticles
HUVEC	Human umbilical vein endothelial cells
C3A	Immortalized human hepatoma cell line
CaCo-2	Human epithelial colorectal adenocarcinoma cell line
ILT 0	Target tissues bioreactor
ILT 2	Intestinal cell bioreactor
ILT system	New connected three tissues dynamic culture
SMSM	Surface and Metabolic Scaling Model
CNSM	Cell Number Scaling Model
LDH	Lactate dehydrogenase
GSH	Glutathione (γ-L-glutammil-L-cisteinilglicina)
GSSG	Glutathione disulfide
ICAM-1	Inter-Cellular Adhesion Molecule 1
IL 8	Interleukin 8
vWF	Von Willebrand factor
TNF-α	Tumor Necrosis Factor-α
Fas-L	Fas-Ligand or CD95L
CYP450	Cytochrome P 450
FFA	Free Fatty Acid
TRITON-X 100	$C_{14}H_{22}O(C_2H_4O)_n$) a non-ionic surfactant
LC_{50}	Half lethal concentration
TEER	Trans epithelial electrical resistance

ELISA	Enzyme-linked immunosorbent assay

Bibliography

1. Animals in Research, Public Policy Statement, www.toxicology.org
2. The society of toxicology, www.toxicology.org
3. www.wikipedia.org
4. Rollin B.E.; Theoretical Medicine and Bioethics (2006), 27 (4): 285–304.
5. Questions and answers on revising the directive for the protection of animals used in scientific experiments. MEMO/08/677, www.europa.eu
6. BBC Science and Nature, www.bbc.co.uk
7. Vignais P.M. et al.; Berlin: Springer (2010), ISBN 90-481-3766-7
8. Eisenbrand G. et al.; Food and chemical toxicology (2002), 40 (2-3): 193-236
9. Andersen M.E. et al.; Toxicological Science (2009), 107 (2), 324–330
10. Mahto S.K. et al.; Annu. Rev. Public Health (2011), 32:161–78
11. Krewski D. et al.; Annu. Rev. Public Health (2011), 32:161–78
12. Gueguen-guillouzo C. et al.; Exp. Cell Res. (1983), 143,47–54
13. Zinchenko S. et al.; Tissue Eng (2006) 12, 8
14. Jamil E.-A. et al.; Nature (2006), 442: 403-411
15. Sung J.H. et al.; Lab Chip (2010), 10: 446-455
16. Sung J.H. et al.; Lab Chip (2009), 9: 1385–94
17. Viravaidya K. et al.; Biotechnol. Prog. (2004), 20: 316–23
18. Sung J.H. et al.; Biotechnol.Bioeng (2009), 104: 516–25
19. Ma B. et al.; Lab Chip (2009), 9:232–38
20. Ges I.A. et al.; Biosens. Bioelectron (2010), 26: 828–33
21. Xiao C. et al.; Biotechnol. Prog. (2003), 19: 1000–5

22. Curtis T.M. et al.; Lab Chip (2009), 9: 2176–83
23. Male K.B. et al.; Anal. Chem. (2008), 80: 5487–93
24. Ravindran S. et al.; Tissue Eng Part A. (2012), Vol. 18, 3-4: 295-309
25. Pagliari S. et al.; Adv Mater. (2011), 23 (4): 514-8
26. Talukdar S. et al., Biomaterials (2011), Epub ahead of print
27. Mahler G.J. et al., Biotechnol. Bioeng. (2009), 104: 193–205
28. Esch M.B. et al.; J Biotechnol. (2010), 148 (1):64-9.
29. www.clubofamsterdam.com
30. Faraday M.; Phil. Trans. Roy. Soc. London. (1857),147: 145–181
31. Turner T.; Proc. Roy. Soc. Lond. A. (1908), 81 (548): 301.
32. http://science.energy.gov
33. Buffat Ph. et al.; Physical Review A. (1976), 13 (6): 2287.
34. Julson A. J. et al.; Appl. Catal. B: Environ. (2006), 65, 315–325.
35. U.S. Food and Drug Administration, Sunscreen. www.fda.gov
36. Mitchnick M.A. et al.; Journal of the American Academy of Dermatology. (1999), 40 (1): 85–90
37. Zhang C. et al.; J Phys Chem B. (2011), 115(13):3392-9.
38. Gerberich W.W. et al.; Journal of the Mechanics and Physics of Solids. (2003), 51 (6) 979-992
39. www.infineon.com
40. www.eagle.fi
41. Mavroidis C., Annu Rev Biomed Eng. (2004), 6:363-95
42. http://www.niac.usra.edu/
43. Quinn J. et al.; Environ Sci Technol. (2005), 39 (5): 1309-18
44. http://ipp.nasa.gov
45. http://www.thermablok.com/
46. The Textiles Nanotechnology Laboratory, http://nanotextiles.human.cornell.edu/
47. Kong J. et al.; Science. (2000); 287 (5453): 622-5.
48. Beck-Broichsitter M., et al.; J Control Release. (2011), Epub ahead of print

49. Rana S. et al.; Adv Drug Deliv Rev. (2011), Epub ahead of print
50. Donev R. et al.; World J Biol Psychiatry. (2011) Suppl 1:44-51.
51. Taheri A. et al.; Int J Nanomedicine. (2011), 6: 1863-74.
52. Wang C. et al.; Int J Nanomedicine. (2011), 6: 1929-35.
53. Ryan J.J.; J Immunol. (2007), 179 (1): 665-72.
54. Arnaud F. et al.; J Vasc Surg. (2009), 50 (3): 632-9.
55. Arnaud F. et al.; J Trauma. (2009), 67 (4): 848-55.
56. Jokerst J.V. et al.; Acc Chem Res. (2011), Epub ahead of print
57. Neumeyer A. et al.; Nanomedicine. (2011), 7 (4): 410-9.
58. Rosen J.E. et al.; Nanomedicine. (2011), Epub ahead of print
59. Yan F. et al.; J Nanosci Nanotechnol. (2004), 4 (1-2): 72-6.
60. Martínez-Gutierrez F. et al.; Nanomedicine. (2011), Epub ahead of print
61. www.inmat.com
62. Li X.H. et al.; Food Sci Technol Int. (2010), 16 (3): 225-32.
63. Nanoscience and Nanotechnologies: Opportunities and Uncertainties. The Royal Society and The Royal Academy of Engineering, London. (2004), ISBN 0 85403 604 0
64. Ying J.; New York: Academic Press. (2001), ISBN 0127444513.
65. www.europa.eu
66. Oberdörster G. et al.; Environmental Health Perspectives. (2005), 113: 823–840
67. Donaldson K. et al.; Toxicol. Lett. (1996), 88, 293–298
68. Xia T. et al.; ACS Nano. (2008), 2, 2121–2134
69. Xia T. et al.; ACS Nano. (2008), 2, 85–96.
70. Donaldson K. et al.; Toxicol. Sci. (2006), 92, 5–22
71. Poland C. A. et al.; Nat. Nanotechnol. (2008), 3, 423–428.
72. Oberdörster G.; J of Internal Medicine. (2010), 267 (1): 89-105
73. Rivera Gil P. et al.; ACS Nano. (2010), 4 (10): 5527-31.
74. Drinker P. et al.; J. Ind. Hyg. (1927), 9, 98–105.
75. Oberdörster G. et al.; Ann. Occup. Hyg. (1994), 38, 295–302.

76. Geiser M. et al.; Environ. Health Perspect. (2005), 113, 1555 – 1560.
77. Oberdörster G. et al.; J. Nanosci. Nanotechnol. (2009), 9, 4996 – 5007.
78. Ryman-Rasmussen J. P. et al.; Toxicol. Sci. (2006), 91, 159 – 165.
79. Baroli B. et al.; Journal of Investigative Dermatology. (2007), 127 (7):1701-1712.
80. Korting H. C. et al.; Eur. J. Clin. Pharmacol. (1990), 39, 349 – 351.
81. Riehemann K. et al.; Angew. Chem. (2009), 121, 886 – 913
82. Dobrovolskaia M. A. et al.; Nat. Nanotechnol. (2007), 2,469 – 478.
83. Kanno S. et al.; Toxicol. Sci. (2007), 97, 398 –406.
84. Simon-Deckers A. et al.; Toxicology (2008), 253, 137 –146.
85. Rothen-Rutishauser B. M.; Environ. Sci. Technol. (2006), 40, 4353 – 4359.
86. Jin H. et al.; ACS Nano (2009),3, 149 – 158
87. Schleh C. et al.; Respir. Res. (2009), 10, 90.
88. Krug H. F. et al.; Angew. Chem. Int. (2011), 50, 1260 – 1278
89. Brunner T. J.; Environ. Sci. Technol. (2006), 40, 4374 – 4381
90. Gojova A.; Environ. Health Perspect. (2007), 115, 403 – 409.
91. National Academy of Sciences. Risk Assessment in the Federal Government: Managing the Process. (1983) Washington, DC: NAS.
92. Kroll A. et al.; European Journal of Pharmaceutics and Biopharmaceutics (2009), (72) 370–377
93. Mazzei D. et al.; Biotechnol Bioeng. (2010), 106(1):127-37.
94. Sbrana T. et al.; Landes Bioscience, Springer Science (2012); ISBN 978-1-4614-3054-4
95. Vinci B. et al.; Biotechnol. J. (2011), 6(5): 554–564
96. Guzzardi M.A. et al.; Biotechnol Bioeng. (2010), 106 (1): 127-37.
97. Vinci B. et al.; Biotechnol J. (2010), 5 (2): 232-41.
98. Vinci B et al.; Biotechnol J. (2010), 5 (6): 618-26.
99. Vinci B et al.; Biotechnol J. (2012), 7, 117–126
100. Vozzi F. et al., in prep.

101. Ucciferri N. et al., in prep.
102. Baudin B. et al., Nature Protocols (2007), 2 (3): 481-5
103. Beken S.; Methods Mol Biol. (1998), 107: 303-9.
104. Senft A. P.; Anal. Biochem. (2000), 280 (1): 80-6.
105. Clift M.D. et al; Toxicology and Applied Pharmacology (2008), 232:418–427
106. Galbusera M. et al.; Blood (1997) 90 (4): 1558-1564
107. Phillips J.W.; Eur. J. Biochem. (1995), 227, 352–358.
108. Stacpoole PW.; Metabolism. (1997); 46 (3): 306-21.
109. Westerink W.M. et al.; Toxicol In Vitro. (2007), (8):1581-91.
110. Brunner T. J et al.; Environ. Sci. Technol. (2006), 40, 4374 – 4381
111. Rasmus F. et al.; Toxicology Letters (2009), 190, (2): 156–162
112. Lee Y.S. et al.; Archives of Toxicology, 85, (12) 1529-1540
113. Park H.S. et al.; Cancer Prevention Research (2010), 3, I12, Supplement 2
114. Hussain S. et al.; Particle and Fibre Toxicology (2010), 7:10
115. Park E.-J. et al.; Toxicology in Vitro (2010) 24, 3: 872–878
116. Khan M. I. et al.; Biomaterials (2012) 33, 5: 1477–1488
117. Satoh S. et al.; Immunology. (1994), 82 (4): 571–576.
118. McHale J.F. et al.; The Journal of Immunology, (1999), 163, 7
119. Couffinhal T. et al.; Arteriosclerosis, thrombosis and vascular biology American Heart Association (1993) 13, 3: 407-414
120. Kermanizadeh A. et al.; Nanotoxicology, (2012), Epub ahead of print
121. Schleh et al.; Nanotoxicology, (2012), 6 (1): 36-46